High Temperature Studies of Sodalites

A Thesis for the MRes in Materials Chemistry and Nanochemistry

Tabasum Fazal

[redacted]

Department of Chemistry

The University of Birmingham

February 2011

Acknowledgements

I am heartily thankful to my supervisor, Dr Joseph Hriljac, whose encouragement, guidance and support from the initial to the final level enabled me to complete my thesis.

I would also like to thank my family and friends for their continual love and support.

Contents

4. Effects of ion exchange on the structure of halosodalites
    a. Ion exchange on Bromosodalite
    b. Ion exchange on Chlorosodalite
    c. Discussion of changes
5. High temperature studies of halosodalites
    a. High temperature studies of bromosodalite
    b. High temperature studies of chlorosodalite
    c. High temperature studies of iodosodalites
    d. Discussion of High temperature studies of halosodalites
6. High temperature studies of ion exchanged halosodalites
    a. High temperature studies on ion exchanged bromosodalites
    b. High temperature studies of ion exchanged chlorosodalites
7. Discussion of Thermal expansion coefficients
8. Discussion of Tetrahedral tilt angles

6. Conclusions

7. Further work

8. References & Bibliography

9. Appendices

1. Introduction

The use of porous framework compounds to encapsulate nanoscale atomic clusters gives many possibilities to produce novel materials (Johnson et al., 1999). A particular family of crystalline microporous solids, the so-called sodalite family, contains many members with various chemical, topological, geometrical, and crystallographic aspects (Depmeier, 2005). Most sodalites can be described by the general formula $M_8[ABO_4]_6X^{n-}_{2/n}$, where M is a monovalent cation such as Na^+, Li^+ and Ag^+, A and B are tetrahedral forming species such as Al and Si, and X can be a variety of mono- or di-valent anions, including Cl, Br, I, ClO_3^-, MnO_4^{2-} and CrO_4^{2-} (Weller and Wong, 1989). The aluminosilicates are by far the most well known and characterised sodalites (Hassan and Grundy, 1984; Weller, 2000). Sodalites are generally synthesised with Na^+ as the non-framework cation, which can then be exchanged in aqueous solution by a range of other monovalent cations such as Li^+, K^+, Rb^+ and Ag^+ (Weller, 2000).

There are a multitude of possible sodalites depending on the cation and anion involved along with the Si/Al ratio of the framework (Acar et al., 2003). Table 1 shows some of the sodalites available and their framework composition (Weller, 2000):

Table 1: Framework compositions of sodalite type structures

Framework atoms	Example
Si,Al	$Na_8[SiAlO_4]_6Cl_2$
Si	$[SiO_2]_{12}(C_2H_4(OH)_2)_2$
Si,Ga	$Na_8[SiGaO_4]_6(HCO_2)_2$
Ge,Al	$Na_8[GeAlO_4]_6(MnO_4)_2$
Ga,Al,Si	$Ca_8[GaAlSiO_6]_4(OH)_8$
Ge,Ga	$Na_8[GeGaO_4]_6(ClO_4)_2$
Al,Be,Si	$Na_8[AlBeSi_4O_{12}]_2Cl_2$
BeSi	$Cd_8[BeSiO_4]_6Se_2$
Al	$Ca_8[AlO_2]_{12}Te_2$
B	$Ca_8[BO_2]_{12}S_2$
Al/P	$[AlPO_4]$
Mg	$Na_8[Mg_3Si_9O_{24}](OH)_2$
ZnP/ZnAs	$Na_6[ZnAsO_4]_6 \cdot 8H_2O$
P	$H_4Co_5[P_{12}N_{24}]Cl_2$
Zn/Cu	$[HN(CH_3)_3][Zn_5CuCl_{12}]$
Co/P	$[NMe_4][CoPO_4]$

In this study the sodium and silver forms of basic halosodalites have been studied. Sodalites occur as a number of natural minerals, and have been noted as being particularly good in the absorption and retention of halides (Barrer and Cole, 1970).

1.1. Structure of sodalites

The structure of the mineral sodalite, $Na_8(SiAlO_4)_6Cl_2$ was first determined by Pauling in 1930 and the structure further studied by Lons and Schulz in 1967 and then by Hassan and Grundy in 1984, based on room temperature X-ray diffraction data. The sodalite framework consists of alternating SiO_4 and AlO_4 units with Si/Al ratio of 1. These corner sharing tetrahedral units are shown in Figure 1 and these form eight 6-rings and six 4-rings which make up the cuboctahedral cage called a β- or a sodalite cage (Stein and Ozin, 1992a).

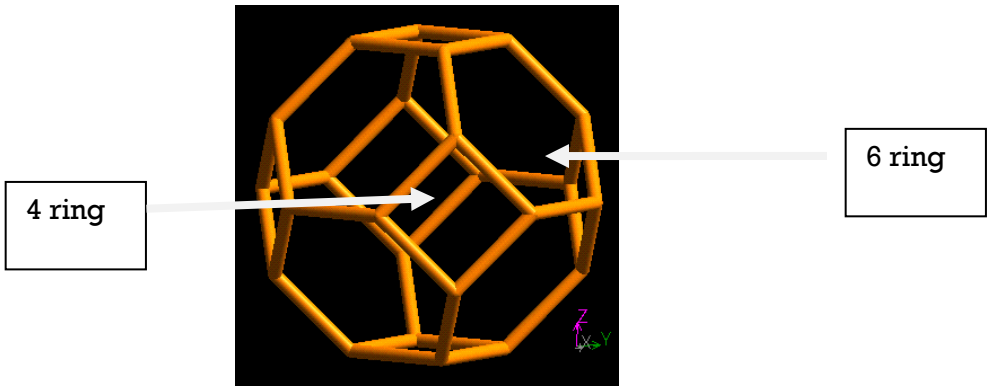

Figure 1: Sodalite cage composed of eight six-rings and six four-rings (Johnson et al., 1999).

These cages are ~ 6.5 Å in diameter and are accessible through six-membered rings of 2.2 Å diameter (Zilli and Bagnato, 1984). The Si and Al atoms of a given ring are coplanar. The oxygen atoms alternate above and below the plane (Weller et al., 1999) (Figure 2a).

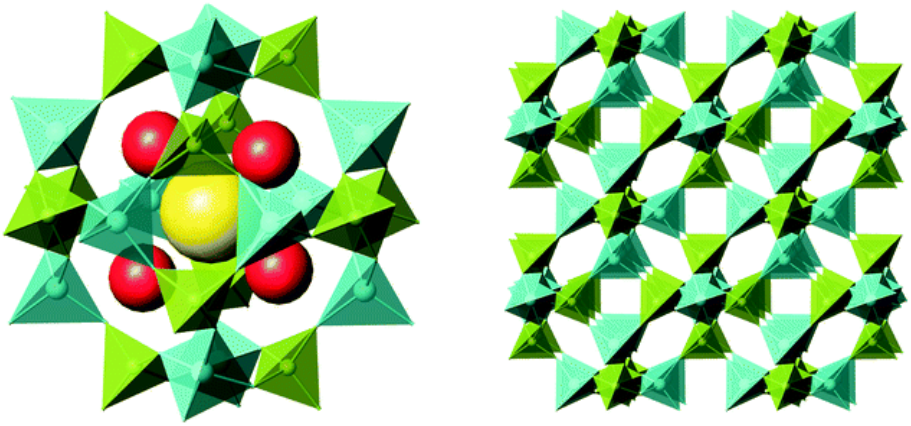

Figure 2a: The sodalite structure. The linking SiO_4 (green) and AlO_4 (blue) tetrahedra forms a body centered arrangement of framework beta cages, right. Each cage contains a central anion (yellow) surrounded tetrahedrally by cations (red), left; the cations also interact strongly with three framework oxygen atoms to produce a distorted tetrahedral environment for these ions (Weller, 2000).

The β-cages are directly linked through six rings and the structure is described as being semi-condensed (Weller, 2000). The six-membered rings form continuous channels that offer diffusion paths for intraframework cations. The channels are too small to permit the adsorption of small molecules such as ammonia (Johnson et al., 1999).

In ordered aluminosilicate sodalites, the lattice symmetry is P43n and has Td point symmetry (Zilli and Bagnato, 1984). The cubic symmetry of the sodalite is a result of the close packing of the interconnected six fold rings of (Al, Si) O4 tetrahedra. The six-membered rings are stacked parallel to {111} in an ABCABC… type of sequence. The stacking sequence of 6-rings in the sodalite is seen in Figure 2b. The structure is further characterised by (Al, Si)0_4 rings of four tetrahedra parallel to {100}.

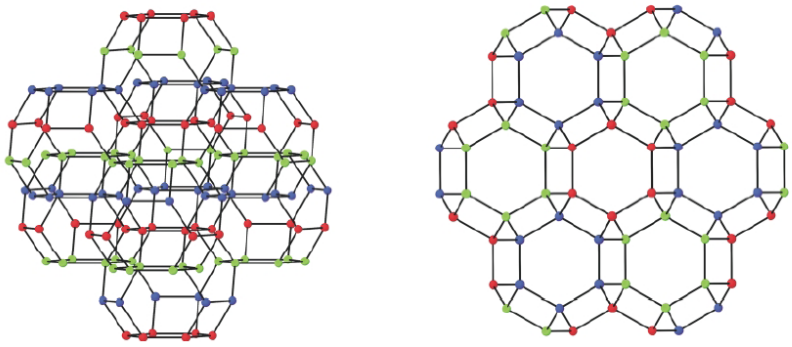

Figure 2b: The stacking sequence of 6-rings in the sodalite (ABCABC…), left. The derived pore structures (right). The red, blue and green represent the different positions of the vertically stacked layers (Weller, 2000).

The overall linkage of (Al, Si)O_4 tetrahedra results in a cubo-octahedral cavity (Hassan and Grundy, 1984). The six membered rings form continuous channels that offer diffusion paths for interframework ions (Barrer and Vaughan, 1971).

With the possibly unique exception of hydroxide, anions are irrevocably trapped within the cages. It is not possible to place the anion within the cage after formation, nor is it possible to remove the anion without destroying the cage or decomposing the anion itself (Acar et al., 2003).

One interesting aspect of sodalites is their structural flexibility. The flexibility of cages is attributed to the change of bond angles rather than a change in bond distances. Due to this, the sodalite framework is termed partially collapsed (Acar et al., 2003). This owes to the rotation of the (Al, Si) O_4 tetrahedra so that the Na atom is within reasonable bonding distance to both the framework oxygen's and the halide atoms (Hassan and Grundy, 1984).

The unit cell size of the halosodalites varies with the type of halide and the types and relative concentrations of cations present (Stein and Ozin, 1992a). The halide effect is mainly a space-filling effect, the large anion causing an expansion of the sodalite cage. An increase in temperature also causes an expansion of the unit cell and the ring dimensions. Replacement of Na^+ by Ag^+ causes a contraction of the cage (Acar et al., 2003).

1.2. Uses of sodalites

Sodalites have received considerable attention during the last few decades. Studies have shown they have many useful properties, for example sodalite based materials are used as pigments (Volynets et al., 1984; Vakhidov et al., 1976) and as containments for radioactive waste prior to disposal (Koyama, 1994). These applications revolve around the fact that the guest material is contained within a regular structure that does not allow for diffusion.

The study of a large range of sodalite data may provide pointers as to the favoured anions and cations for entrapment, the preferred size of sodalites for different framework compositions and the ability of the sodalite structure to adapt to different anion and cation sizes. The extent to which certain structural parameters, such as tetrahedral tilts and framework bond angles, can deviate from the ideal may also provide information regarding which sodalites can realistically be expected to form and with stand high temperatures (Koyama, 1994; Stein et al., 1992a).

Applications such as optical data storage media, novel semiconductor assemblies, and chemical transducer materials have also been suggested (Stein et al. 1992a). Silver sodalites have been observed to manifest various optical properties including photochromic, barochromic, thermochromic, and fluorescent behaviour (Volynets et al., 1984; Vakhidov et al., 1976).

1.3. Synthesis of Halosodalites

Sodalites have been synthesised by various techniques, such as solid state reactions, hydrothermal growth, and transformation of zeolites (Suzuki et al., 1985).

The most popular method of synthesising halosodalites is hydrothermally using Stein's method (Stein et al., 1992a). The advantages of using hydrothermal method are listed below (Stein et al., 1992a; Stein et al. 1992b):

- Good mixing of reagents. By using a solvent it ensures that the reagents are mixed well for the formation of a homogeneous product, which is particularly important for mixed anions.
- Metastable/ Kinetically stable products are formed due to the mild conditions applied
- Control over the particle size by fine tuning of the flexible reaction conditions.
- Single step method which considerably simplifies synthesis when compared to more traditional solid state/ ceramic methods
- Mild conditions drastically reduce the potential costs of application to industry

Structure conversion method

The "structure conversion method" by Chang (1974) has also been used to make halosodalites. This method converts a complex sodium-aluminosilicate structure into a sodalite structure while at the same time incorporating an alkali halide and activator compounds to form cathodochromic or photochromic sodalites.

Ion exchange

Hydrothermally produced sodium halosodalites have then further been modified to load silver into the structure, replacing some or all of the Na cations in the framework with silver cations. $AgNO_3$ melt and hydrothermal aqueous exchanges have been used to replace Na^+ ions by Ag^+ ions (Acar et al., 2003).

Mixed halide sodalites

Mixed halide sodalites can also be produced as outlined by Weller and Wong (1989). The new type of sodalite containing more than one type of anion cage species have been synthesised and Weller discussed the structural effects of introducing a proportion of a second halide. The structures of $Na_8(AlSiO_4)_6(Cl, Br)_2$ and $Na_8(AlSiO_4)_6(Cl\ Br)_2$ have been refined from powder neutron diffraction data. No evidence of halide ordering was found and the structure was expressed in terms of average cell content with a gradual expansion of the framework Si-O-Al bond angle as the heavier anion replaces chloride.

1.4. High temperature studies and Thermal expansion

High temperature studies on halosodalites have been carried out previously, showing normal (positive) thermal expansion (Henderson and Taylor, 1984). Thermal Expansion is the tendency of matter to change in volume in response to a change in temperature (Tipler and Mosca, 2008). Thermal expansion can either be positive or negative i.e contraction. When a substance is heated, its constituent particles move around more vigorously and by doing so generally maintain a greater average separation. This is known as positive thermal expansion. Most solids expand on heating, some materials, however, shrink when they are heated, which is known as negative thermal expansion (O'Mara et al., 1990). Materials that contract with an increase in temperature are very uncommon; it only occurs within limited temperature ranges (Tipler and Mosca, 2008). The degree of expansion divided by the change in temperature is called the material's coefficient of thermal expansion and generally varies with temperature (Tipler and Mosca, 2008).

Thermal expansion can be calculated using:

Thermal expansion	$\alpha = \frac{1}{V}\left(\frac{\partial V}{\partial T}\right)$

A good way of measuring the entire expansion tensor is to perform powder diffraction on the material during a heating or cooling run and monitor the position of its diffraction peaks.

In this study we investigate the effect of high temperature on a variety of halosodalites to correlate thermal expansion with changes in the cations and anions. The thermal expansions of

several sodalites and structurally related compounds have been previously reported by high temperature powdered X-ray diffraction (Taylor, 1968; Henderson & Taylor, 1978).

The results from these studies (Taylor, 1968; Henderson & Taylor, 1978) suggested that there were anomalous increases in their cell dimensions with temperature over the range 293-1100K. The changes in the framework bonds would be slight; in some cases an apparent contraction of the framework bonds was observed and this may be attributed to the anisotropic thermal motion of the framework oxygen's. The distances between the cavity ions increased on heating (Dempsey and Taylor, 1980).

The geometric relationship between the cell edge of a cubic sodalite, a, the length of the framework tetrahedron edge, E, and the tilt angle, Φ is (Dempsey and Taylor, 1980)

$$a = 2E\cos\Phi + 1.414E$$

The tilt angle is the angle through which a tetrahedron is tilted relative to its position in the ideal fully-expanded structure. Due to the sodalite having a partially collapsed structure, the main structural change upon heating was a decrease in the tilt angle, Φ, and a resulting increase in the T-O-T angle. There will also be an increase in bond lengths of the cavity ions (Dempsey and Taylor, 1980).

The thermal expansion behaviour of the aluminosilicate sodalites has been interpreted by means of a computer model of the cubic sodalite structure by Henderson and Taylor in 1978. It was concluded that a discontinuity should only be expected for aluminosilicate sodalites containing

large cavity anions, for example iodine, and that the discontinuity occurs when the coordinates of the cavity cation become 0.25.

Dempsey and Taylor (1980), described how the distance least squares (DLS) structure modelling technique was used to determine the room temperature structures of the sodalite $Na_8(AlSiO_4)_6Cl_2$. This technique also calculated the thermal expansion behaviour of $Na_8(AlSiO_4)_6I_2$ assuming that the discontinuity in its thermal expansion curve occurred either when the ideal fully expanded state was achieved or when the x-coordinate of the sodium atom became 0.25. Results were given as plots of bond lengths and bond angles as a function of temperature. Estimates indicated that the expansion of the Na-O and Na-I bonds were 9% and 27.4% respectively, between room temperature and 810°C, and there was an apparent shortening of the framework bond distances of about 1.5Å (Dempsey and Taylor, 1980).

2. **Aim**

Previous work on members of the sodalite family by Taylor and Henderson (1978) concentrated towards understanding the nature of the bonding in framework structures, particularly the T-O-T angles, interpreting the infra-red spectra of framework structures and interpreting the thermal expansion of the halosodalites. The aim of my project is to expand upon this work to study the effect of high temperature on a variety of halosodalites and silver ion exchanged halosodalites and to correlate thermal expansion with changes in both the cations and anions, where the balance of the ionic and covalent bonding of the cage contents changes.

High temperature experiments have been carried out on the aluminosilicate sodalites, $Na_8(Al_6Si_6O_{24})Br_2$, $Na_8(Al_6Si_6O_{24})Cl_2$ and $Na_8(Al_6Si_6O_{24})I_2$ in the past and thermal expansion and discontinuity in some of the aluminosilicate sodalites have been observed (Hassan and Grundy, 1984; Henderson and Taylor, 1978; Dempsey and Taylor, 1980). So far no high temperature studies on silver exchanged aluminosilicates have been carried out and the aim of this project is to see if thermal expansion behaviour is different in the silver and sodium forms due to changes in the M–X bonding and subsequent effects on the M–O bonding to the framework.

The first objective was to examine various ways to make sodalites, in order to be able to produce the most crystalline sodalite for further studies. After finding the best method in producing crystalline halosodalites, the second objective was to carry out silver ion exchange on these sodalites and examine changes in the structures due to the replacement of Na by Ag. The final

objective was to carry out high temperature studies on the ion exchanged halo sodalites and see how composition affects thermal expansion. The study was carried out to 997°C using the D5000 and D5005 X-ray powder diffractometers and Rietveld structure refinements. From measurements of the coefficients of thermal expansion it was possible to determine how changes in the cations and anions affect this property.

There are a number of reasons why the structures and thermal expansion properties of the compounds are of interest. One of the reasons is that these are simple model systems and the results could be useful for studies of more complex aluminosilicates. Another is because the structures are so well behaved and understood they form a systematic study to see how changing the species inside the pores of aluminosilicates in a controlled fashion can affect thermal expansion behaviour. Finally, sodalites with silver in the pores have been proposed to have many potential applications such as optical data storage data media, novel semiconductor assemblies and chemical transducer materials (Ozin et al. 1990; Stein et al., 1992a, 1992b) and some of these would be affected by temperature so understanding the thermal expansion is important.

A further study of how the cation exchange affects high pressure behaviour was planned, but due to time limitations and the lack of synchrotron X-ray beam time this was not possible.

3. Experimental

3.1. Hydrothermal synthesis of Sodium halosodalites

The sodium sodalites, $Na_8(AlSiO_4)_6Br_2$, $Na_8(AlSiO_4)_6Cl_2$ and $Na_8(AlSiO_4)_6I_2$ were initially prepared hydrothermally using Stein's (Stein et al., 1992a; Stein et al., 1992b) method and then with an alteration to the prep. The gel compositions and reagents used to make the sodalites are listed in Table 2.

Since only sodalites with a Si/Al ratio of unity have been produced, the synthesis was carried out in aqueous media and without any templates other than the salt desired in the final product (i.e., no organic templates have been used).

The raw materials used were reagent-grade sodium hydroxide pellets (Mallinckrodt, 98.7%), Sodium aluminate [$NaAlO_2$. xH_2O] (8% water), sodium halides (NaBr, NaCl, NaI) and ammonium stabilised colloidal silica (Ludox HS-40).

Table 2: Reagents and gel composition used to make the Sodalites

Sodalite type	Batch composition
$Na_8[SiAlO_4]_6Br_2$	Solution A – 52 NaBr : 20 NaOH : 5 Silica Solution B – 9 NaOH : 3 $NaAl_2O_2.XH_2O$
$Na_8[SiAlO_4]_6Cl_2$	Solution A – 29 NaCl : 20 NaOH : 5 Silica Solution B – 9 NaOH : 3 $NaAl_2O_2.XH_2O$
$Na_8[SiAlO_4]_6I_2$	Solution A – 83 NaI : 20 NaOH : 5 Silica Solution B – 9 NaOH : 3 $NaAl_2O_2.XH_2O$

In a typical synthesis, solution A contained the sodium salt, sodium hydroxide, and silica source and solution B contained sodium hydroxide and the alumina source. These were prepared as follows. For solution A, the NaOH and the sodium salt to be occluded in the sodalite were dissolved in the deionised water. An aqueous colloidal silica solution was added to the above solution. The solution was mixed and heated to 95ºC. Solution B was prepared by dissolving the sodium aluminate and the sodium hydroxide in deionised water and heated to 95ºC. The hot solutions A and B were mixed rapidly. A gel formed almost immediately upon mixing. The gel was shaken for 5 minutes and the mixture was heated at 95ºC for 72 hours in a 500ml capped Teflon bottle. After crystallisation the white, microcrystalline products were cooled to ambient temperature and then filtered. They were washed with deionised water until the filtrate was hydroxide free and the pH fell below 8. The sodalite was then dried at 110˚C and ground in a mortar and pestle, weighed and stored in a vial.

A second set of materials were made by using half as much of the aluminate and silicate sources, this is referred to as “the modified Stein prep”.

3.2. Aqueous exchange

The sodalites were subsequently modified in order to obtain silver loaded forms. The silver loading was done by aqueous ion exchange, whereby the sodium cations in the framework were replaced by silver from the solution phase. Ion exchange was carried out on the sodalites produced hydrothermally in 500ml Teflon bottles. Silver-containing sodalites were prepared by aqueous ion exchange of a mixture containing the parent sodium sodalite and 0.1M of $AgNO_3$ (fisher, 99.8%). About ~ 1.5g of sodium sodalite was added to an aqueous solution containing stoichiometric amounts of silver nitrate. The mixture was stirred in the dark for 24 hours at room

temperature. The products were filtered, washed in the dark and dried in air. Due to their light sensitivity, the white to yellow coloured dry powders were stored in the dark in sample vials.

The XRD patterns indicated that the ion exchange of the sodalites was successful but chemical analysis was carried out to calculate the amount of sodium in each sodalite and from this then the amount of silver present was calculated. About 100 mg of the compound was added to 10 ml solution of diluted HNO_3 (nitric acid and distilled water in a ratio of 1:10) in order to dissolve the aluminosilicate framework. The solution was stirred and heated in order to dissolve properly. The solution was transferred into a 250 ml volumetric flask and bought up to volume with deionised water.

Standards of sodium were also prepared in order to determine the amount of sodium in each sodalite and therefore calculate how much silver was present. A flame photometry machine (Figure 3) was used for the measurements.

Figure 3: Flame photometry machine

Stein and Stucky (1992b) carried out far-infrared spectroscopy which showed that replacement of sodium ions by silver ions did proceed to completion or nearly so and that proton exchange is unlikely at a neutral pH.

3.3. Other synthesis routes

In another experiment, the above hydrothermal method was used to synthesise halosodalites but instead of putting the gel mixture in the 500ml capped Teflon bottles, autoclaves were used and the gel mixture was heated for 24hrs at 200˚C.

Structure Conversion Method (SCM)

The basic mechanism of the SCM is the conversion of complex sodium-aluminosilicate structure into a sodalite structure while at the same time incorporating the alkali halide to form the halosodalites (Chang, 1974). The structure conversion method is different from the hydrothermal method in that it is not a synthesis from the oxide and the salt components in water. Two types of structural conversion methods were carried out. In the first structure conversion method, commercial Linde 4Å molecular sieve was used as the starting Na-Al-silicate and was added to the halide salt. These starting materials (all in powder form) were ground together in a mortar and pestle for five minutes and transferred into a quartz boat. The boat was then placed in an oven and heated to 850˚C for 24 hours. In the second structure conversion method, 0.25g of the product from the first structure conversion method was taken and excess sodium halide was added to this, since the excess salt can be leached out after the heating process. The sodalite was again heated to 850°C for 24 hours and was then cooled to ambient temperature and washed with deionised water to remove the excess halide.

4. Characterisation

Powder X-ray Diffraction

The samples investigated in this thesis were all crystalline powders. The term 'powder' really means that the crystalline domains are randomly oriented in the sample. The positions and the intensities of the peaks from a simple diffraction experiment are used for identifying the underlying structure of the material.

Laboratory equipment

Two laboratory diffractometers were used during these studies. X-ray diffraction data was gathered using a Bruker D5000 and a Bruker D5005 diffractometer. The D5000 diffractometer was used for the routine measurement of samples, checking for phase changes, ion exchange, i.e. variation in peak intensities and structure crystallinity confirmation. X-ray data was gathered using the Bruker D5005 diffractometer utilising Cu $K\alpha_1$, $K\alpha_2$ radiation and additionally, for the variable temperature work, an Anton Parr HTK 1200 heating stage for the in-situ X-ray examination of products over a given heating regime.

D5000 Diffractometer

The instrument operates in transmission mode with the primary X-ray beam passing through the rotating sample. The sample for analysis was dispersed between two strips of Scotch 'magic tape' which, in general, gives negligible scattering in comparison to the crystalline sample. The magic tape was then attached to an aluminium X-ray disc, which was fitted to the diffractometer such that the x-ray beam passes through the sample Figure 4.

Figure 4 : D5000 Diffractometer

The products from the hydrothermal synthesis and silver exchanges were analysed using the D5000 Diffractometer using Cu $K\alpha_1$ radiation (λ=1.5406Å). XRD at room temperature was carried out over a 2theta range of 6 – 60 over 20 minutes.

D5005 Diffractometer

This is a general purpose Cu K_α X-ray powder diffractometer. It is used primarily for phase identification.

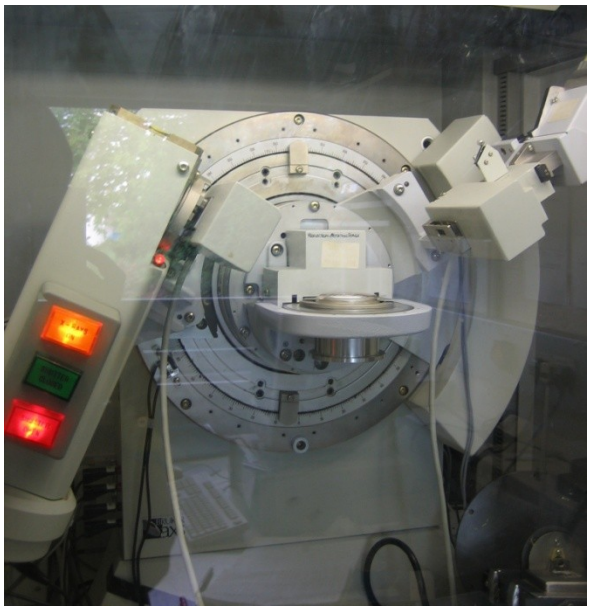

Figure 5: D5005 Diffractometer

In addition an Anton Parr HTK 1200 heating stage was used for the high temperature work. Variable temperature XRD scans were carried out over a temperature range of ambient (~25˚C) to 847˚C with multiple scans of the same temperature. Only the significant scans have been included here. This is because they were initially carried out to 997˚C, but the sample started to decompose after 847˚C.

Rietveld structure refinements

Rietveld refinement is a technique devised by Hugo Rietveld for use in the characterisation of crystalline materials (Rietveld, 1969). The neutron or X-ray diffraction of powder samples results in a pattern characterised by peaks in intensity at certain positions. The height, width and position of these peaks can be used to determine many aspects of the materials structure.

The Rietveld method uses a least squares approach to refine a theoretical line profile until it matches the measured profile. The introduction of this technique was a significant step forward in the diffraction analysis of powder samples as, unlike other techniques at that time; it was able to deal reliably with strongly overlapping reflections (Rietveld, 1969). A powder data set can be thought of as a series of data points with a certain intensity, which is contributed to by the reflections of one or more crystalline phases within the sample studied. The Rietveld method seeks to obtain the best fit between this pattern (the observed) and that generated from a structural model (the calculated). The process of Rietveld refinement involves inputting a model structure and constraints for subsequent refinement. Each available parameter is then varied according to the constraints in an iterative fashion to achieve an improved fit (Rietveld, 1969).

The diffraction traces collected from the D5005 were treated with the Rietveld method, using the GSAS and EXPGUI programs. For the room temperature structures, the starting atomic coordinates, cell parameter, isotropic displacement parameters, and space group, P43n, were those of Weller and Tong (1989). The refined atomic coordinates were then used as input for the next higher temperature structure. The site occupancies were fixed to the idealised chemical formula for sodalite. No actual attempts were made to refine the Na/Ag occupancies to verify the elemental analysis because the quantitative exchange is well accepted in literature (Stein and Stucky, 1992b). Also this is experimentally backed up in that the Rietveld refinements with the fixed compositions give reasonable and consistent temperature factors.

5. Results and Discussion

5.1. Synthesis

A number of experiments were carried out in order to produce pure crystalline sodalites $Na_8(SiAlO_4)_6Br_2$, $Na_8(SiAlO_4)_6Cl_2$, and $Na_8(SiAlO_4)_6I_2$. The XRD patterns are shown in Figure 6a, 6b and 6c and the measured full width at half maximum for the peak at ca. 24.5°2θ for each sample are shown in Tables 3, 4 and 5.

The first attempt was using Stein's method (Stein et al., 1992a).The samples were produced successfully but the peaks were not very sharp, therefore the method was modified by diluting the amounts of silicate and aluminate in solution to slow crystallisation, as outlined in the experimental section. The new samples were analysed using the EVA software, limiting the elements in the search/match to Si, Al, Na and the halide. The compositions of the sodium sodalites were consistent with the expected sodalite structure and no extra peaks were observed. The peaks were a lot sharper as can be seen in Figure 6a, 6b and 6c (stack f), but other experimental methods were also carried out to see if there was an alternative method that would produce more crystalline halosodalites. The halosodalites were produced in autoclaves in order to heat at very high temperatures, but the XRD patterns showed that the halosodalites were not more crystalline. Another method used was Chang's "structure conversion method" (Chang, 1974). Chang's method produced impure halosodalites which contained nepheline. This method was then modified further by adding more halide to the sample but the halosodalites were not pure enough so this method was not further used. In the end the modified method of Stein was scaled up to make large batches of the halosodalites that were used for the ion exchanges and variable temperature studies.

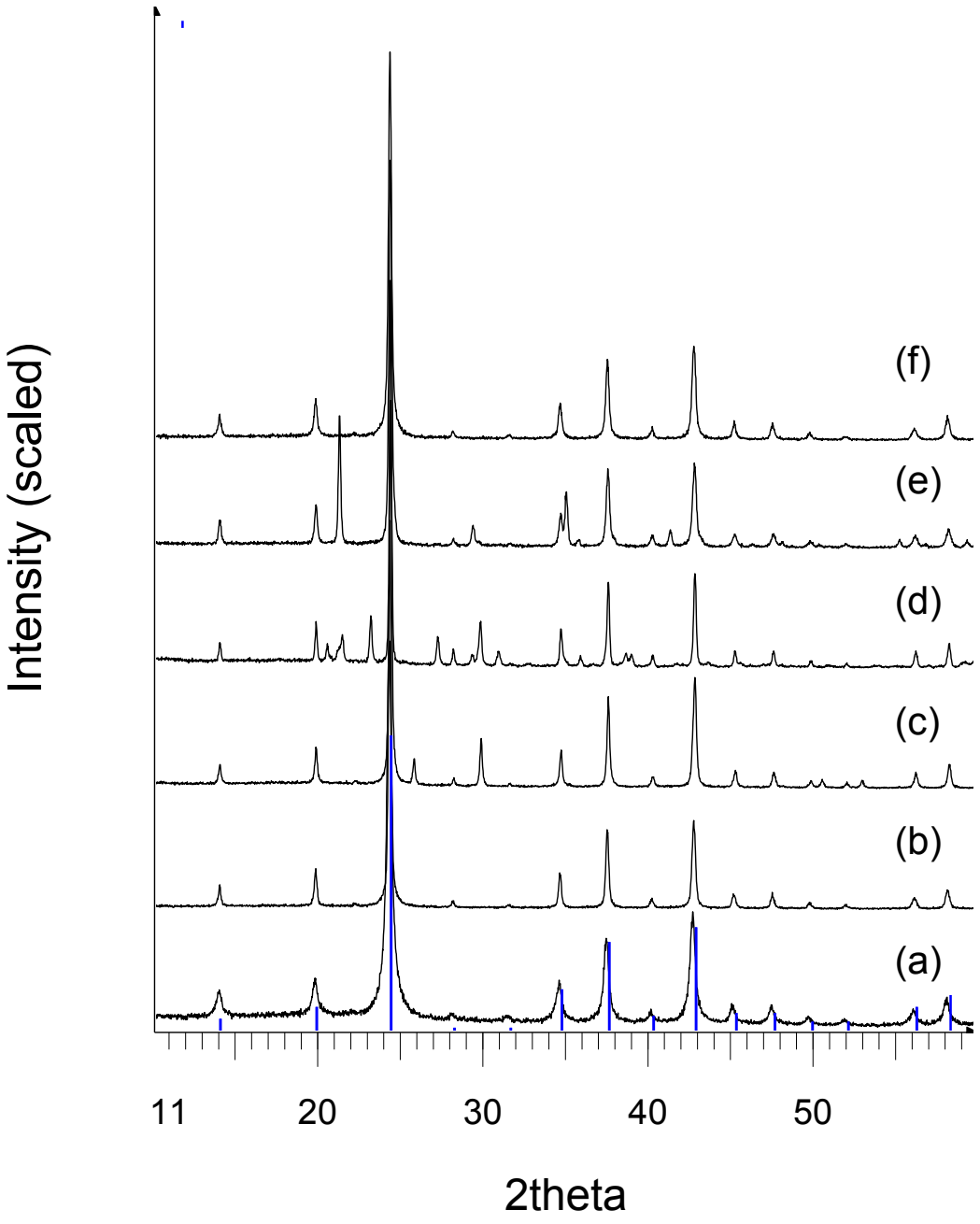

Figure 6a: XRD plots of (a) bromosodalite produced using Stein's preparation, (b) bromosodalite produced using Stein's method with alterations made to the method, (c) bromosodalite produced in autoclaves, (d) structure conversion method 1, (e) structure conversion method 2, (f) large batch using Stein's prep with modifications. The blue line shows the ICSD pattern for sodium bromosodalite (00-037-0476).

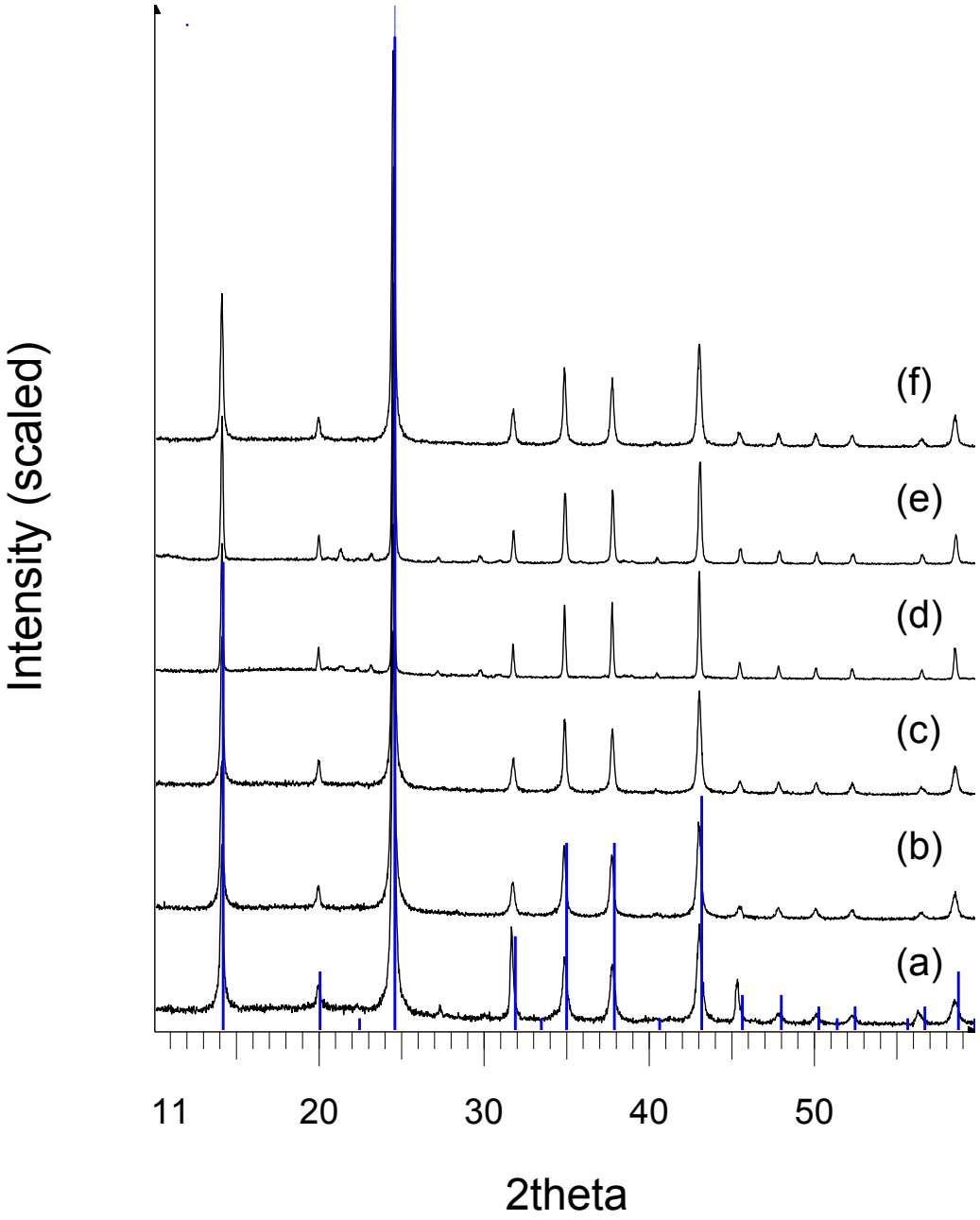

Figure 6b: XRD plots of (a) chlorosodalite produced using Stein's preparation, (b) chlorosodalite produced using Stein's method with alterations made to the method, (c) chlorosodalite produced in autoclaves, (d) structure conversion method 1, (e) structure conversion method 2, (f) large batch using Stein's prep with modifications. The blue line shows the ICSD pattern for sodium chlorosodalite (00-032-1032)

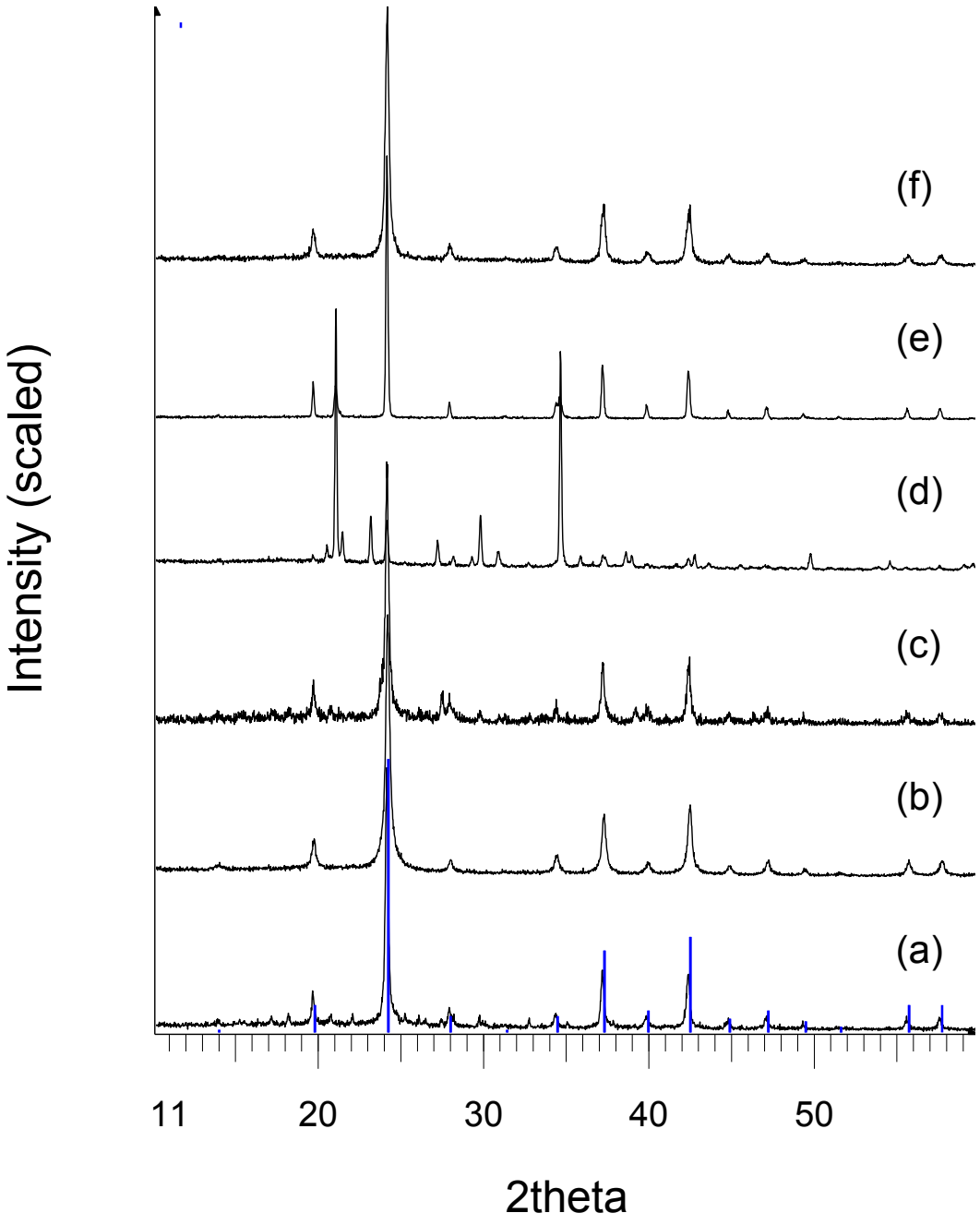

Figure 6c: XRD plots of (a) iodosodalite produced using Stein's preparation, (b) iodosodalite produced using Stein's method with alterations made to the method, (c) iodosodalite produced in autoclaves, (d) structure conversion method 1, (e) structure conversion method 2, (f) large batch using Stein's prep with modifications. The blue line shows the ICSD pattern for sodium iodosodalite (00-032-1031)

Table 3: The variation in peak width with synthesis method for bromosodalite.

Method	FWHM (°) of peak at 24.5° 2θ
Basic Stein's preparation	0.353
Modified Stein's method	0.182
Autoclaves	0.168
Structure conversion method 1 – original prep	0.137
Structure conversion method 2 – extra halide	0.198
Large batch using the modified Stein's method	0.202

Table 4: The variation in peak width with synthesis method for chlorosodalite.

Method	FWHM (°) of peak at 24.5° 2θ
Basic Stein's preparation	0.239
Modified Stein's method	0.204
Autoclaves	0.198
Structure conversion method 1 – original prep	0.128
Structure conversion method 2 – extra halide	0.160
Large batch using the modified Stein's method	0.199

Table 5: The variation in peak width with synthesis method for iodosodalite.

Method	FWHM (°) of peak at 24.5° 2θ
Basic Stein's preparation	0.194
Modified Stein's method	0.285
Autoclaves	0.217
Structure conversion method 1 – original prep	0.129
Structure conversion method 2 – extra halide	0.139
Large batch using the modified Stein's method	0.285

5.2. Ion exchange

Once the halosodalites were synthesised using the hydrothermal method as outlined in the experimental procedure, the next step was to exchange the sodium ions with silver ions. The ion exchange was successfully carried out for the bromo and chlorosodalites using the method described in the experimental procedure and the following samples were produced successfully:

$Na_{8-x}Ag_x[SiAlO_4]_6Br_2$ with x = 2, 4, 6 and 8

$Na_{8-x}Ag_x[SiAlO_4]_6Cl_2$ with x = 2, 4, 6 and 8

Although the ion exchange for the bromo- and chlorosodalites was successful, ion exchange for the iodosodalite was unsuccessful. Each time the silver nitrate solution was added to the iodosodalite the sample turned yellow and when left for 24 hrs so that the ion exchange could occur, a dark brown/black solution was produced. After analysis the XRD patterns showed no signs of sodalite. The dark colour suggests that the silver in the solution was reduced to produce

particles of silver, silver oxide or silver hydroxides, which would all lead to dark materials. The iodide could have reduced the silver. The difference could be due to the I^- being more easily oxidized to I_2, which is also dark than Br^- or Cl^-. Due to time constraints in the project I could not pursue this further to find out what the problem was. Further analysis was not done and after several attempts this was abandoned.

5.3. Analysis

Both sodium and silver halosodalites were characterised by powder diffraction and the sodium contents determined using flame photometry. As noted earlier, all of the X-ray diffraction patterns of the sodium sodalites were consistent with the expected sodalite structure based on matching to the PDF database. The ion exchange for the bromo- and chlorosodalites was carried out successfully and samples checked by XRD to ensure they remained crystalline and changes in relative intensities of the peaks are indicative of changes in the number and type of cations. The compositions are given in Table 6; in all cases the silver content is based on eight cations per formula unit and the assumption that sodium and silver are the only cations present. Extreme selectivity towards silver over sodium was observed during ion exchange regardless of the temperature being used as can be seen from the XRD patterns in the appendix and from the sodium and silver content values from the flame photometry. Acar and Culfaz (2003) carried out a similar experiment on Chlorosodalites and also observed the same result.

Table 6: Sodalite composition – sodium and silver content

Nominal composition	Sodalite composition produced
$Na_8[SiAlO_4]_6Br_2$	$Na_{7.2}[SiAlO_4]_6Br_2$
$Na_6Ag_2[SiAlO_4]_6Br_2$	$Na_{5.7}\ Ag_{2.3}[SiAlO_4]_6Br_2$
$Na_4Ag_4[SiAlO_4]_6Br_2$	$Na_4Ag_4[SiAlO_4]_6Br_2$
$Na_2Ag_6[SiAlO_4]_6Br_2$	$Na_{2.7}\ Ag_{5.3}[SiAlO_4]_6Br_2$
$Na_0Ag_8[SiAlO_4]_6Br_2$	$Na_{0.3}\ Ag_{7.7}\ [SiAlO_4]_6Br_2$
$Na_8[SiAlO_4]_6Cl_2$	$Na_{7.2}[SiAlO_4]_6Cl_2$
$Na_6Ag_2[SiAlO_4]_6Cl_2$	$Na_{5.7}Ag_{2.3}[SiAlO_4]_6Cl_2$
$Na_4Ag_4[SiAlO_4]_6Cl_2$	$Na_{3.9}Ag_{4.1}[SiAlO_4]_6Cl_2$
$Na_2Ag_6[SiAlO_4]_6Cl_2$	$Na_{2.2}Ag_{5.8}[SiAlO_4]_6Cl_2$
$Na_0Ag_8[SiAlO_4]_6Cl_2$	$Na_{0.6}Ag_{7.4}[SiAlO_4]_6Cl_2$

5.4. Effect of Ion exchange on the Structures of the Halosodalites

5.4a. Ion exchange on Bromosodalite

Ion exchange on bromosodalite was carried out as outlined in the experimental section. The samples were then analysed and the atomic coordinates and thermal factor values are shown in Table 7. The Rietveld fit plots for each sample are shown in Figures 7-11. No attempt was made to vary the Na/Ag ratios; these were fixed at the values from the analysis and as the metal thermal parameters are reasonable and consistent, this appears to be a good assumption.

Tables 7a & b: Atomic coordinates and thermal factors values for ion exchanged bromosodalites.

Sodalite	*a* / Å	M	O		
		x	*x*	*y*	*z*
$Na_{7.2}[SiAlO_4]_6Br_2$	8.92601 (3)	0.187422 (2)	0.140608 (3)	0.443530 (9)	0.152567 (3)
$Na_{5.7}Ag_{2.3}[SiAlO_4]_6Br_2$	8.92134 (4)	0.176727 (1)	0.140672 (2)	0.445956 (2)	0.151873 (1)
$Na_4Ag_4[SiAlO_4]_6Br_2$	8.91437 (4)	0.170074 (5)	0.137652 (3)	0.449680 (6)	0.150665 (4)
$Na_{2.7}Ag_{5.3}[SiAlO_4]_6Br_2$	8.91402 (4)	0.172968 (1)	0.141994 (2)	0.446707 (6)	0.156683 (1)
$Na_{0.3}Ag_{7.7}[SiAlO_4]_6Br_2$	8.91532 (5)	0.173216 (1)	0.134360 (1)	0.446899 (1)	0.152689 (1)

Sodalite	M	O	Al	Si	X	CHI*2
	U_{iso} *x100*	U_{iso} *x100*	U_{iso} *x100*	U_{iso} *x100*	U_{iso} *x100*	
$Na_{7.2}[SiAlO_4]_6Br_2$	5.185 (2)	3.122 (1)	4.847 (1)	3.373 (1)	9.672 (1)	1.471
$Na_{5.7}Ag_{2.3}[SiAlO_4]_6Br_2$	6.318 (1)	3.537 (3)	4.107 (1)	3.411 (1)	9.463 (1)	1.224
$Na_4Ag_4[SiAlO_4]_6Br_2$	7.448 (3)	3.318 (4)	4.931 (1)	3.438 (1)	8.162 (3)	1.224
$Na_{2.7}Ag_{5.3}[SiAlO_4]_6Br_2$	8.281 (1)	4.400 (2)	3.999 (1)	2.143 (1)	8.275 (1)	1.276
$Na_{0.3}Ag_{7.7}[SiAlO_4]_6Br_2$	8.699 (1)	0.892 (2)	1.634 (1)	0.884 (1)	5.535 (1)	1.288

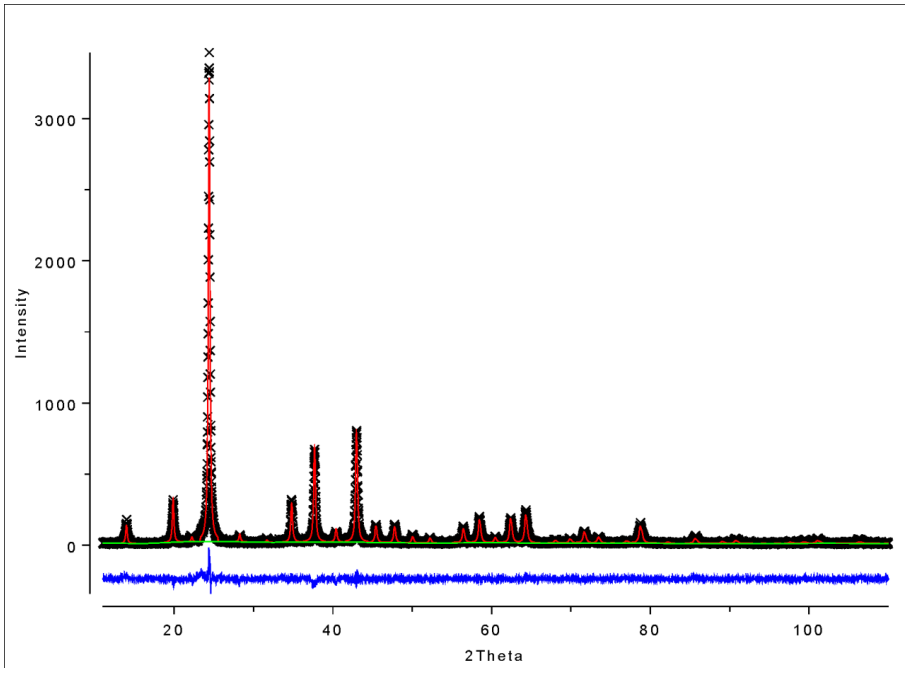

Figure 7: Rietveld fit for $Na_8[SiAlO_4]_6Br_2$ where the observed points are crosses. The calculated pattern is the red line and the difference curve is the blue line.

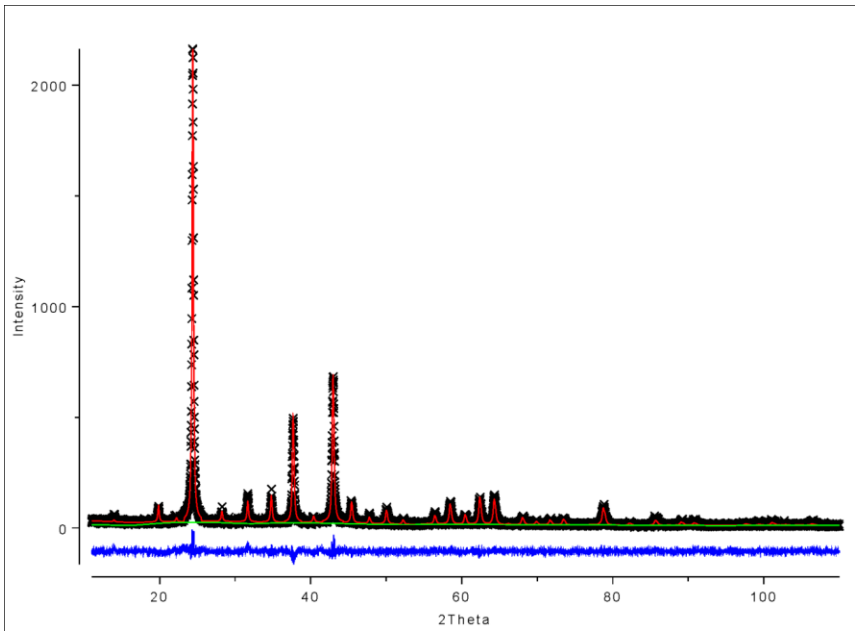

Figure 8: Rietveld fit plot for $Na_6Ag_2[SiAlO_4]_6Br_2$ where the observed points are crosses. The calculated pattern is the red line and the difference curve is the blue line.

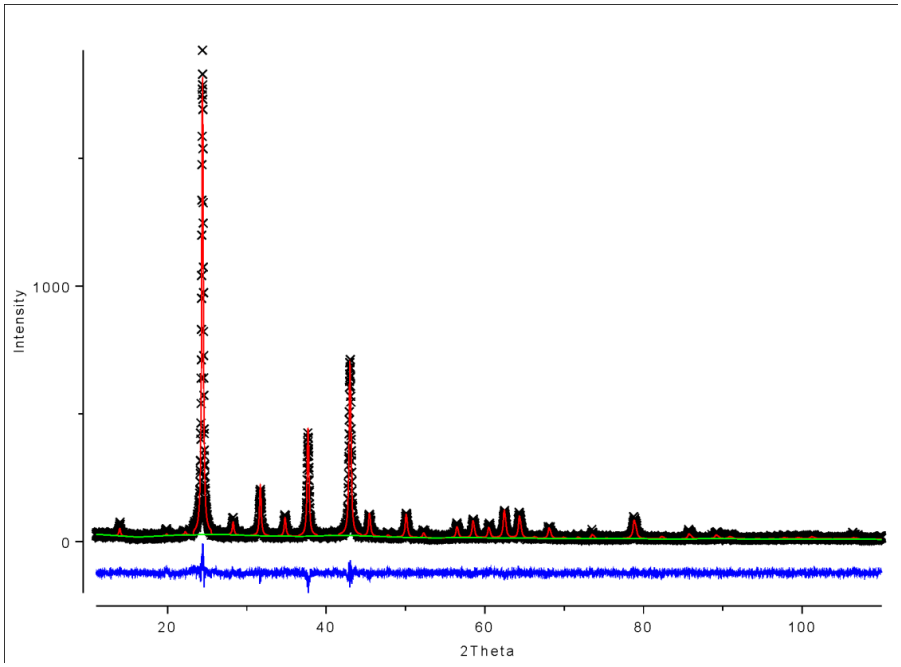

Figure 9: Rietveld fit plot for $Na_4Ag_4[SiAlO_4]_6Br_2$ where the observed points are crosses. The calculated pattern is the red line and the difference curve is the blue line.

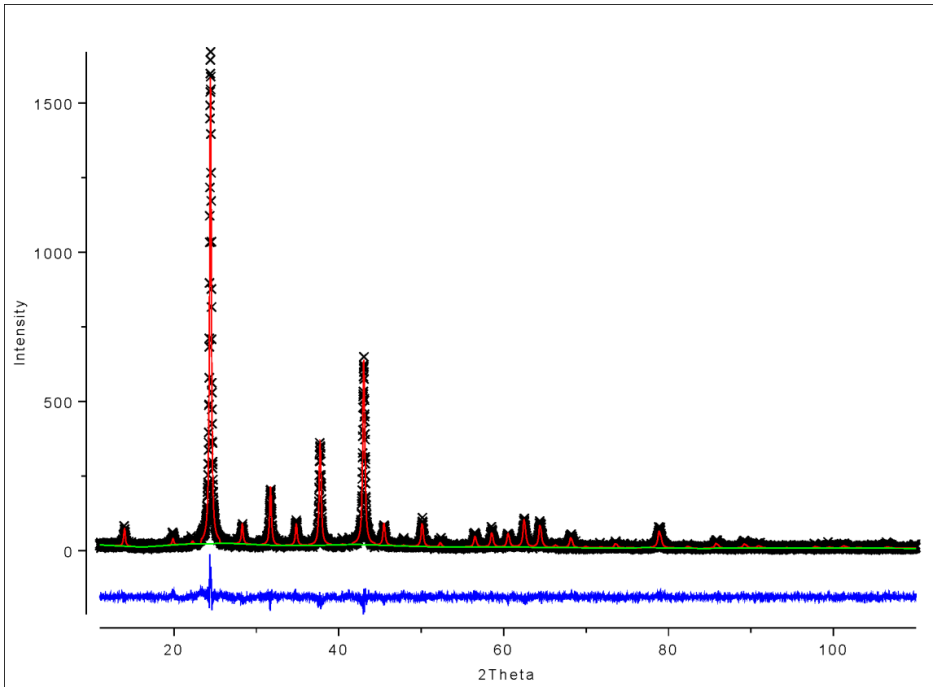

Figure 10: Rietveld fit plot for $Na_2Ag_6[SiAlO_4]_6Br_2$ where the observed points are crosses. The calculated pattern is the red line and the difference curve is the blue line.

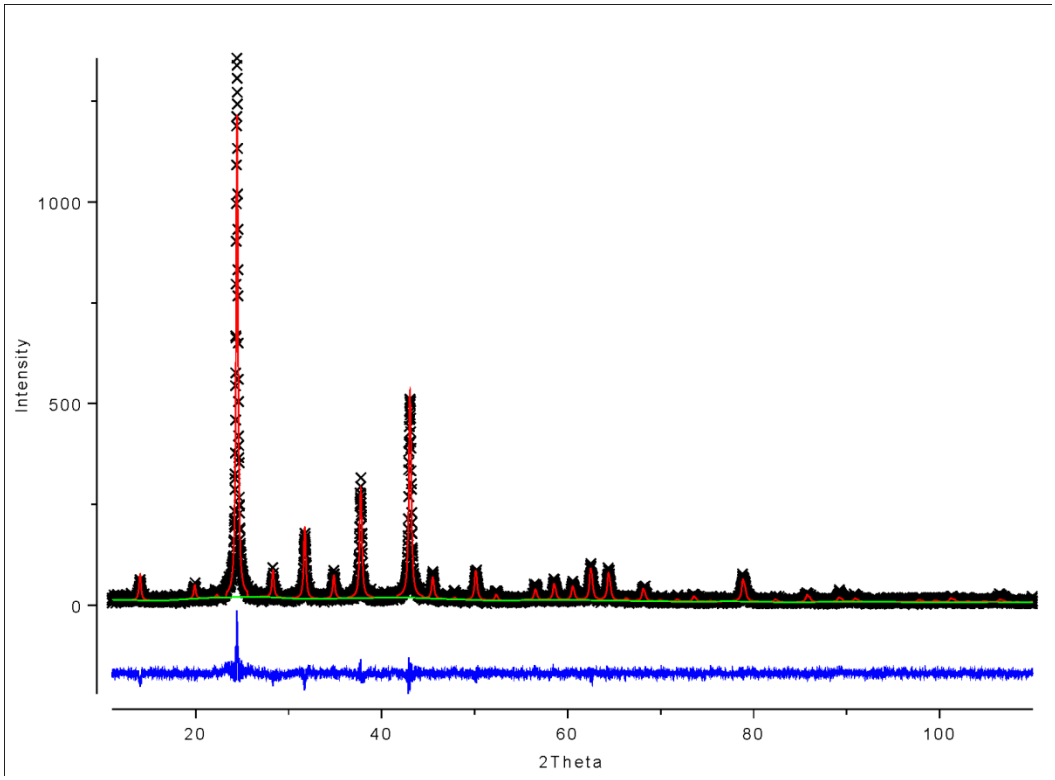

Figure 11: Rietveld fit plot for $Na_0Ag_8[SiAlO_4]_6Br_2$ where the observed points are crosses. The calculated pattern is the red line and the difference curve is the blue line.

As can be seen from the values in Table 8 and the graphs in Figures 12-16, respectively, as the fully loaded sodium cations are replaced by the silver cations there is a decrease in the unit cell size and M-X bond distance whereas there is an increase in the M-O bond. The changes in the Al-O and Si-O are relatively small after taking the ESD values into account and therefore are not very significant.

Table 8: Structural changes based on Rietveld refinements from room temperature data for the bromosodalites when the sodium cations are replaced by silver ions

Sodalite	Unit cell /Å	M-X bond /Å	M-O bond /Å	Al-O bond /Å	Si-O bond / Å
$Na_{7.2}[SiAlO_4]_6Br_2$	8.92601(3)	2.898(4)	2.345(4)	1.735(4)	1.608(5)
$Na_{5.7}Ag_{2.3}[SiAlO_4]_6Br_2$	8.92134(4)	2.731(4)	2.434(5)	1.738(8)	1.604(8)
$Na_4Ag_4[SiAlO_4]_6Br_2$	8.91437(4)	2.626(4)	2.515(8)	1.734(10)	1.587(10)
$Na_{2.7}Ag_{5.3}[SiAlO_4]_6Br_2$	8.91402(4)	2.618(2)	2.561(9)	1.732(12)	1.578(12)
$Na_{0.3}Ag_{7.7}[SiAlO_4]_6Br_2$	8.91532(5)	2.605(3)	2.571(9)	1.722(13)	1.553(13)

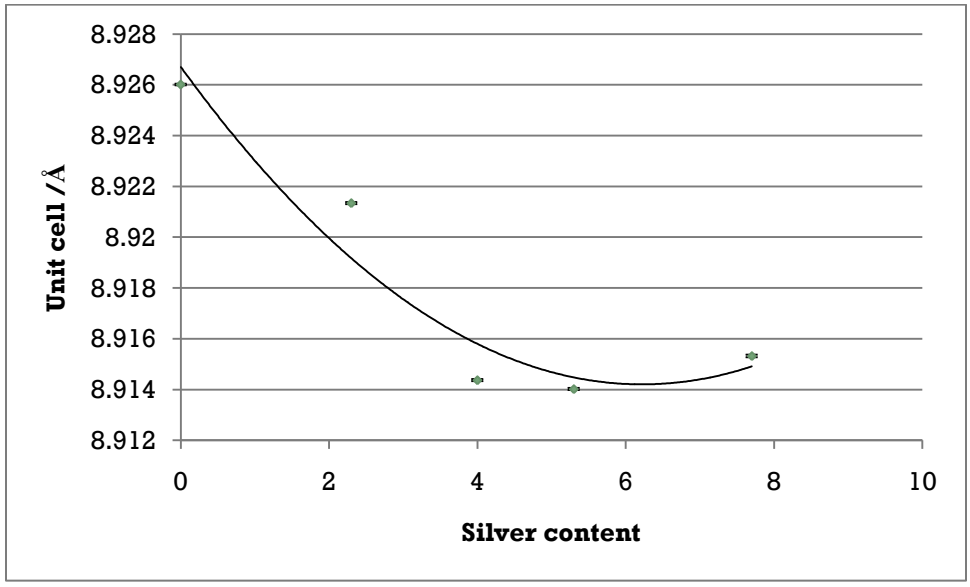

Figure 12: Graph showing change in unit cell as the silver content changes. Error bars represent 1 esd.

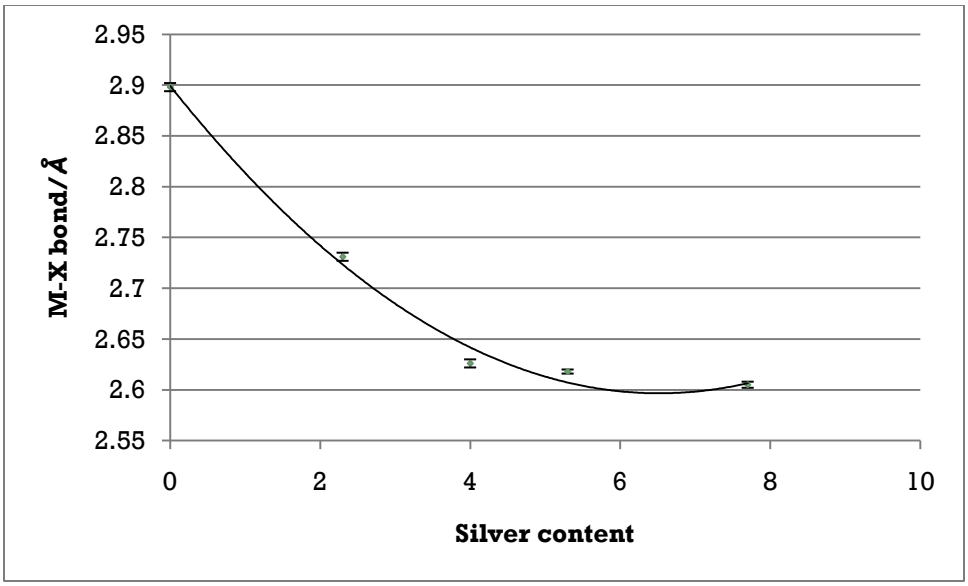

Fig 13: Graph showing changes in M-X bond length as the silver content increases. Error bars represent 1 esd.

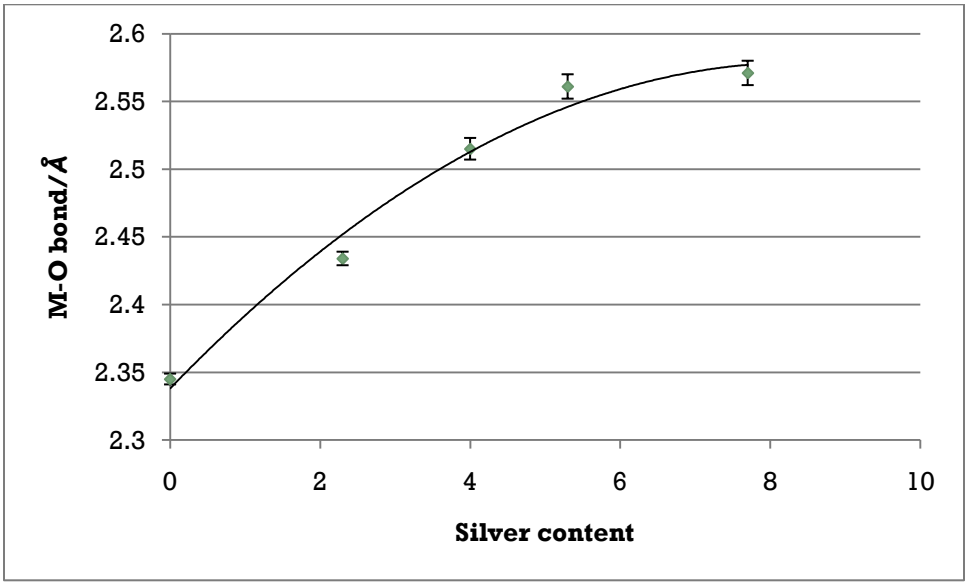

Fig 14: Graph showing changes in M-O bond length as the silver content increases. Error bars represent 1esd.

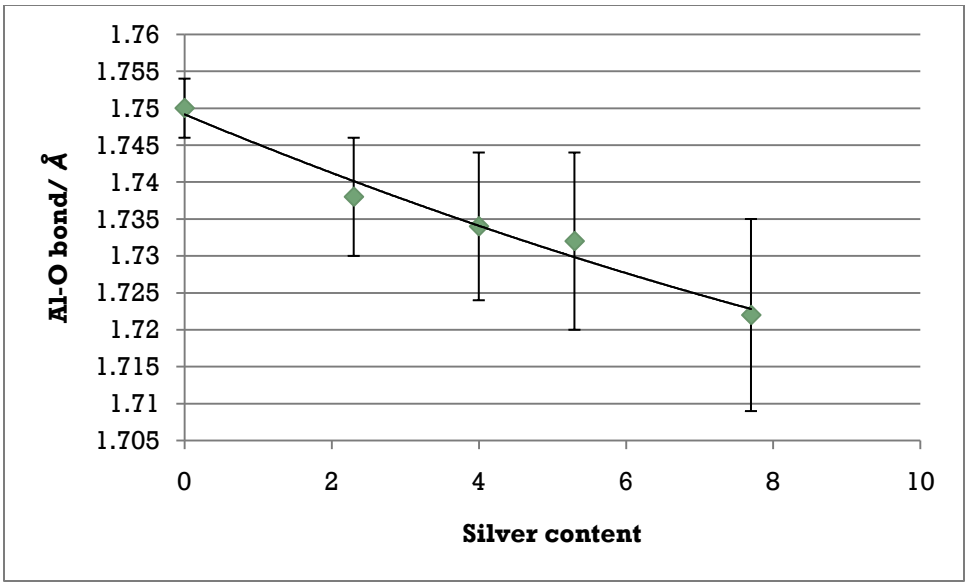

Fig 15: Graph showing changes in Al-O bond length as the silver content increases

Error bars represent 1esd.

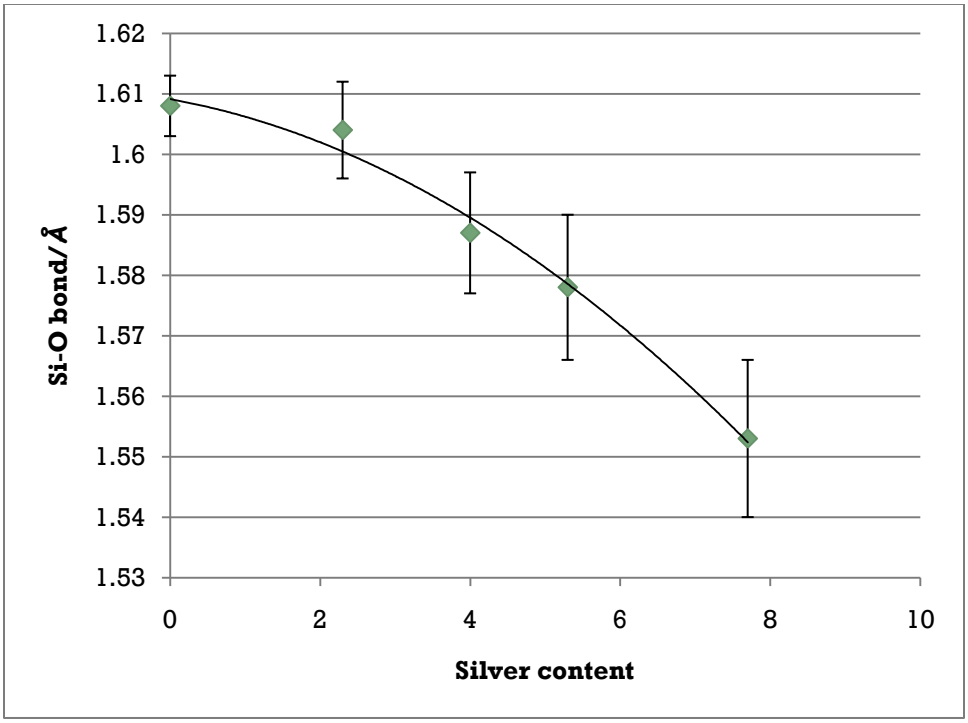

Fig 16: Graph showing changes in Si-O bond length as the silver content increases. Error bars represent 1 esd.

5.4b Ion exchange on Chlorosodalites

Ion exchange on bromosodalite was carried out as outlined in the experimental section. The samples were then analysed and the atomic coordinates and thermal factor values are shown in Table 9. The Rietveld fit plots for each sample are shown in Figures 17-21. No attempt was made to vary the Na/Ag ratios; these were fixed at the values from the analysis and as the metal thermal parameters are reasonable and consistent, this appears to be a good assumption.

Table 9: Atomic coordinates and thermal factor values for chlorosodalites when sodium is replaced by silver.

Sodalite	*a* / Å	M	O		
		x	*x*	*y*	*z*
$Na_{7.2}[SiAlO_4]_6Cl_2$	8.87965 (3)	0.178490(1)	0.141439 (2)	0.439844 (3)	0.150827 (1)
$Na_{5.7}Ag_{2.3}[SiAlO_4]_6Cl_2$	8.87409 (4)	0.168649(1)	0.142286(1)	0.444855(1)	0.147289(1)
$Na_{3.9}Ag_{4.1}[SiAlO_4]_6Cl_2$	8.87543 (5)	0.170083(1)	0.140009(1)	0.440072(2)	0.148847(2)
$Na_{2.2}Ag_{5.8}[SiAlO_4]_6Cl_2$	8.8297 (4)	0.165769(10)	0.144661 (7)	0.438508(1)	0.149302(1)
$Na_{0.6}Ag_{7.4}[SiAlO_4]_6Cl_2$	8.887969(5)	0.164247(36)	0.136913 (3)	0.439771 (16)	0.150429 (3)

Sodalite	M	O	Al	Si	X	CHI*2
	U_{iso} *x100*	U_{iso} *x100*	U_{iso} *x100*	U_{iso} *x100*	U_{iso} *x100*	
$Na_{7.2}[SiAlO_4]_6Cl_2$	5.230 (1)	3.467 (1)	3.254 (1)	4.610 (1)	6.983 (1)	1.38
$Na_{5.7}Ag_{2.3}[SiAlO_4]_6Cl_2$	6.056 (1)	3.805 (1)	4.562 (1)	3.639 (2)	7.637 (1)	1.197
$Na_{3.9}Ag_{4.1}[SiAlO_4]_6Cl_2$	6.905 (1)	4.722 (1)	6.337 (1)	2.959 (1)	12.645 (2)	1.346
$Na_{2.2}Ag_{5.8}[SiAlO_4]_6Cl_2$	6.747 (2)	4.356 (1)	4.563 (1)	2.683 (2)	7.034 (2)	1.347
$Na_{0.6}Ag_{7.4}[SiAlO_4]_6Cl_2$	6.648 (22)	0.074 (33)	0.956 (5)	0.297 (5)	1.484 (19)	1.233

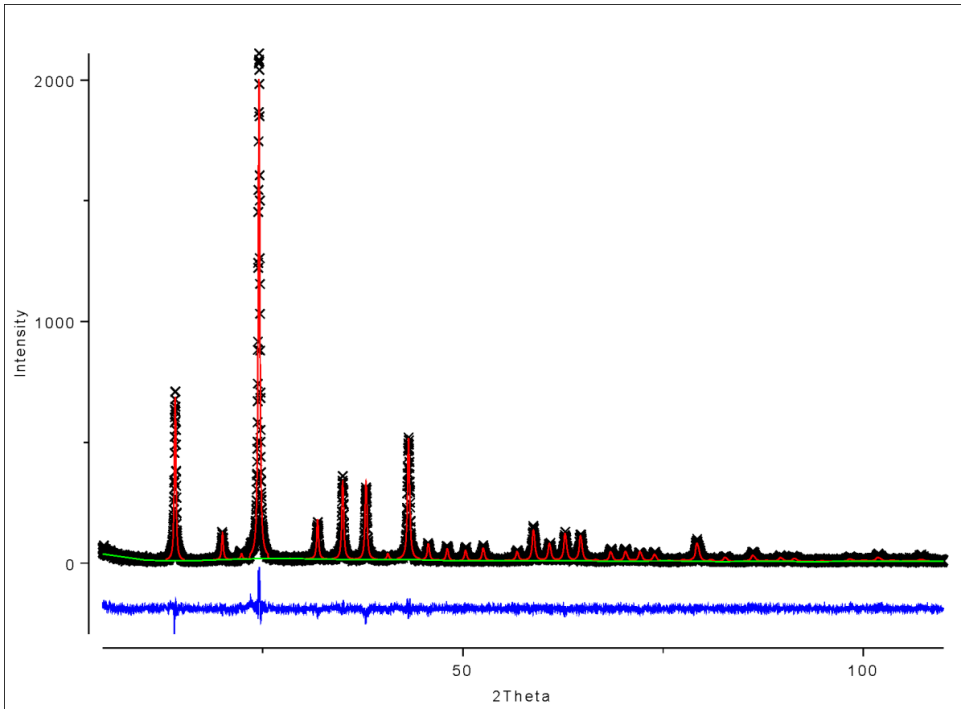

Figure 17: Rietveld fit plot for $Na_8[SiAlO_4]_6Cl_2$ where the observed points are crosses. The calculated pattern is the red line and the difference curve is the blue line.

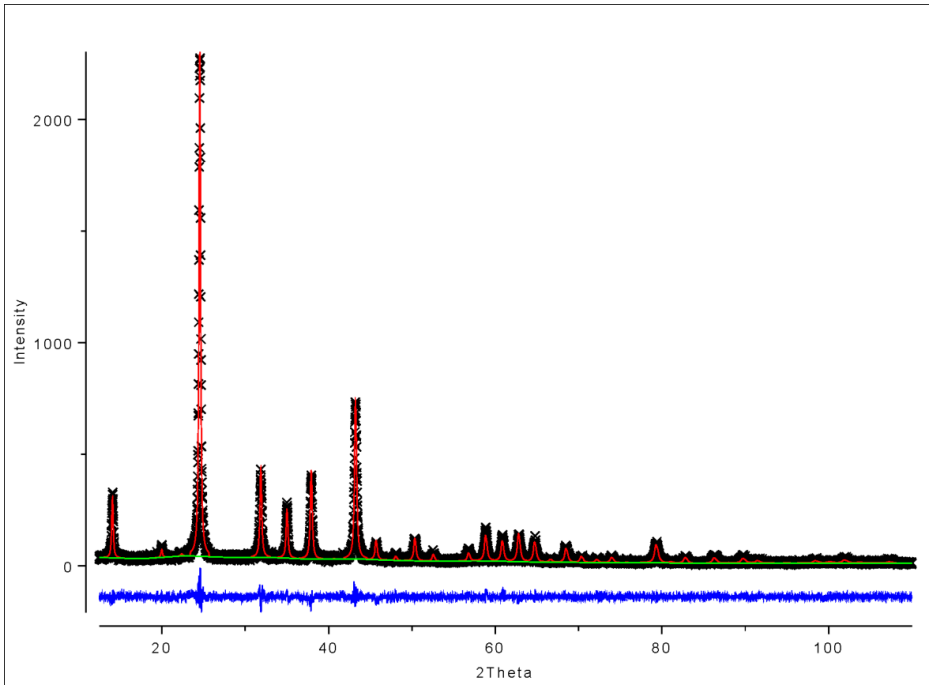

Figure 18: Rietveld fit plot for $Na_6Ag_2[SiAlO_4]_6Cl_2$ where the observed points are crosses. The calculated pattern is the red line and the difference curve is the blue line.

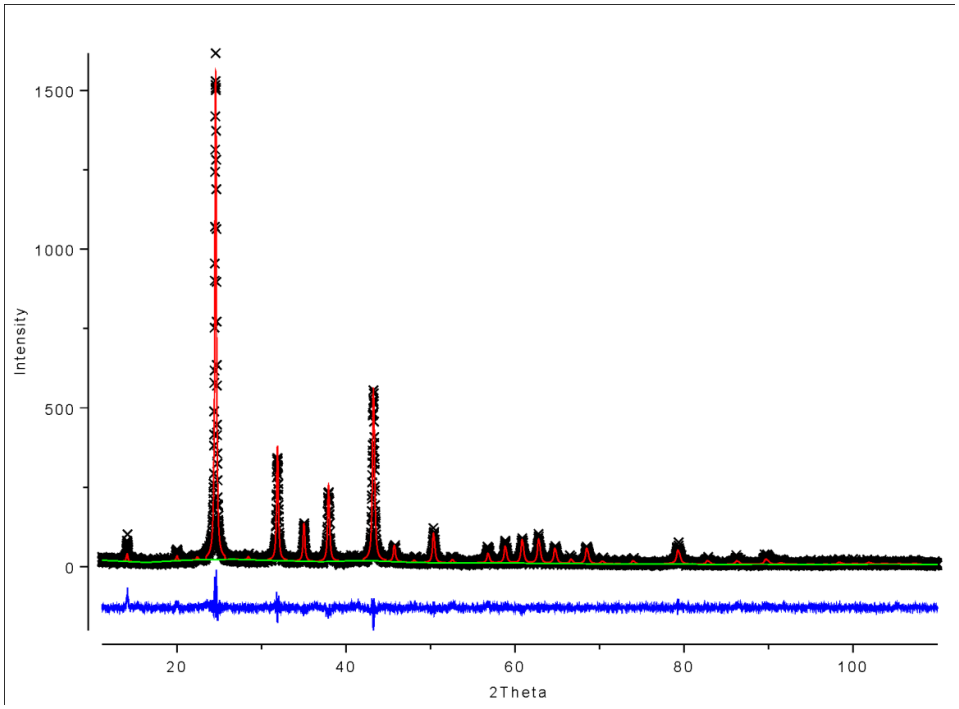

Figure 19: Rietveld fit plot for $Na_4Ag_4[SiAlO_4]_6Cl_2$ where the observed points are crosses. The calculated pattern is the red line and the difference curve is the blue line.

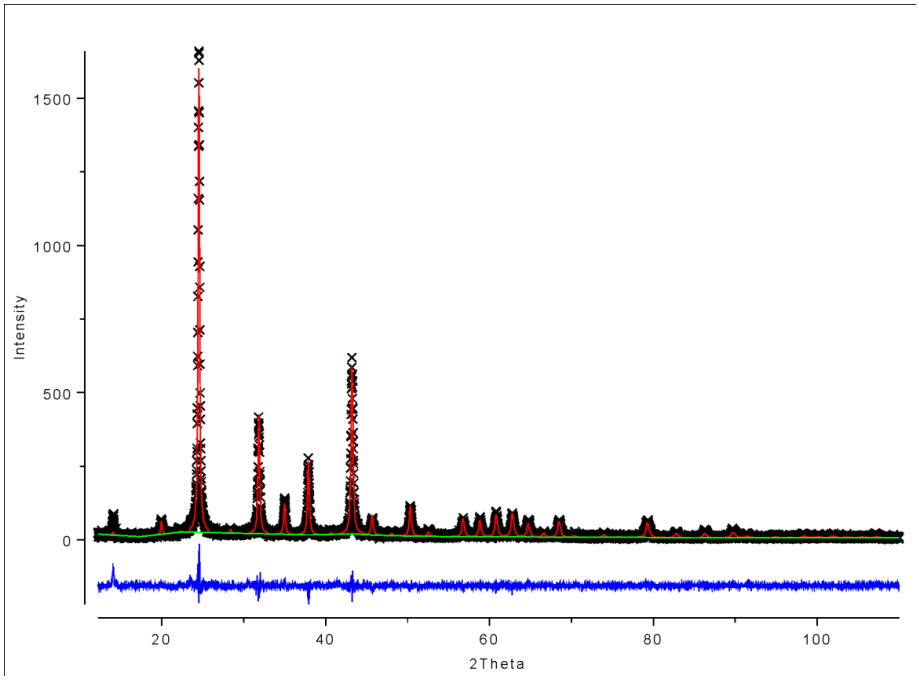

Figure 20: Rietveld fit plot for $Na_2Ag_6[SiAlO_4]_6Cl_2$ where the observed points are crosses. The calculated pattern is the red line and the difference curve is the blue line.

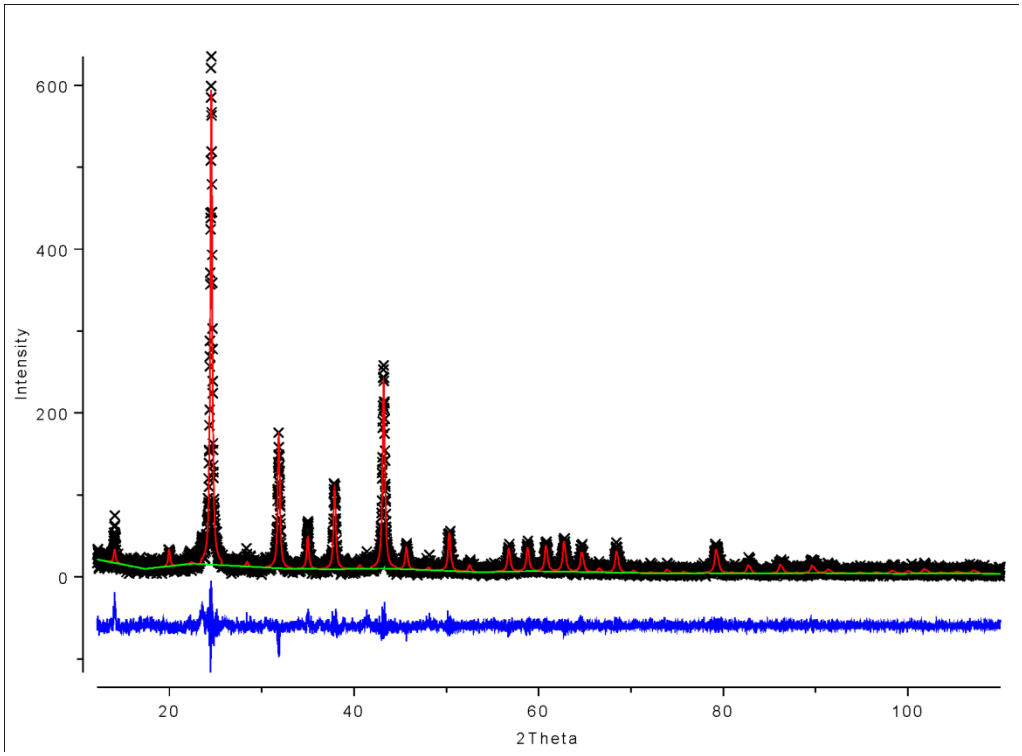

Figure 21: Rietveld fit plot for $Na_0Ag_8[SiAlO_4]_6Cl_2$ where the observed points are crosses. The calculated pattern is the red line and the difference curve is the blue line.

For the chlorosodalites similar patterns were observed for structural changes as for the bromosodalites, as can be seen from Table 10 and Figures 22-26. As the sodium cations are replaced by the silver cations, again there is a decrease in the unit cell size and M-X bond whereas there is an increase in the M-O bond. The decrease in M-X distance and unit cell size show that the silver ions cause a contraction within the sodalite when replacing the sodium ions. Again, within errors, the Si-O and Al-O bonds are not affected.

Table 10: The structural changes at room temperature on the chlorosodalites when the sodium cations are replaced by silver ions

Sodalite	Unit cell /Å	M-X bond /Å	M-O bond /Å	Al-O bond /Å	Si-O bond / Å
$Na_{7.2}[SiAlO_4]_6Cl_2$	8.87965(3)	2.745(4)	2.357(4)	1.735(5)	1.624(5)
$Na_{5.7}Ag_{2.3}[SiAlO_4]_6Cl_2$	8.87409(3)	2.615(4)	2.417(5)	1.727(9)	1.632(9)
$Na_{3.9}Ag_{4.1}[SiAlO_4]_6Cl_2$	8.87343(4)	2.592(4)	2.418(9)	1.711(11)	1.623(10)
$Na_{2.2}Ag_{5.8}[SiAlO_4]_6Br_2$	8.87297(4)	2.548(4)	2.43(9)	1.692(23)	1.656(23)
$Na_{0.6}Ag_{7.4}[SiAlO_4]_6Br_2$	8.87169 (5)	2.513(5)	2.445(10)	1.683(24)	1.661(24)

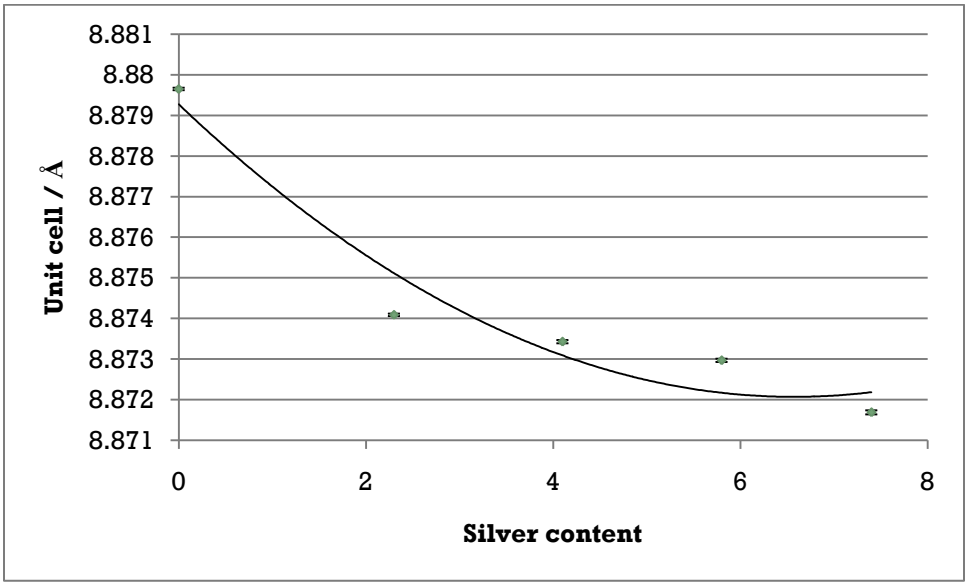

Fig 22: Graph showing changes in Unit cell size as the silver content increases. Error bars represent 1 esd.

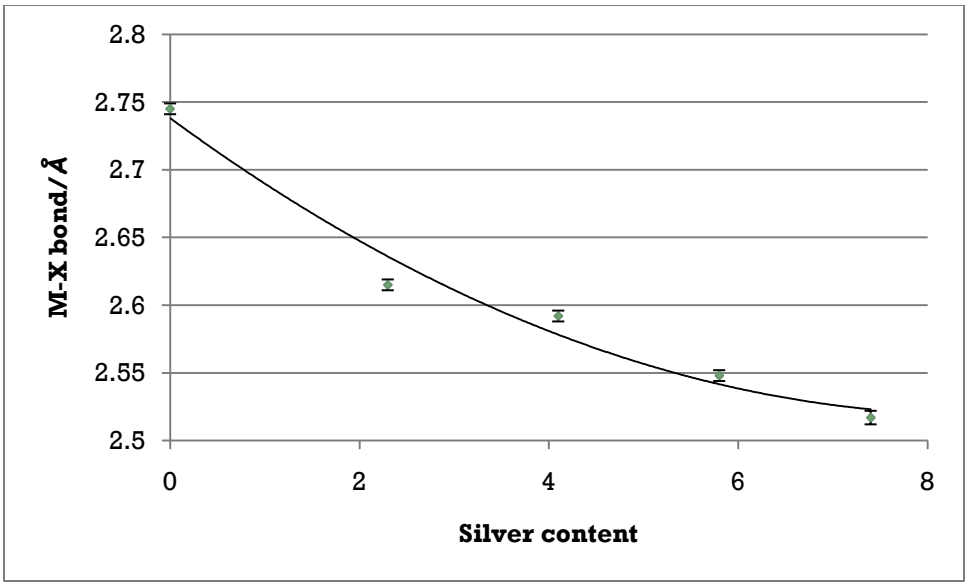

Fig 23: Graph showing changes in M-X bond length as the silver content increases. Error bars represent 1 esd.

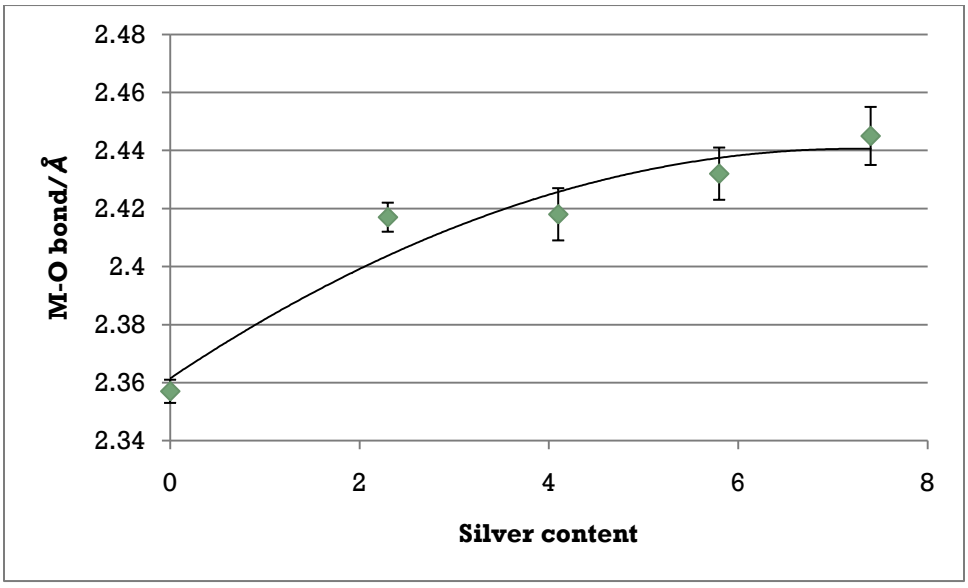

Fig 24: Graph showing changes in M-O bond length as the silver content increases. Error bars represent 1 esd.

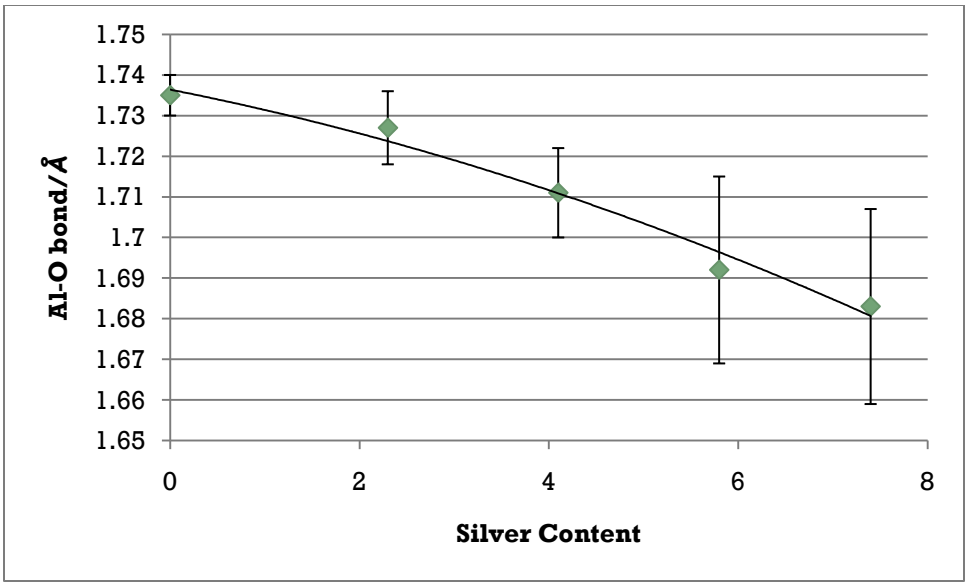

Fig 25: Graph showing changes in Al-O bond length as the silver content increases. Error bars represent 1esd.

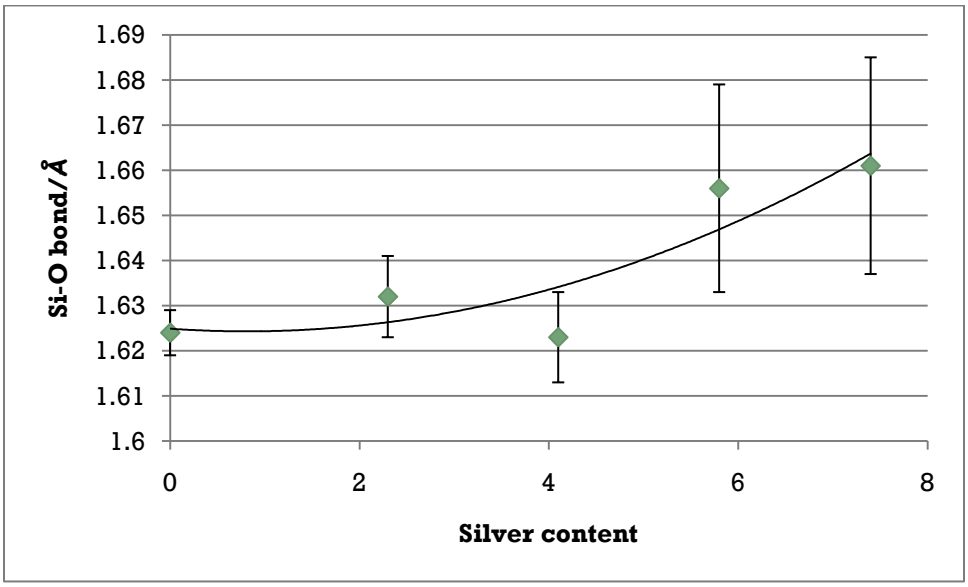

Fig 26: Graph showing changes in Si-O bond length as the silver content increases. Error bars represent 1 esd.

Iodosodalite

Ion exchange was not possible for the Iodosodalite. Table 11 and Figure 27 show the atomic coordinate and thermal factor values and Rietveld plot respectively at 27°C.

Tables 11a and b: Table of atomic coordinates and thermal factors for sodium iodosodalite.

Sodalite	*a* / Å	M	O		
		x	*x*	*y*	*z*
$Na_8[SiAlO_4]_6I_2$	8.99726(4)	3.859 (1)	0.141827 (2)	0.448432 (1)	0.158158 (1)

Sodalite	M	O	Al	Si	X	CHI*2
	U_{iso} *x100*	U_{iso} *x100*	U_{iso} *x100*	U_{iso} *x100*	U_{iso} *x100*	
$Na_8[SiAlO_4]_6I_2$	0.199174 (1)	2.374 (1)	2.672 (1)	1.560 (1)	8.709 (2)	1.209

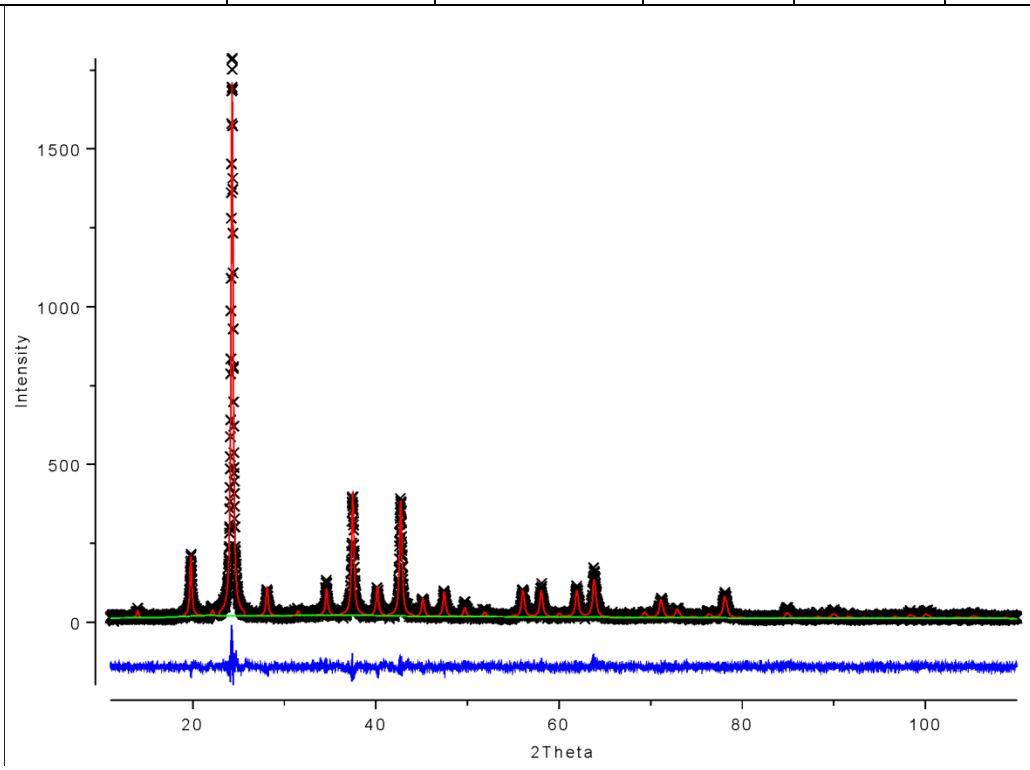

Figure 27: Rietvield fit plot for $Na_8[SiAlO_4]_6I_2$ where the observed points are crosses. The calculated pattern is the red line and the difference curve is the blue line.

5.4c Discussion of the Changes

Similar results were observed with both systems as the silver content increased; there was a decrease in the unit cell and M-X bond, whereas the M-O bond length increased. A picture of the sodalite cage can be seen in Figure 28. According to Hassan and Grundy, 1984, there should be no change in the Si-O and Al-O bonds as the cations or anion change and the size of the unit cell alters due to tilts of the SiO_4 and AlO_4 tetrahedra to accommodate the O-M-X bonds. Analyzing my data I would agree with Hassan and Grundy (1984); taking the ESD values into account there is a relatively small change in the Al-O and Si-O bonds for both halosodalites series.

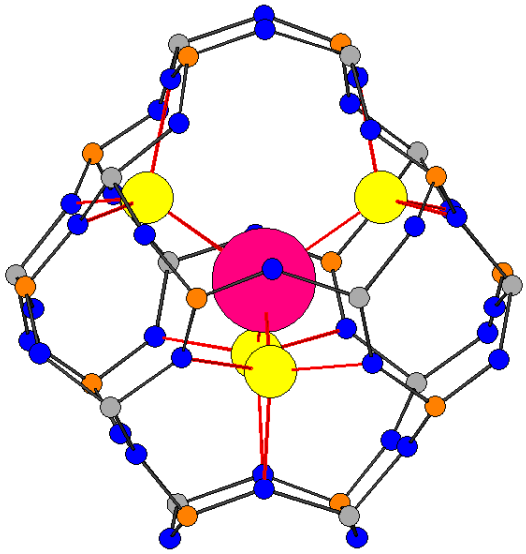

Figure 28: Picture of a Sodalite cage. The red sphere is the anion, yellow spheres Na/Ag, blue spheres O atoms, brown Si atoms and grey Al atoms.

For the sodium end members, the Na-X and Na-O bonding should be effectively purely ionic. As shown in Table 12a, the bond lengths match very well to those determined using the effective ionic radii of Shannon (1976).

Table 12a: Observed and Calculated Na-X and Na-O bond lengths (Å)

Bond	**This work**	**Shannon (1976)**
Na-X (Br)	2.90	2.96
Na-O (Br)	2.35	2.36
Na-X (Cl)	2.75	2.81
Na-O (Cl)	2.36	2.36

Factors which affect radii additivity are polyhedral distortion, partial occupancy of cation sites, covalence and metallic character. Taking into account that the effective ionic radius of Ag^{+} is 1.00Å and Na^{+} is 0.99Å, the decrease in M-X bond length as silver substitutes for sodium for both bromo- and chlorosodalites suggests that this deviation is due to increased covalent character. There is a change from ionic bonding to covalent bonding which strongly shortens the M-X bond as the electronegativity difference of X and M decreases. Based on the Pauling scale, the differences are 1.1 (Ag) vs. 2.1 (Na) for M-Cl and 0.9 (Ag) vs. 1.9 (Na) for M-Br. For the end members the decrease in the M-Cl bond is 8.4% whereas that for the M-Br bond is 10.1%, consistent with the electronegativity differences. As the M-X bond lengths decrease, the M-O bonds increase. This is probably due to two factors; the first is reduced ionic M-O bonding as a greater fraction of the effective nuclear charge of Ag is used in M-X bonding, and some resistance to moving the oxygen atoms as they are relatively rigidly held by the aluminosilicate

framework. No structural studies have been carried out on fully loaded and partially loaded silver halosodalites, which makes it difficult to compare data. This is the first time someone is looking at partially loaded silver halosodalites and carrying out high temperature studies on these.

Table 12b shows Ag-Br, Ag-Cl and Ag-I bond lengths from other zeolites and inorganic structures for comparison against the results from this thesis.

Bond	This work	Stein (1989)	Takahashi (1987), Swanson (1921), Wright (1934), respectively
Ag-Br	2.605 (3)	2.671 (2)	2.888 (2)
Ag-Cl	2.5135 (5)	2.537 (2)	2.774 (2)
Ag-I	-	2.779 (2)	2.830 (2)

My bond lengths match well to Stein's et al (1989) bond lengths of the halosodalites whereas they are slightly lower than Takahashi (1987), Swanson (1921) and Wright's (1934) bond lengths, which relate to the simple salts AgCl, AgBr and AgI, respectively, in the alpha form.

5.5 High temperature studies of various sodalites

High temperature X-ray powder diffraction studies were carried out on both the halosodalites and the ion exchanged halosodalites. Studies were carried out at room pressure and the sodalites were heated from 27^{o}C to 847^{o}C; above that temperature some systems showed colour changes that indicated decomposition. The structural behaviour was determined using Rietveld refinement. The samples were heated at a rate of 9^{o}C/min and X-ray patterns were collected at intervals of about 25^{o}C. High temperatures studies were carried out to see the effect of thermal expansion.

5.5a High Temperature studies of Bromosodalite

A high temperature study was carried out on the bromosodalite and the atomic coordinate and thermal factor values are shown in Table 13.

Table 13: Atomic coordinate and thermal factor values for bromosodalite at various temperatures

Temp	*a* / Å	M		O				Al	Si	X	CHI*2
		x	U_{iso} *x100*	*x*	*y*	*z*	U_{iso} *x100*	U_{iso} *x100*	U_{iso} *x100*	U_{iso} *x100*	
27	8.92601(3)	0.187422 (2)	5.185 (2)	0.140608 (3)	0.443530 (9)	0.152567 (3)	3.122 (1)	4.847 (1)	3.373 (1)	8.724 (1)	1.471
122	8.93714(4)	0.189111(2)	5.491(2)	0.140059 (2)	0.445590 (5)	0.153349 (2)	3.053 (2)	4.127(2)	3.829(2)	9.231 (1)	1.469
222	8.95348(4)	0.191017(2)	6.532 (1)	0.139596(3)	0.448834 (2)	0.151994 (1)	3.070 (2)	4.824 (2)	2.559 (1)	10.563 (2)	1.445
322	8.97001(5)	0.193894(3)	6.576 (2)	0.136885(4)	0.451066 (3)	0.152323 (2)	2.949 (3)	4.176 (2)	2.631 (1)	12.276 (1)	1.426
422	8.98807(5)	0.196347 (2)	7.063 (1)	0.13880 (1)	0.454736 (1)	0.153990 (1)	3.537 (2)	4.662 (1)	2.892 (1)	14.094 (1)	1.292
522	9.00522(6)	0.199292 (1)	7.393 (1)	0.134761 (1)	0.456109 (1)	0.153741 (2)	3.206 (4)	4.117 (1)	2.998 (1)	15.464 (1)	1.311
622	9.02348(8)	0.201780 (1)	8.413 (1)	0.134586 (5)	0.459309 (1)	0.151922 (6)	3.380 (2)	4.370 (1)	2.719 (1)	17.858 (1)	1.294
722	9.05777(8)	0.203405 (1)	8.918 (1)	0.135430 (1)	0.462693 (1)	0.152863 (1)	3.412 (1)	4.549 (4)	2.943 (1)	21.191 (1)	1.16
822	9.0707(9)	0.207352 (1)	8.946 (3)	0.137266 (4)	0.467010 (1)	0.152892 (4)	4.180 (2)	4.483 (4)	3.064 (2)	24.991 (1)	1.162

As can be seen from Table 14 and figures 29-33 there is an increase in the size of the unit cell, Na-X, and Na-O bonds therefore suggesting that there is positive thermal expansion. No significant change was seen in the Al-O and Si-O bond length and the graphs for these show no correlation. Within a three esd error there are no consistent correlations in any of these with composition and temperature.

Table 14: The effect of high temperature on bromosodalite

Temperature / °C	Unit cell /Å	Na-X bond/Å	Na-O bond/Å	Al-O bond/Å	Si-O bond/Å
27	8.92601(3)	2.898(4)	2.345(4)	1.750(4)	1.608(5)
122	8.93714(4)	2.927(5)	2.356(4)	1.755(5)	1.597(5)
222	8.95348(4)	2.962(5)	2.38(5)	1.743(5)	1.594(5)
322	8.97001(5)	3.012(6)	2.392(5)	1.758(6)	1.571(6)
422	8.98807(5)	3.057(6)	2.410(5)	1.766(6)	1.558(6)
522	9.00522(6)	3.108(8)	2.420(7)	1.755(6)	1.543(6)
622	9.02348(8)	3.154(11)	2.443(9)	1.760(8)	1.547(7)
722	9.05777(8)	3.215(11)	2.468(10)	1.754(9)	1.557(8)
822	9.0707(9)	3.258(11)	2.489(10)	1.748(9)	1.555(9)

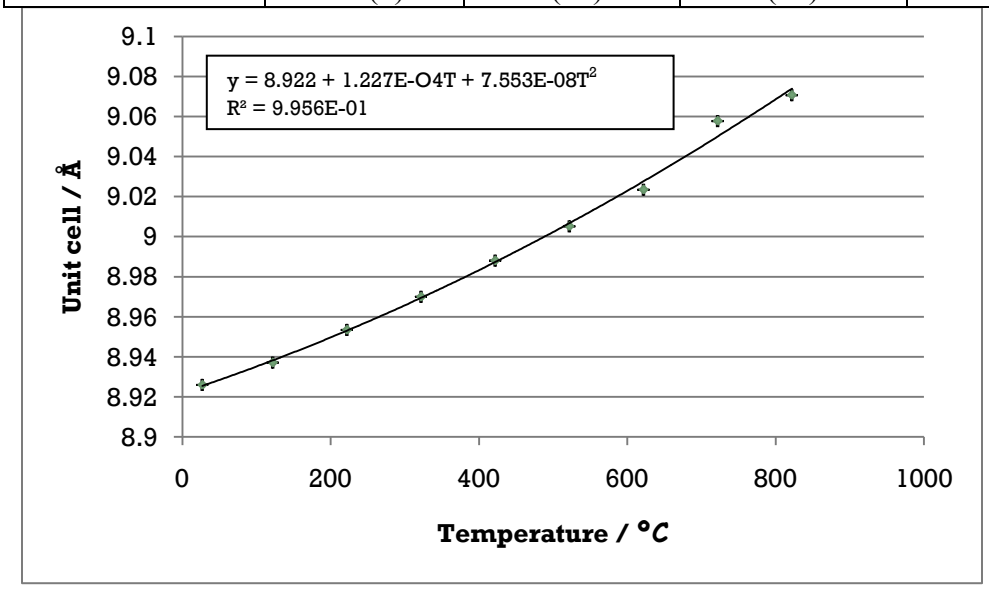

Fig 29: Graph showing change in unit cell size as temperature increases. Error bars represent 1 esd.

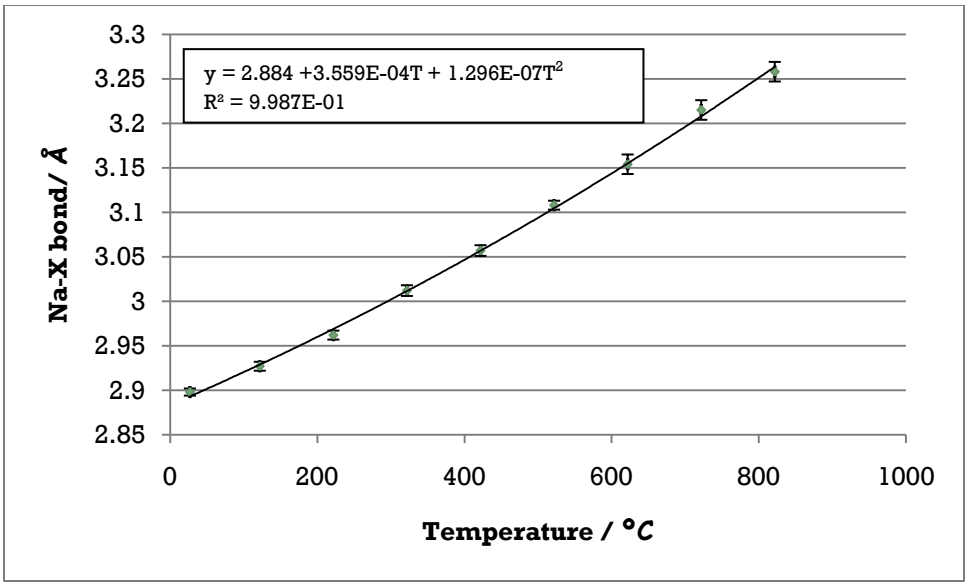

Fig 30: Graph showing change in Na-X bond length as temperature increases. Error bars represent 1 esd.

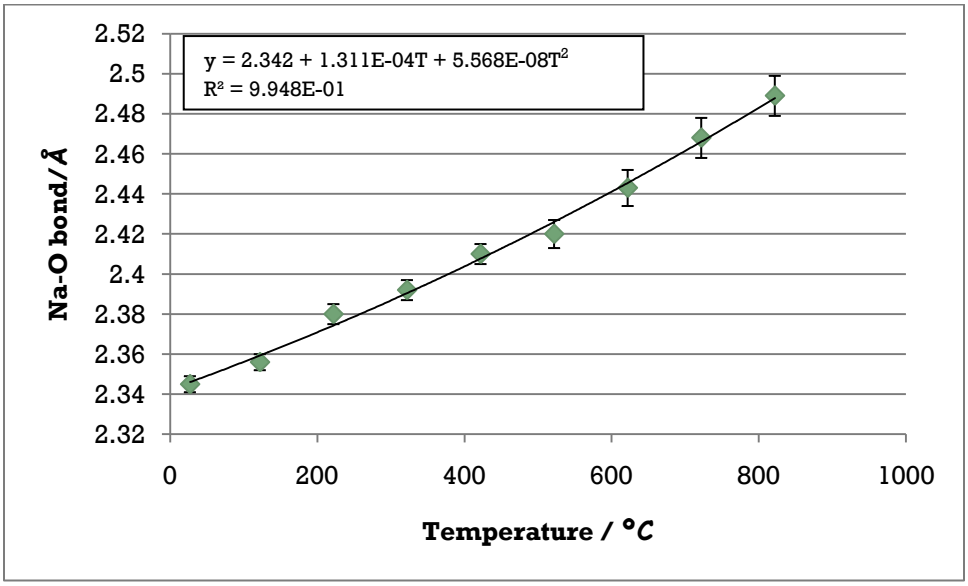

Fig 31: Graph showing change in Na-O bond length as temperature increases. Error bars represent 1 esd.

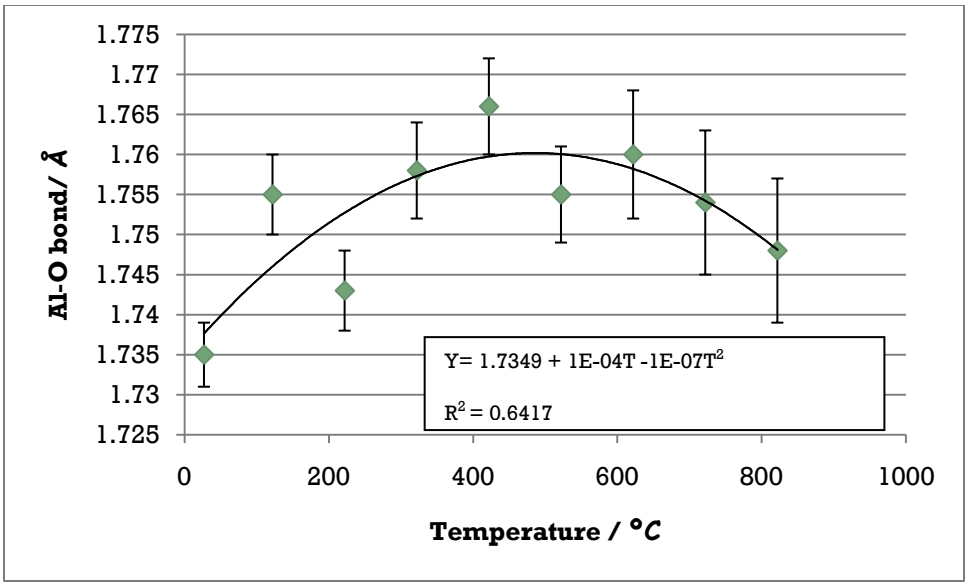

Fig 32: Graph showing change in Al-O bond length as temperature increases. Error bars represent 1 esd.

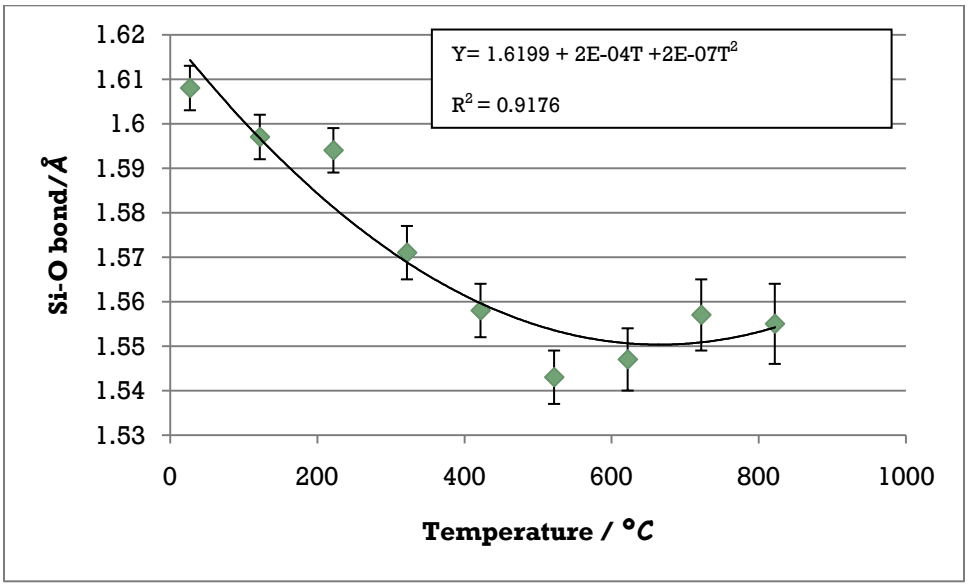

Fig 33: Graph showing change in Si-O bond length as temperature increases. Error bars represent 1 esd.

5.5b High temperature studies of Chlorosodalite

High temperature study was carried out on the chlorosodalite and the atomic coordinate and thermal factor values are shown in Table 15.

Table 15: Atomic coordinate and thermal factor values for chlorosodalite at various temperatures

Temp	*a* / Å	M		O				Al	Si	X	CHI*2
		x	$U_{iso}x100$	*x*	*y*	*z*	$U_{iso}x100$	$U_{iso}x100$	$U_{iso}x100$	$U_{iso}x100$	
27	8.87965(3)	0.178490 (1)	5.230 (1)	0.141439 (2)	0.439844 (3)	0.150827 (1)	3.467 (1)	3.254 (1)	4.610 (1)	6.983 (1)	1.388
122	8.88984(4)	0.180184 (1)	5.453 (1)	0.138466 (3)	0.439672 (2)	0.151295 (1)	3.703 (1)	3.518 (1)	4.163 (1)	7.531 (1)	1.36
222	8.90421(4)	0.180983 (2)	6.638 (7)	0.140288 (3)	0.441537 (8)	0.153043 (11)	3.694 (11)	4.693 (2)	4.645 (1)	9.345 (2)	1.427
322	8.92126(5)	0.183562 (1)	7.358 (1)	0.140942 (1)	0.444006 (1)	0.151873 (1)	4.597 (1)	5.949 (1)	3.909 (1)	10.815 (3)	1.43
422	8.93750(5)	0.185184 (2)	8.916 (1)	0.141096 (1)	0.444623 (5)	0.153072 (4)	4.705 (3)	5.638 (1)	3.803 (1)	11.706 (2)	1.358
522	8.95442(6)	0.188592 (1)	8.781 (1)	0.138927 (2)	0.448856 (2)	0.152083 (2)	4.886 (1)	5.504 (1)	3.515 (1)	14.522 (1)	1.345
622	8.96874(6)	0.187270 (1)	9.801 (1)	0.141275 (1)	0.451107 (1)	0.154302 (1)	4.304 (1)	4.995 (1)	3.321 (1)	15.521 (2)	1.309
722	8.98908(7)	0.190985 (1)	9.919 (1)	0.139193 (1)	0.452240 (1)	0.153770 (1)	4.329 (1)	4.950 (1)	3.656 (1)	18.939 (1)	1.293
822	9.00979(8)	0.192957 (1)	11.012 (1)	0.139365 (1)	0.455072 (1)	0.155685 (1)	4.241 (1)	3.617 (1)	2.823 (1)	23.511 (1)	1.26

The same pattern is observed with high temperature studies of chlorosodalite as was with bromosodalite, see Table 8 and Figures 20-22. There is an increase in the unit cell size, Na-Cl and Na-O bond length as the temperature increases thus indicating positive thermal expansion. Within a three esd error there are no consistent correlations in the of Al-O and Si-O bond lengths with composition and temperature.

Table 16: High temperature studies of chlorosodalite

Temperature / °C	Unit cell /Å	Na-X bond/Å	Na-O bond/Å	Al-O bond/Å	Si-O bond/Å
27	8.87965(3)	2.745(3)	2.357(3)	1.738(3)	1.569(3)
122	8.88984(4)	2.774(5)	2.351(4)	1.757(4)	1.581(4)
222	8.90421(4)	2.792(5)	2.361(4)	1.749(5)	1.592(5)
322	8.92126(5)	2.836(6)	2.371(4)	1.747(5)	1.589(5)
422	8.93750(5)	2.867(6)	2.369(5)	1.751(6)	1.608(6)
522	8.95442(6)	2.925(7)	2.395(6)	1.741(6)	1.612(6)
622	8.96874(6)	2.909(8)	2.421(6)	1.756(6)	1.605(6)
722	8.98908(7)	2.974(9)	2.417(7)	1.755(7)	1.604(7)
822	9.00979(8)	2.997(11)	2.439(8)	1.735(7)	1.624(7)

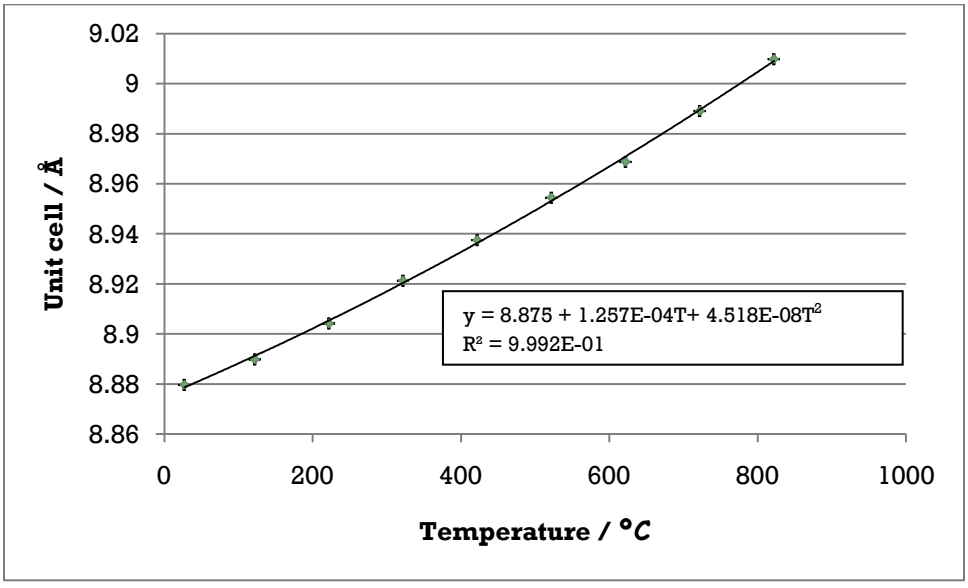

Fig 34: Graph showing change in unit cell size as temperature increases. Error bars represent 1 esd.

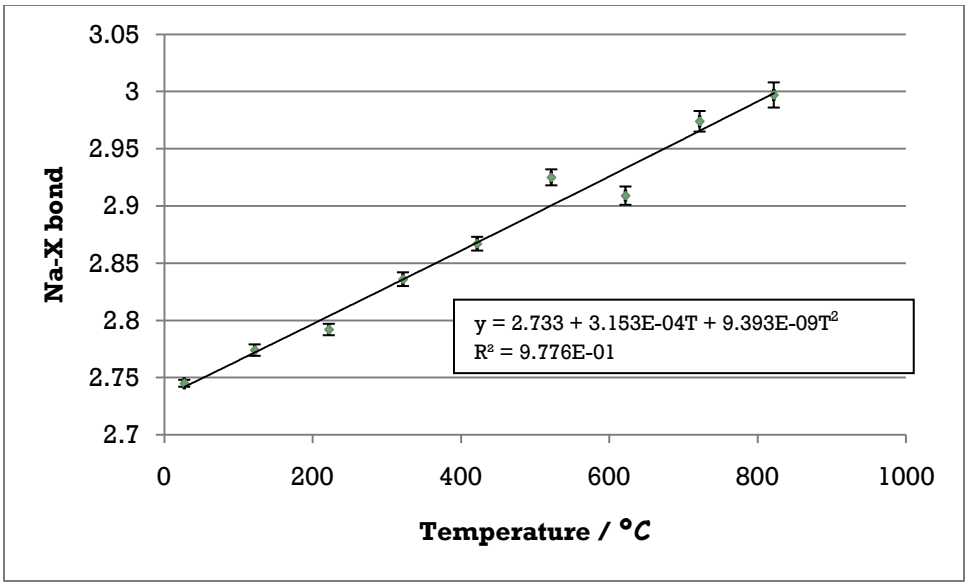

Fig 35: Graph showing change in Na-X bond length as temperature increases. Error bars represent 1 esd.

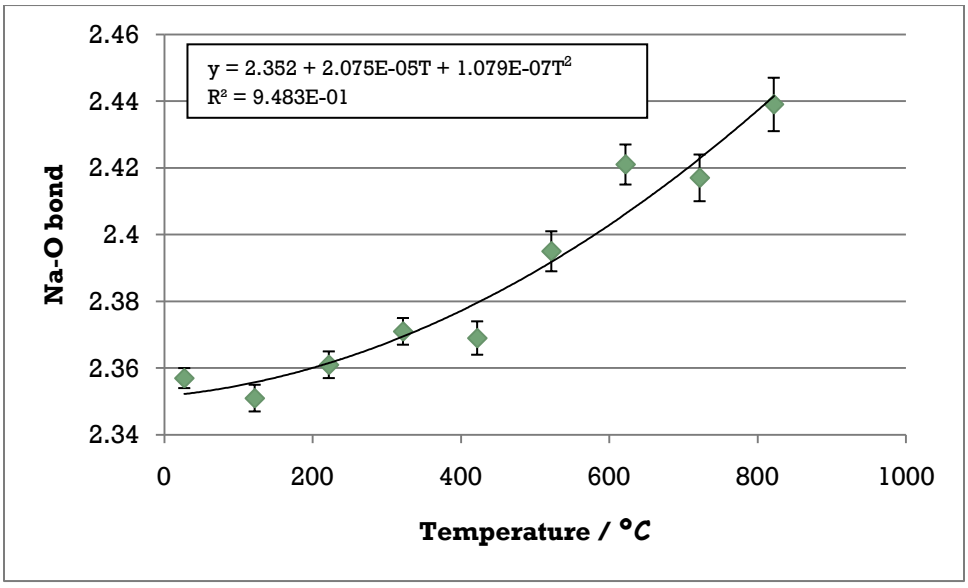

Fig 36: Graph showing change in Na-O bond length as temperature increases. Error bars represent 1 esd.

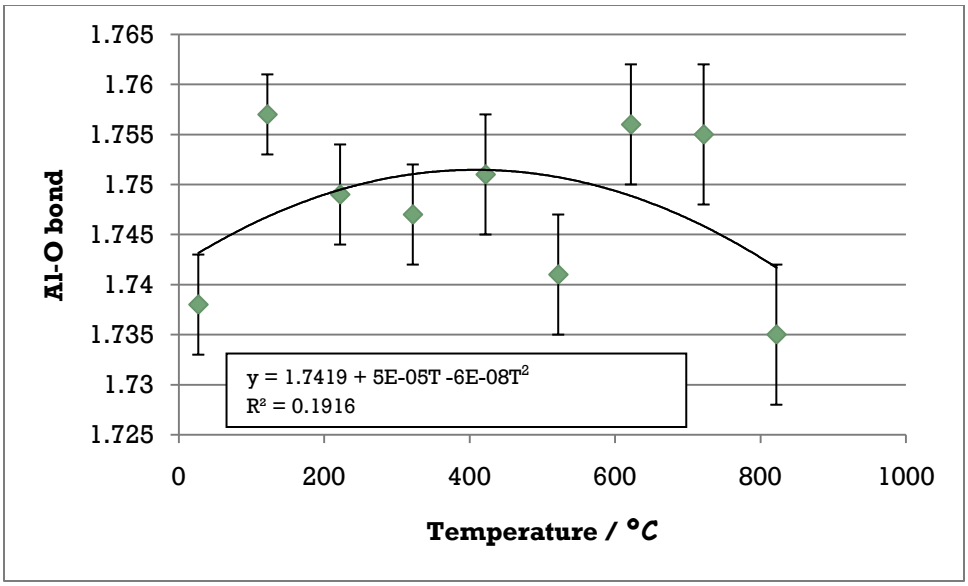

Fig 37: Graph showing change in Si-O bond length as temperature increases. Error bars represent 1 esd.

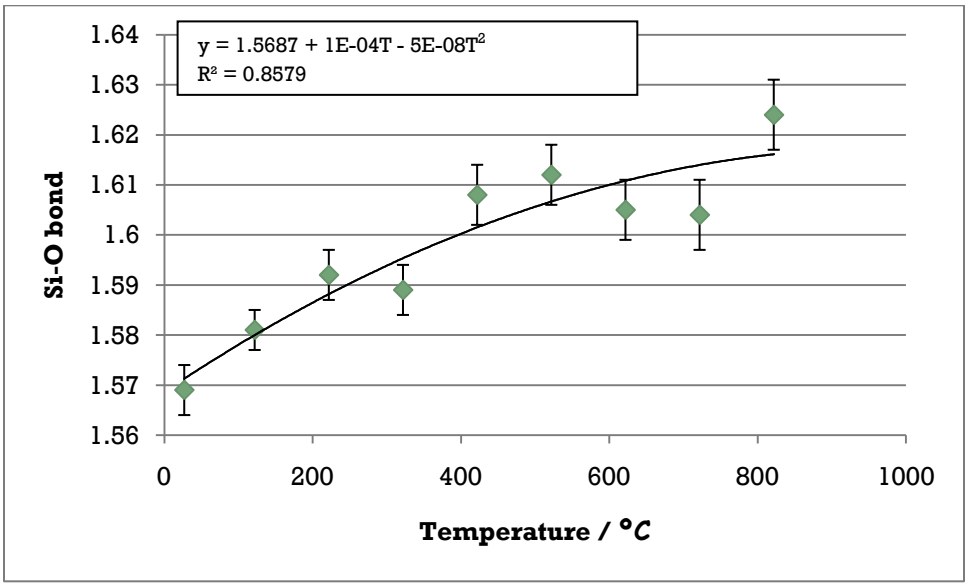

Fig 38: Graph showing change in Si-O bond length as temperature increases. Error bars represent 1 esd.

5.5c. High temperature studies of Iodosodalite

High temperature study was carried out on the iodosodalite and the atomic coordinate and thermal factor values are shown in Table 17.

Table 17: Atomic coordinate and thermal factor values for iodosodalite at various temperatures

Temp	*a* / Å	M		O				Al	Si	X	CHI*2
		x	$U_{iso}x100$	*x*	*y*	*z*	$U_{iso}x100$	$U_{iso}x100$	$U_{iso}x100$	$U_{iso}x100$	
27	8.99726(4)	0.199174 (1)	3.859 (1)	0.141827 (2)	0.448432 (1)	0.158158 (1)	2.374 (1)	2.672 (1)	1.560 (1)	8.709 (2)	1.209
122	9.00915(5)	0.199666 (1)	4.668 (1)	0.141001 (1)	0.450155 (2)	0.157477 (2)	2.134 (1)	3.640 (1)	2.581 (1)	10.349 (1)	1.171
222	9.02936(5)	0.202601 (1)	6.620 (1)	0.144283 (1)	0.453482 (1)	0.158045 (1)	3.525 (2)	5.154 (1)	2.220 (1)	13.005 (1)	1.192
322	9.04958(6)	0.206569 (1)	7.648 (1)	0.143235 (1)	0.453482 (1)	0.160572 (1)	2.697 (1)	4.894 (1)	2.810 (1)	14.385 (1)	1.147
422	9.06901(7)	0.208457 (1)	7.798 (1)	0.142890 (1)	0.456286 (1)	0.158982 (2)	3.635 (2)	3.889 (1)	3.856 (1)	15.983 (1)	1.176
522	9.08937(8)	0.208488 (1)	9.363 (1)	0.143742 (1)	0.459252 (1)	0.159458 (2)	3.899 (3)	6.330 (1)	3.380 (1)	17.752 (1)	1.167
622	9.111190(9)	0.215107 (1)	9.782 (2)	0.145288 (3)	0.466366 (1)	0.161623 (2)	5.484 (4)	5.378 (1)	3.481 (1)	20.749 (1)	1.165
722	9.13667(11)	0.215017 (4)	8.070 (3)	0.145876 (10)	0.469104 (7)	0.160167 (2)	7.432 (8)	5.196 (1)	3.752 (1)	23.494 (4)	1.108
822	9.15769(8)	0.220512 (1)	9.696 (1)	0.145287 (2)	0.477320 (1)	0.160188 (1)	5.904 (3)	5.294 (1)	3.116 (1)	25.894 (1)	1.149

As can be seen from Table 18 and Figures 39-43, the iodosodalite also behaves the same with an increase in the Unit cell, M-X and M-O bonds thus suggesting that there is positive thermal expansion. Again within a three esd error there are no consistent correlations in the Al-O and Si-O with composition and temperature

Table 18: High temperature studies of Iodosodalites

Temperature / °C	Unit cell /Å	Na-X bond/Å	Na-O bond/Å	Al-O bond/Å	Si-O bond/Å
27	8.99726(4)	3.104(6)	2.331(6)	1,785(7)	1.590(7)
122	9.00915(5)	3.116(6)	2.349(6)	1.783(7)	1.584(7)
222	9.02936(5)	3.169(7)	2.36(7)	1.767(8)	1.601(8)
322	9.04958(6)	3.238(8)	2.344(8)	1.795(8)	1.585(8)
422	9.06901(7)	3.274(9)	2.368(9)	1.783(9)	1.587(9)
522	9.08937(8)	3.282(10)	2.396(10)	1.780(9)	1.588(10)
622	9.111190(9)	3.395(11)	2.425(13)	1.781(11)	1.580(11)
722	9.13667(11)	3.402(14)	2.456(14)	1.768(14)	1.592(14)
822	9.15769(8)	3.498(17)	2.512(18)	1.765(13)	1.578(13)

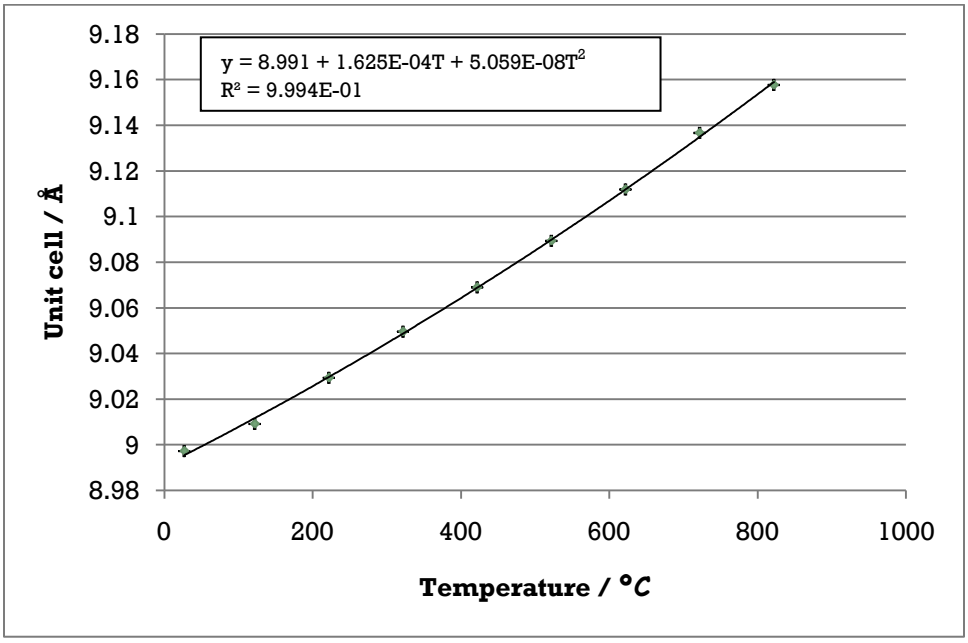

Fig 39: Graph showing change in unit cell size as temperature increases. Error bars represent 1 esd.

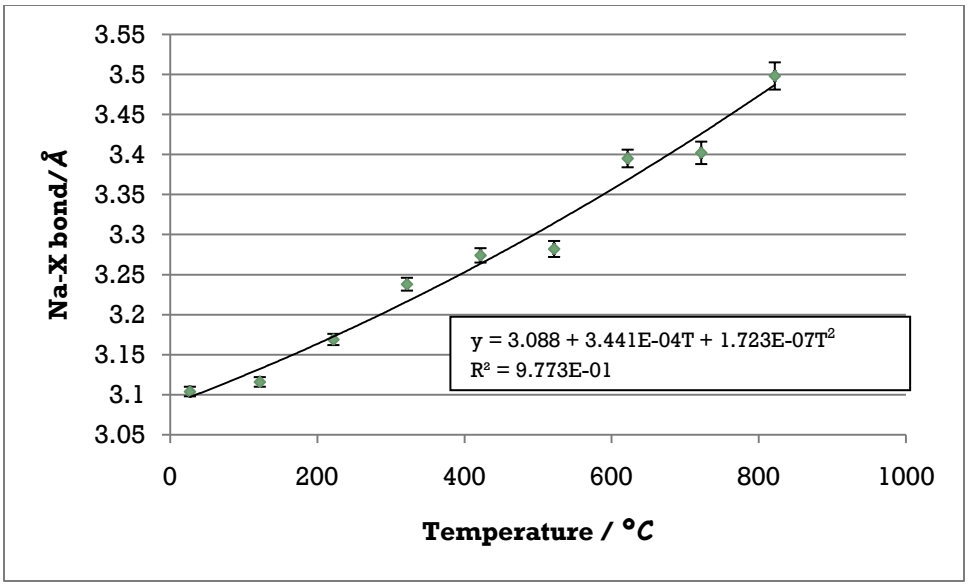

Fig 40: Graph showing change in Na-X bond length as temperature increases. Error bars represent 1 esd.

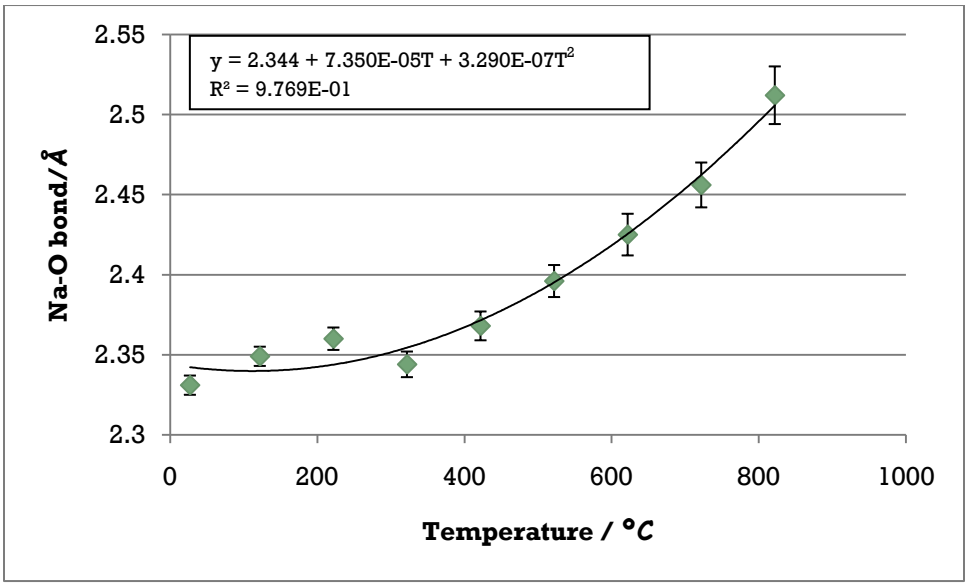

Fig 41: Graph showing change in Na-O bond length as temperature increases. Error bars represent 1 esd.

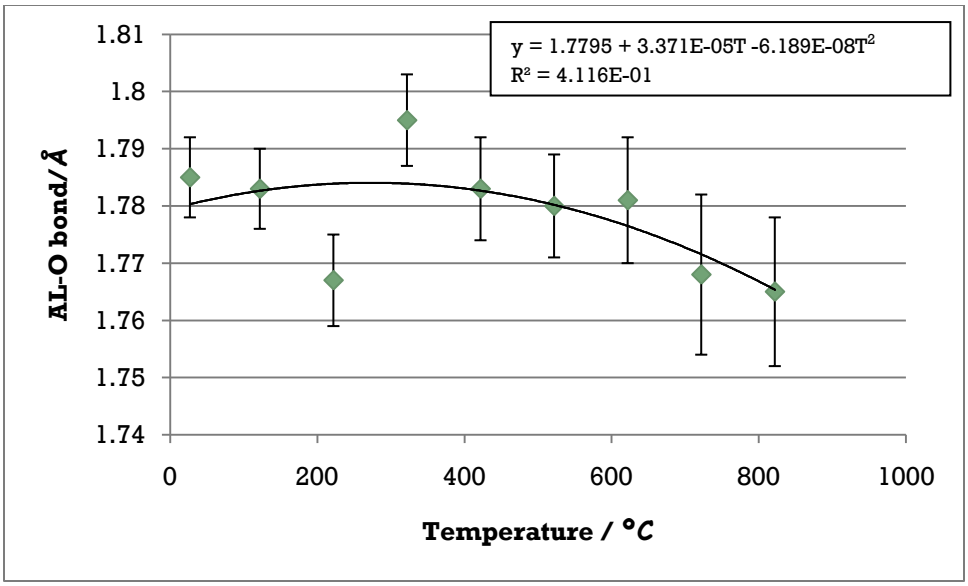

Fig 42: Graph showing change in Al-O bond length as temperature increases. Error bars represent 1 esd.

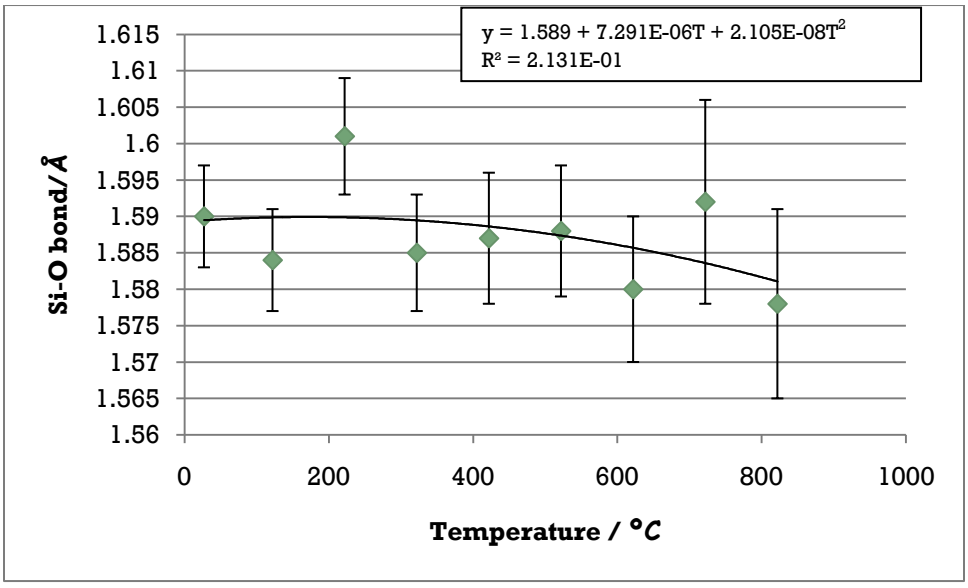

Fig 43: Graph showing change in Si-O bond length as temperature increases. Error bars represent 1 esd.

5.5d Discussion of High temperature studies of Halosodalites

Structure of sodalite

The general structural features of a sodalite have been described in the introduction, and the structure obtained by Hassan and Grundy (1984) is shown in figure 44. For bromosodalite, the Al-O and Si-O distances are 1.75Å and 1.608Å, respectively; for chlorosodalite Al-O and Si-O distances are 1.74Å and 1.624Å, respectively; and for iodosodalite Al-O and Si-O distances are 1.78Å and 1.6Å, respectively, indicating that the Al and Si atoms are fully ordered.

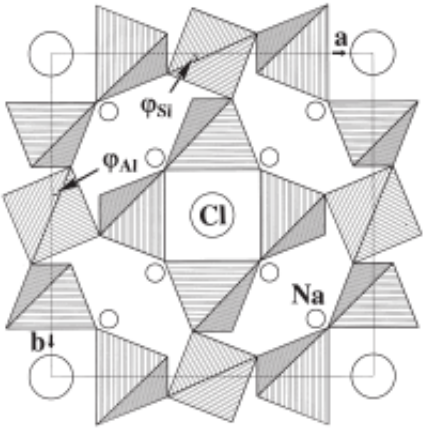

Fig 44: projection of the structure of sodalite down [001] showing the lower half of the unit cell. The TO_4 tetrahedra are ordered and the angles of rotation of these tetrahedra are indicated by φAl and φSi. Φ is the angle between the cell edge and the projection of the tetrahedral edge on (001).

Effect of temperature on the unit cell parameter

The unit cell parameters increase with temperature for all three halosodalites, indicating there is standard positive thermal expansion. The data yields smooth expansion curves without any changes or discontinuities up to 822^{o}C.

Antano and Hassan (2002) reported that sodalites melt at about 1079^{o}C and begin to lose their salt. I was unable to heat the sodalites to this temperature range; therefore the halo-sodalites did not change composition significantly in the temperature range I used for this study.

Effect of temperature change on the framework

The framework of sodalites consists of corner linked TO_4 units, as described in the introduction. Taking into account the ESD values, no clear pattern was observed in the Al-O and Si-O bond lengths for all three halosodalites.

Effect of temperature on Cage cluster

The Na-X and Na-O bonds in all three halosodalites increased slightly with increased temperature suggesting positive thermal expansion.

Thermal expansion

High temperature studies of the crystal structures of other framework silicates and aluminosilicates have been carried out previously by Hassan and Grundy (1984), Antano and Hassan (2002), Hassan et al (1984), Dempsey and Taylor (1980). Taylor and Henderson (1978) found that at room temperature the cell parameters, atomic coordinates and tilt angles of the sodalites depended on the framework bond lengths and the sizes of the cavity ions. They found that as the temperature was increased there was an expansion in these bond lengths due the

untwisting of the partially-collapsed framework by gradual removal of the tilting. Studies have also suggested that the changes in the framework bonds will be slight and in some cases apparent contraction of the framework bonds would be observed (Young, 1962; Peacor, 1968; Winter et al., 1979).

In my studies there was an increase in the cell parameter, Na-X and Na-O bond lengths as the temperature increased. Expansion data by Taylor (1968) and Henderson and Taylor (1978) also found that the Cl- and Br- bearing aluminosilicate sodalites showed increasing rate of expansion up to the highest temperature studied. The weaker Na-Br/ Na-Cl bond distance increased, as indicated by large displacement parameters for the Na, Br and Cl atoms. The Na migrated towards the plane of the six membered ring as the framework tetrahedra rotate. The AlO_4 and SiO_4 tetrahedra were rotated by angles φAl and φSi respectively (fig 44). These rotations induced a high degree of expansion.

In the case of the I-bearing sodalites, I found no discontinuity whereas studies showed there is a high and increasing rate of expansion to a low and constant rate (Henderson and Taylor, 1978; Dempsey and Taylor, 1980). This discontinuity is due to the iodine being a large cavity anion. A computer model by Henderson and Taylor (1978) implied that the driving force lay in the framework, and that the bonds of the cavity ions vainly attempt to restrain the untwisting of the framework. Dempsey and Taylor (1980) suggest that these discontinuities are due to the ideal fully-expanded state being achieved or that the x coordinates of the sodium atoms became 0.25, with the latter theory being preferred. I was unable to observe this as I only heated the iodo sodalite to 847ºC.

5.6. High temperature studies of Ion exchanged Halosodalites

Previously no high temperature studies of ion exchanged halosodalites have been carried out.

5.6a High temperature study of silver exchanged bromosodalites

- $Na_6Ag_2\,[SiAlO_4]_6.\,Br_2$

High temperature study was carried out on the ion exchanged bromosodalite and the atomic coordinate and thermal factor values are shown in Table 19.

Table 19: Atomic coordinate and thermal factor values for $Na_6Ag_2[SiAlO_4]_6Br_2$ at various temperatures

Temp/ °C	a / Å	M			O				Al	Si	X	CHI*2
		x	$U_{iso}x100$	x	y	z	$U_{iso}x100$	$U_{iso}x100$	$U_{iso}x100$	$U_{iso}x100$		
27	8.92177(4)	0.176727 (1)	6.318 (1)	0.140672 (2)	0.445956 (2)	0.151873 (1)	3.537 (3)	4.107 (1)	3.411 (1)	9.463 (1)		1.224
122	8.93850(4)	0.177671 (1)	6.500 (1)	0.139025 (1)	0.446467 (1)	0.151274 (1)	3.405 (1)	3.861 (1)	3.456 (1)	9.924 (1)		1.24
222	8.94544(5)	0.179769 (1)	7.482 (2)	0.139743 (1)	0.446681 (2)	0.153267 (2)	3.586 (2)	4.039 (1)	3.370 (1)	11.242 (1)		1.164
322	8.96886(6)	0.181338 (1)	8.555 (1)	0.138961 (2)	0.448638 (1)	0.153674 (1)	4.514 (3)	4.585 (1)	3.763 (1)	13.889 (2)		1.164
422	8.98007(6)	0.183134 (1)	9.388 (1)	0.139813 (1)	0.449610 (2)	0.152601 (1)	4.747 (1)	4.882 (1)	3.224 (1)	15.001 (1)		1.174
522	8.99586(7)	0.185151 (1)	9.639 (1)	0.140125 (1)	0.452245 (1)	0.152313 (1)	5.436 (1)	4.716 (1)	3.352 (1)	16.414 (1)		1.17
622	9.01333(7)	0.186778 (1)	10.998 (1)	0.138829 (1)	0.454942 (1)	0.153224 (1)	5.566 (1)	5.255 (1)	2.625 (1)	18.839 (1)		1.099
722	9.03102(9)	0.188485 (1)	12.284 (1)	0.140514 (2)	0.457448 (1)	0.153458 (2)	5.662 (1)	5.239 (1)	2.320 (1)	20.519 (1)		1.117
822	9.06665(11)	0.193751 (1)	13.189 (1)	0.138726 (1)	0.459596 (1)	0.150877 (1)	7.670 (1)	5.521 (1)	2.599 (1)	27.123 (1)		1.086

As can be seen from Table 20 and figures 45-49 there is an increase in the size of the unit cell, M-X, and M-O bonds therefore suggesting that there is positive thermal expansion. Within a three esd error there are no consistent correlations in the Al-O and Si-O with composition and temperature

Table 20: High temperature studies of $Na_6Ag_2[SiAlO_4]_6Br_2$

Temperature / °C	Unit cell /Å	Na-X bond/Å	Na-O bond/Å	Al-O bond/Å	Si-O bond/Å
27	8.92177(4)	2.731(4)	2.434(4)	1.738(6)	1.604(6)
122	8.93850(4)	2.748(5)	2.436(6)	1.742(8)	1.596(8)
222	8.94544(5)	2.785(5)	2.426(6)	1.755(9)	1.593(8)
322	8.96886(6)	2.815(5)	2.439(7)	1.761(9)	1.584(9)
422	8.98007(6)	2.848(6)	2.440(8)	1.750(10)	1.596(9)
522	8.99586(7)	2.885(6)	2.454(9)	1.743(10)	1.596(10)
622	9.01333(7)	2.916(7)	2.474(10)	1.754(10)	1.578(10)
722	9.03102(9)	2.948(8)	2.488(11)	1.745(11)	1.587(11)
822	9.06665(11)	3.043(9)	2.492(12)	1.739(14)	1.589(11)

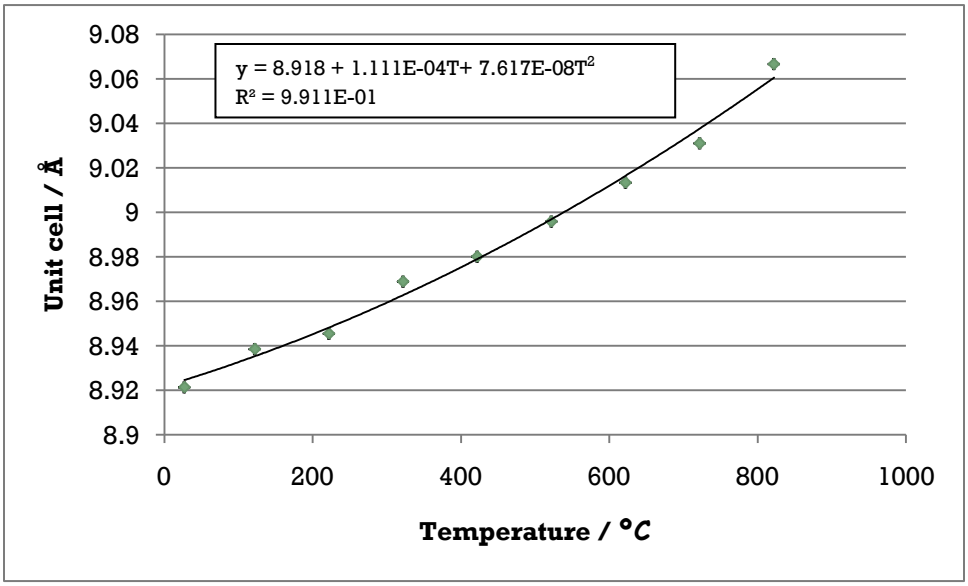

Fig 45: Graph showing change in unit cell size as temperature increases. Error bars represent 1 esd.

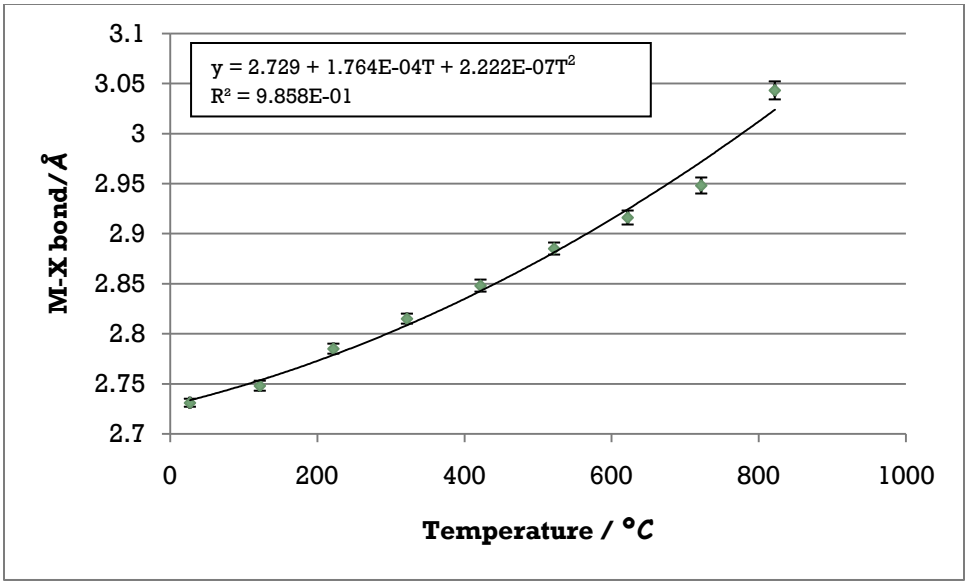

Fig 46: Graph showing change in M-X bond length as temperature increases. Error bars represent 1 esd.

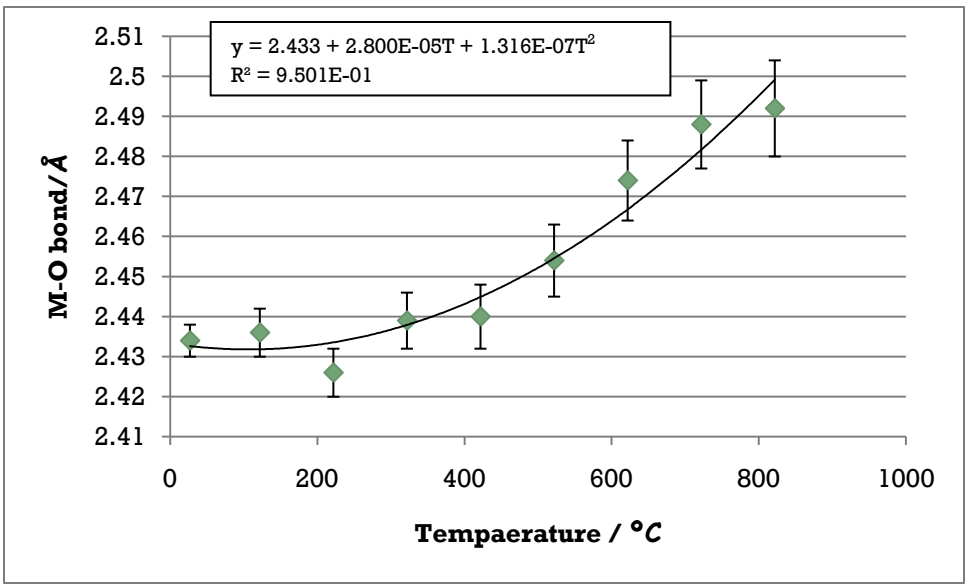

Fig 47: Graph showing change in M-O bond length as temperature increases. Error bars represent 1 esd.

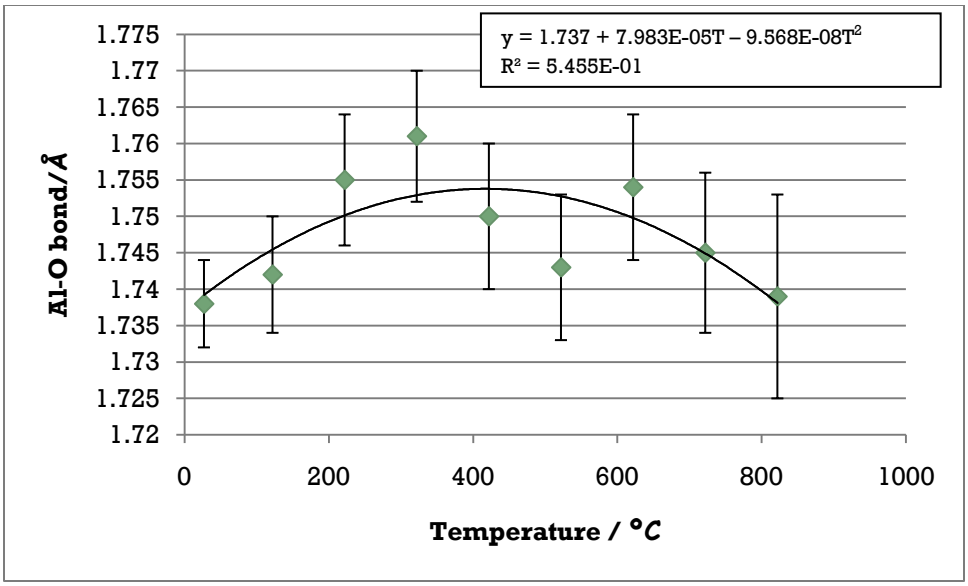

Fig 48: Graph showing change in Al-O bond length as temperature increases. Error bars represent 1 esd.

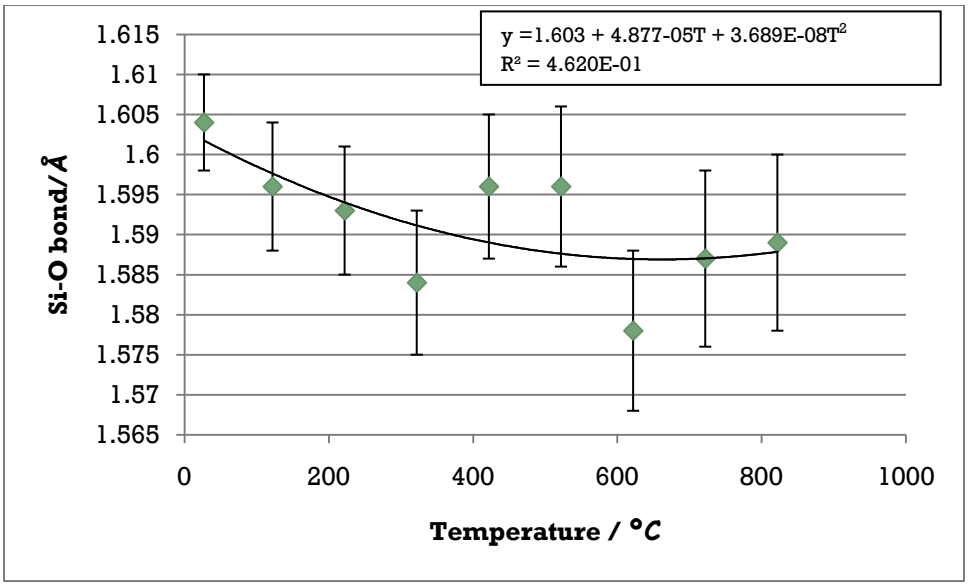

Fig 49: Graph showing change in Si-O bond length as temperature increases. Error bars represent 1 esd.

$Na_4\ Ag_4\ [SiAlO_4]_6.\ Br_2$

High temperature study was carried out on the ion exchanged bromosodalite and the atomic coordinate and thermal factor values are shown in Table 21.

Table 21: Atomic coordinate and thermal factor values for $Na_4Ag_4[SiAlO_4]_6Br_2$ at various temperatures

Temp /°C	*a* / Å	M		O				Al	Si	X	CHI*2
		x	$U_{iso}x100$	*x*	*y*	*z*	$U_{iso}x100$	$U_{iso}x100$	$U_{iso}x100$	$U_{iso}x100$	
27	8.91437(4)	0.170074(5)	7.448(3)	0.137652(3)	0.449680 (6)	0.150665(4)	3.318 (4)	4.931 (1)	3.438 (1)	8.162 (3)	1.244
122	8.92005(4)	0.170510(1)	8.491(1)	0.136444(1)	0.450546 (1)	0.147277(1)	2.689 (1)	5.157 (1)	3.121 (1)	8.869 (2)	1.251
222	8.93668(5)	0.174113(1)	9.002(1)	0.140112(1)	0.446567 (1)	0.149742(1)	4.083 (1)	6.057 (1)	2.194 (1)	11.018 (1)	1.128
322	8.95264(6)	0.174826(1)	10.33 (1)	0.135829(1)	0.448397 (1)	0.151581(1)	3.558 (1)	4.957 (1)	3.095 (1)	12.479 (1)	1.124
422	8.96589(7)	0.177199(1)	11.10 (1)	0.136307(1)	0.450183 (1)	0.151776(1)	5.299 (1)	5.131 (1)	2.911 (1)	14.594 (1)	1.122
522	8.98076(8)	0.178569(1)	12.172(1)	0.135593(1)	0.453095 (1)	0.145521(1)	4.345 (1)	4.789 (1)	2.936 (1)	15.951 (1)	1.104
622	8.99676(9)	0.180848(1)	13.040(1)	0.133084(1)	0.457505 (1)	0.144925(1)	5.012 (1)	4.868 (1)	3.077 (1)	17.960 (1)	1.091
722	9.01650(10)	0.183900(1)	13.901(1)	0.129202(1)	0.460110 (1)	0.146623(1)	4.164 (1)	3.648 (1)	2.354 (1)	20.388 (1)	1.095
822	9.04353(12)	0.187835(1)	13.787(1)	0.124840(2)	0.456091 (1)	0.147660(1)	5.259 (2)	3.401 (1)	2.074 (1)	27.796 (1)	1.135

As can be seen from Table 22 and Figures 50-54 there is an increase in the size of the unit cell, M-X, and M-O bonds therefore suggesting that there is positive thermal expansion. No significant change was seen in the Al-O and Si-O bond length and the graphs for these show no correlation.

Table 22: High temperature studies of $Na_4Ag_4[SiAlO_4]_6Br_2$

Temperature / °C	Unit cell /Å	Na-X bond/Å	Na-O bond/Å	Al-O bond/Å	Si-O bond/Å
27	8.91437(4)	2.626(4)	2.515(8)	1.734(11)	1.578(10)
122	8.92005(4)	2.634(4)	2.525(8)	1.717(11)	1.586(10)
222	8.93668(5)	2.695(5)	2.463(9)	1.727(12)	1.612(12)
322	8.95264(6)	2.711(6)	2.483(10)	1.760(13)	1.571(12)
422	8.96589(7)	2.752(6)	2.485(12)	1.758(14)	1.571(13)
522	8.98076(8)	2.778(7)	2.513(14)	1.715(14)	1.594(13)
622	8.99676(9)	2.818(8)	2.546(17)	1.718(15)	1.573(15)
722	9.01650(10)	2.872(8)	2.561(22)	1.750(20)	1.535(20)
822	9.04353(12)	2.942(9)	2.518(24)	1.795(18)	1.513(18)

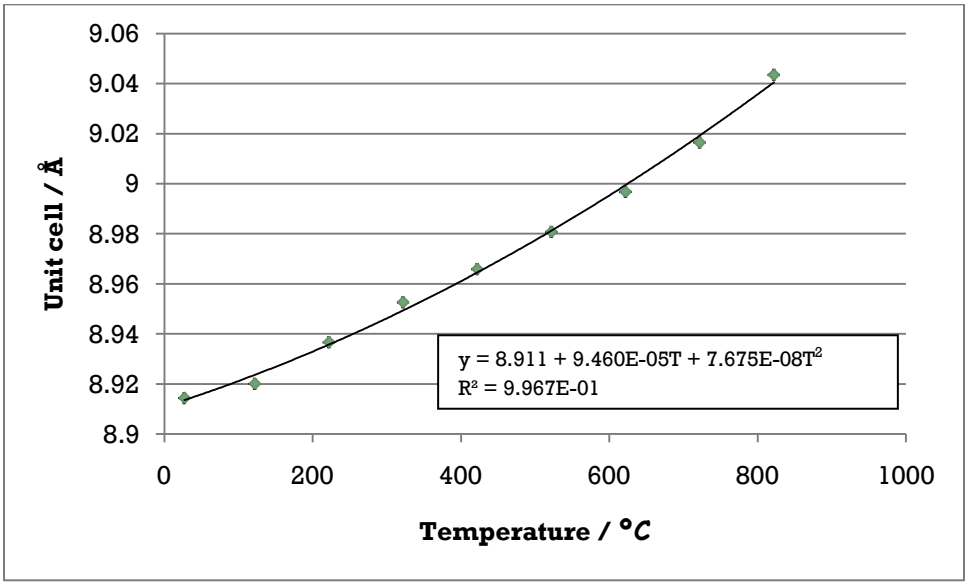

Fig 50: Graph showing change in unit cell size as temperature increases. Error bars represent 1 esd.

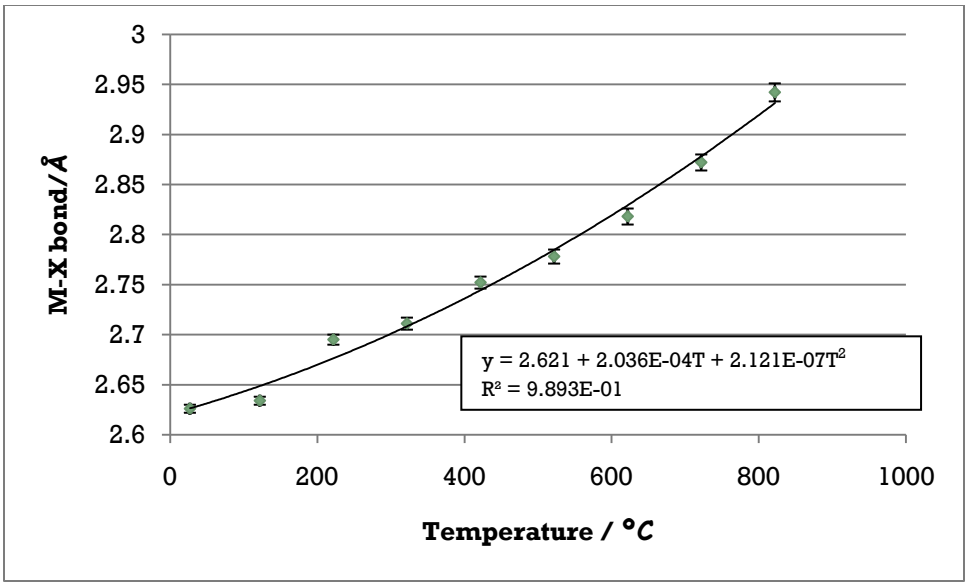

Fig 51: Graph showing change in M-X bond length as temperature increases. Error bars represent 1 esd.

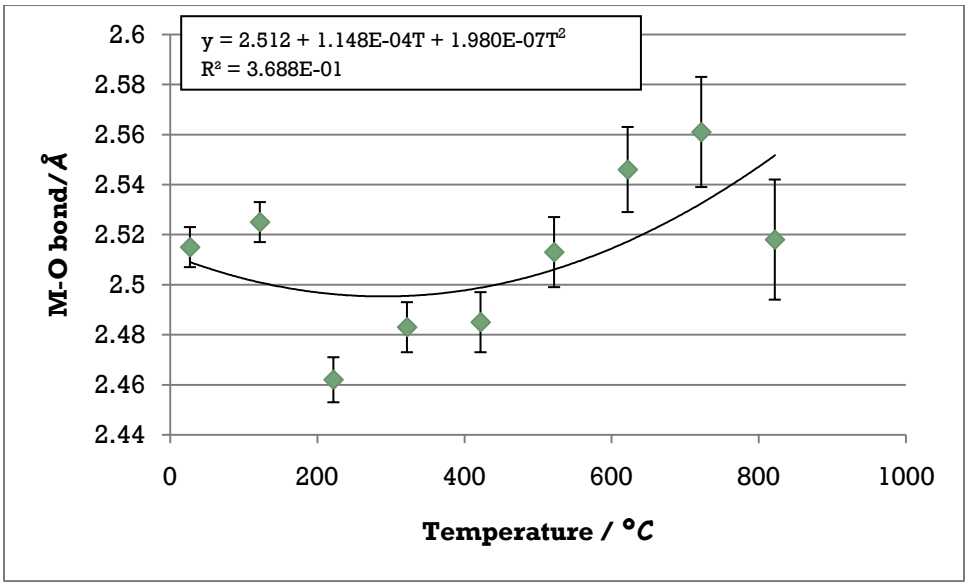

Fig 52: Graph showing change in M-O bond length as temperature increases. Error bars represent 1 esd.

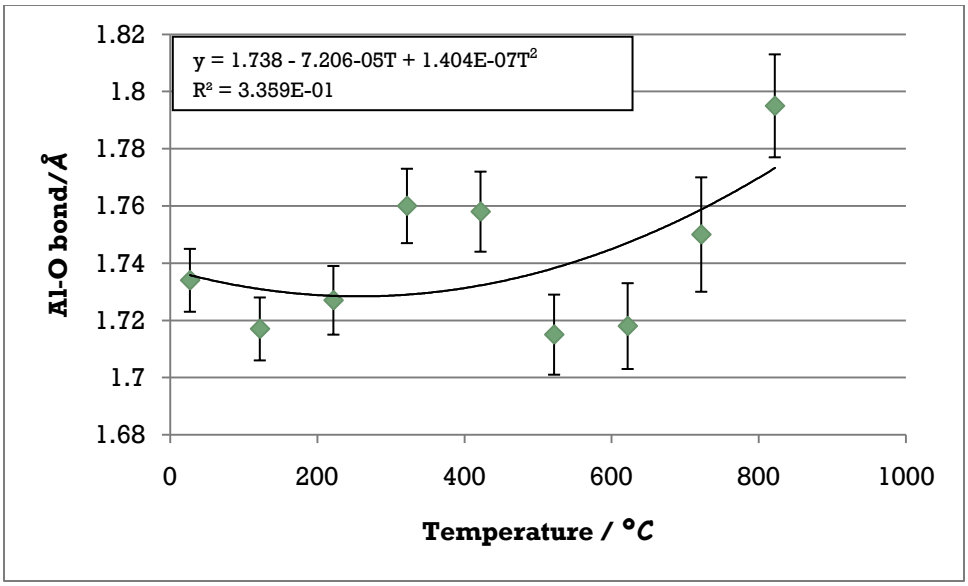

Fig 53: Graph showing change in Al-O bond length as temperature increases. Error bars represent 1 esd.

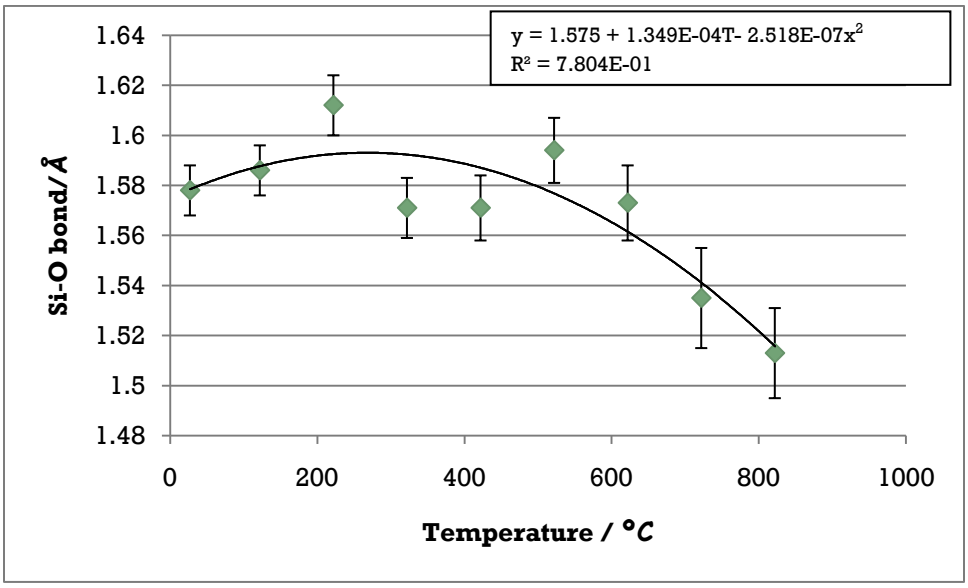

Fig 54: Graph showing change in Si-O bond length as temperature increases Error bars represent 1 esd.

- $Na_2\ Ag_6[SiAlO_4]_6.\ Br_2$

High temperature study was carried out on the ion exchanged bromosodalite and the atomic coordinate and thermal factor values are shown in Table 23.

Table 23: Atomic coordinate and thermal factor values for $Na_2Ag_6[SiAlO_4]_6Br_2$ at various temperatures

Temp/ °C	*a* / Å	M		O				Al	Si	X	CHI*2
		x	U_{iso} *x100*	*x*	*y*	*z*	U_{iso} *x100*	U_{iso} *x100*	U_{iso} *x100*	U_{iso} *x100*	
27	8.91402 (4)	0.172968(1)	8.281(1)	0.141994(2)	0.446707(6)	0.156683 (1)	4.400 (2)	3.999 (1)	2.143 (1)	8.275 (1)	1.276
122	8.91725 (5)	0.173027(1)	8.521(1)	0.138168(2)	0.444230(3)	0.157421 (2)	4.145 (3)	3.711 (1)	2.711 (1)	9.288 (1)	1.22
222	8.93113 (5)	0.173961(1)	10.004(1)	0.138004(1)	0.449894(1)	0.151534 (1)	3.029 (2)	3.369 (1)	1.774 (1)	9.364 (1)	1.179
322	8.94998 (6)	0.175141(1)	11.101(2)	0.133682(1)	0.447229(2)	0.150753 (1)	2.708 (1)	2.779 (1)	2.218 (1)	10.321 (1)	1.129
422	8.96223 (7)	0.175527(1)	12.095(1)	0.132665(1)	0.451448(1)	0.150514 (1)	2.817 (2)	3.446 (1)	1.369 (1)	12.379 (1)	1.124
522	8.97691 (8)	0.177826(1)	13.388(1)	0.132780(1)	0.455079(1)	0.150957 (1)	3.219 (1)	2.569 (1)	1.554 (2)	13.351 (1)	1.109
622	8.99388(9)	0.179815(1)	13.649(1)	0.129380(1)	0.458199(1)	0.150889 (1)	5.495 (1)	3.649 (1)	1.399 (1)	15.866 (1)	1.125
722	9.00722(11)	0.180737(2)	13.110(3)	0.130827(4)	0.469932(8)	0.147557 (1)	6.876 (6)	2.097 (1)	1.221 (1)	17.712 (2)	1.145
822	9.03479(15)	0.185781(1)	14.594(1)	0.118134(1)	0.463502(2)	0.148938 (1)	3.695 (2)	0.374 (1)	2.338 (1)	24.948 (1)	1.123

As can be seen from Table 24 and Figures 55-59 there is an increase in the size of the unit cell, M-X, and M-O bonds therefore suggesting that there is positive thermal expansion. Within a three esd error there are no consistent correlations in the Al-O and Si-O with composition and temperature

Table 24: High temperature studies of $Na_2\ Ag_6[SiAlO_4]_6.\ Br_2$

Temperature / °C	Unit cell /Å	Na-X bond/Å	Na-O bond/Å	Al-O bond/Å	Si-O bond/Å
27	8.91402(4)	2.6705(3)	2.460(9)	1.762(12)	1.587(13)
122	8.91725(5)	2.6724(3)	2.442(10)	1.792(13)	1.564(12)
222	8.93113(5)	2.691(4)	2.493(10)	1.741(12)	1.579(11)
322	8.94998(6)	2.715(4)	2.473(11)	1.768(13)	1.563(13)
422	8.96223(7)	2.725(5)	2.513(13)	1.765(16)	1.549(13)
522	8.97691(8)	2.765(6)	2.533(15)	1.762(15)	1.541(15)
622	8.99388(9)	2.801(7)	2.558(20)	1.778(20)	1.513(20)
722	9.00722(11)	2.820(8)	2.660(24)	1.730(19)	1.521(20)
822	9.03479(15)	2.907(9)	2.604(4)	1.827(130)	1.443(28)

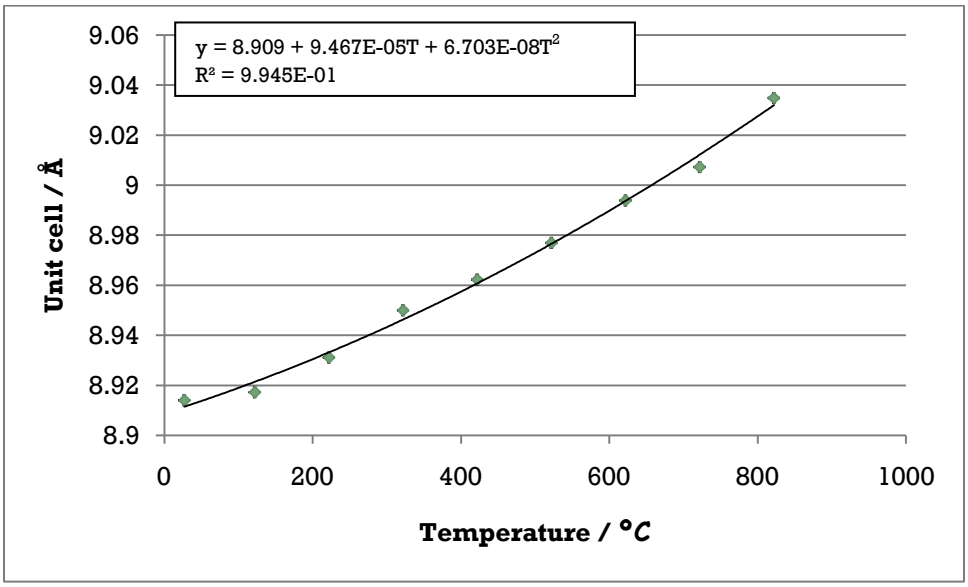

Fig 55: Graph showing change in unit cell size as temperature increases. Error bars represent 1 esd.

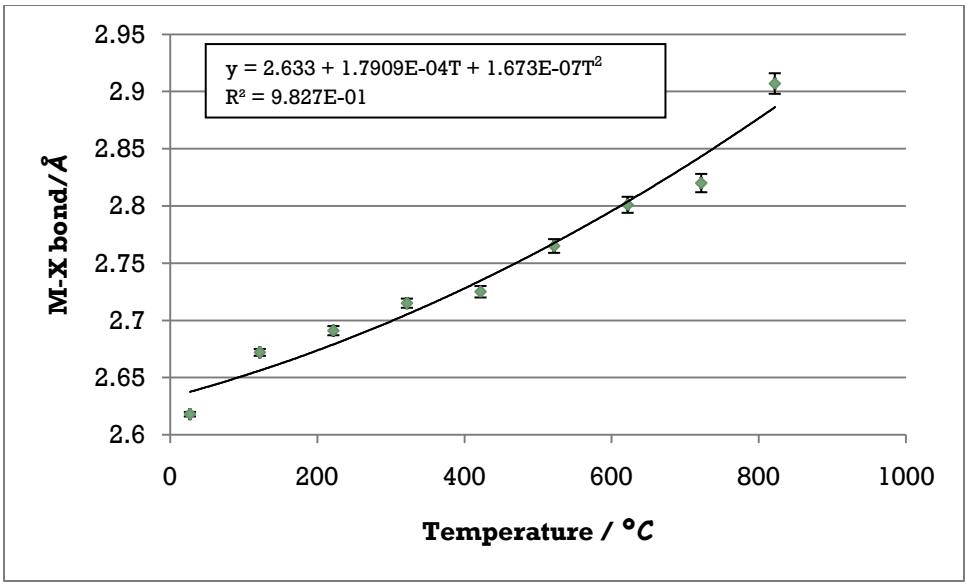

Fig 56: Graph showing change in M-X bond length as temperature increases. Error bars represent 1 esd.

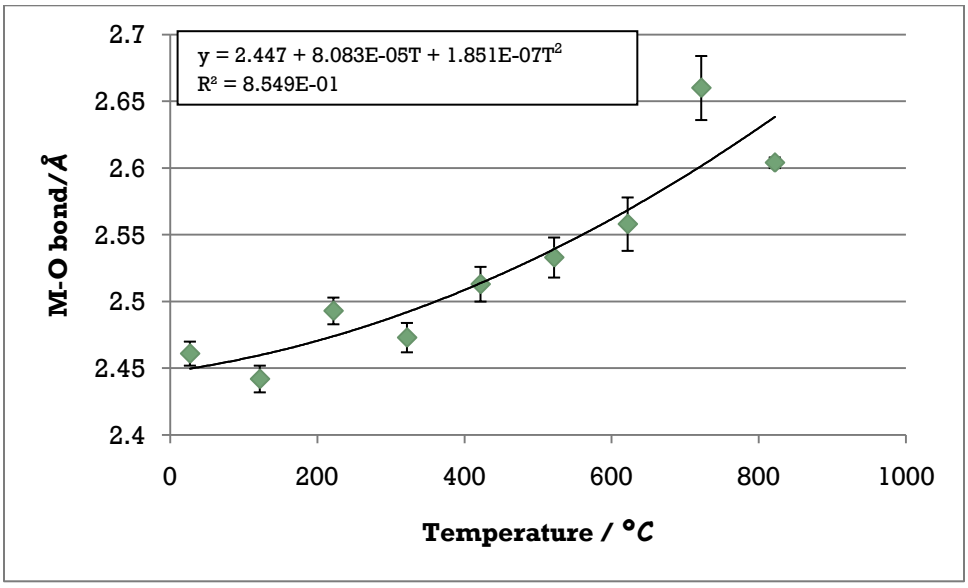

Fig 57: Graph showing change in M-O bond length as temperature increases. Error bars represent 1 esd.

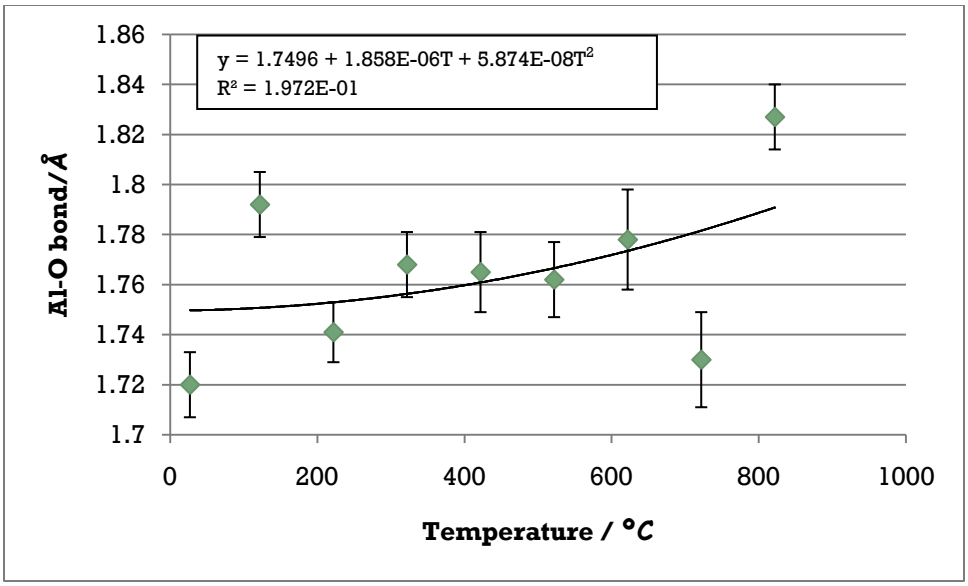

Fig 58: Graph showing change in Al-O bond length as temperature increases. Error bars represent 1 esd.

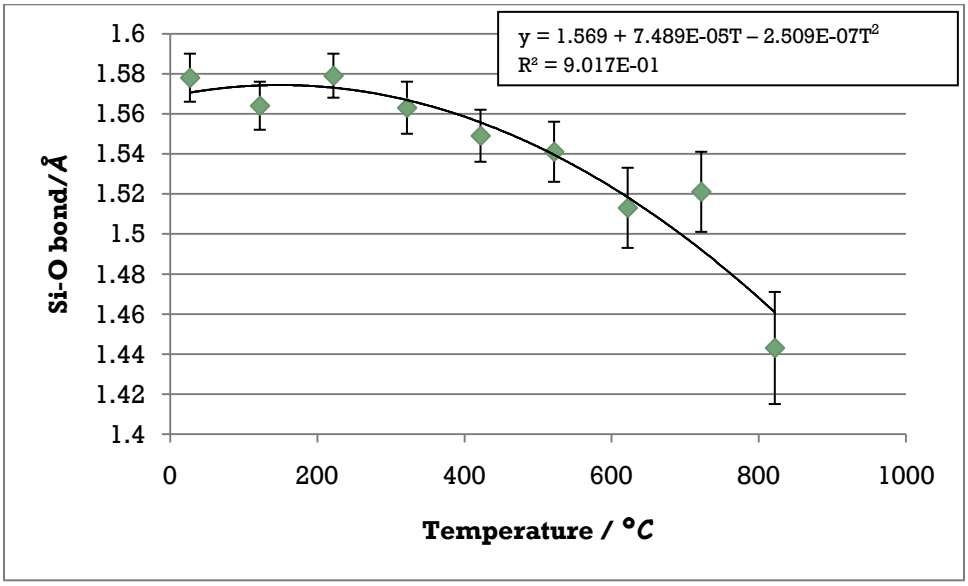

Fig 59: Graph showing change in Si-O bond length as temperature increases. Error bars represent 1 esd.

- $Na_0\ Ag_8[SiAlO_4]_6.\ Br_2$

High temperature study was carried out on the ion exchanged bromosodalite and the atomic coordinate and thermal factor values are shown in Table 25.

Table 25: Atomic coordinate and thermal factor values for $Na_0Ag_8[SiAlO_4]_6Br_2$ at various temperatures

Temp/ °C	*a* / Å	M		O				Al	Si	X	CHI*2
		x	U_{iso} *x100*	*x*	*y*	*z*	U_{iso} *x100*	U_{iso} *x100*	U_{iso} *x100*	U_{iso} *x100*	
27	8.91532(5)	0.173216(1)	8.699(1)	0.134360 (1)	0.446899 (1)	0.152689 (1)	0.892 (2)	1.634 (1)	0.884 (1)	5.535 (1)	1.288
122	8.91887(5)	0.173449 (1)	8.957(1)	0.130990 (1)	0.448996 (2)	0.154423 (1)	0.895 (1)	1.976 (1)	0.865 (1)	5.778 (1)	1.229
222	8.93280(6)	0.174029 (1)	10.678(1)	0.127361 (1)	0.453732 (2)	0.150776 (1)	0.373 (1)	1.786 (3)	0.881 (1)	6.358 (2)	1.257
322	8.94953(6)	0.175589 (2)	12.472 (1)	0.124564 (2)	0.455521 (1)	0.148956 (2)	0.538 (2)	1.767 (2)	1.329 (2)	8.542 (1)	1.209
422	8.96133(7)	0.175455(2)	13.378 (3)	0.128967 (1)	0.455674 (3)	0.145764 (3)	0.245 (1)	2.020 (2)	0.540 (2)	9.014 (2)	1.155
522	8.97394(8)	0.176722 (1)	14.272 (2)	0.125004 (1)	0.467565 (2)	0.148200 (1)	0.823 (2)	2.215 (1)	0.808 (1)	9.008 (2)	1.094
622	8.99002(10)	0.177506 (1)	14.373 (2)	0.124608 (1)	0.470993 (2)	0.146088 (1)	2.285 (1)	1.890 (1)	0.652 (1)	10.622 (1)	1.105
722	9.00473(12)	0.178939 (3)	14.931 (3)	0.120948 (2)	0.484213 (2)	0.148558 (2)	2.876 (2)	3.065 (2)	0.670 (1)	11.643 (1)	1.123
822	9.03816(15)	0.179717 (2)	14.417 (1)	0.121466 (1)	0.503733 (2)	0.142762 (2)	3.463(1)	1.450 (2)	0.450 (2)	13.975 (1)	1.113

As can be seen from Table 26 and Figures 60-64 there is an increase in the size of the unit cell, Na-X, and Na-O bonds therefore suggesting that there is positive thermal expansion. Within a three esd error there are no consistent correlations in the Al-O and Si-O with composition and temperature.

Table 26: High temperature studies of $Na_0Ag_8[SiAlO_4]_6Br_2$

Temperature / °C	Unit cell /Å	Na-X bond/Å	Na-O bond/Å	Al-O bond/Å	Si-O bond/Å
27	8.91532(5)	2.674(3)	2.471(9)	1.772(12)	1.553(11)
122	8.91887(5)	2.679(3)	2.492(9)	1.797(11)	1.516(11)
222	8.93280(6)	2.693(4)	2.542(10)	1.785(12)	1.500(12)
322	8.94953(6)	2.722(4)	2.558(12)	1.788(14)	1.490(13)
422	8.96133(7)	2.723(5)	2.559(13)	1.744(14)	1.538(14)
522	8.97394(8)	2.747(5)	2.663(20)	1.761(18)	1.476(18)
622	8.99002(10)	2.764(6)	2.696(24)	1.750(20)	1.482(19)
722	9.00473(12)	2.791(7)	2.811(22)	1.778(23)	1.429(22)
822	9.03816(15)	2.811(9)	2.884(24)	1.730(4)	1.460(5)

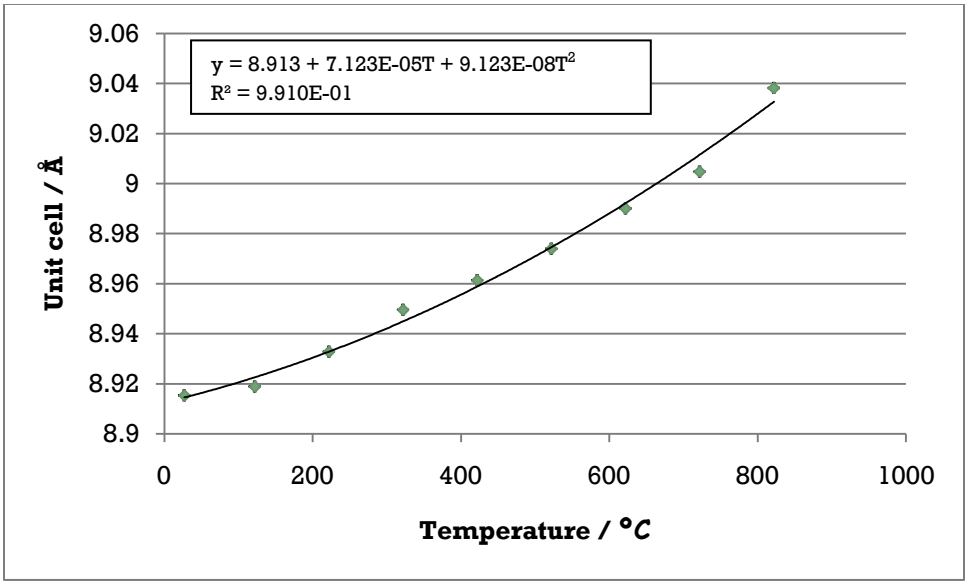

Fig 60: Graph showing change in unit cell size as temperature increases. Error bars represent 1 esd.

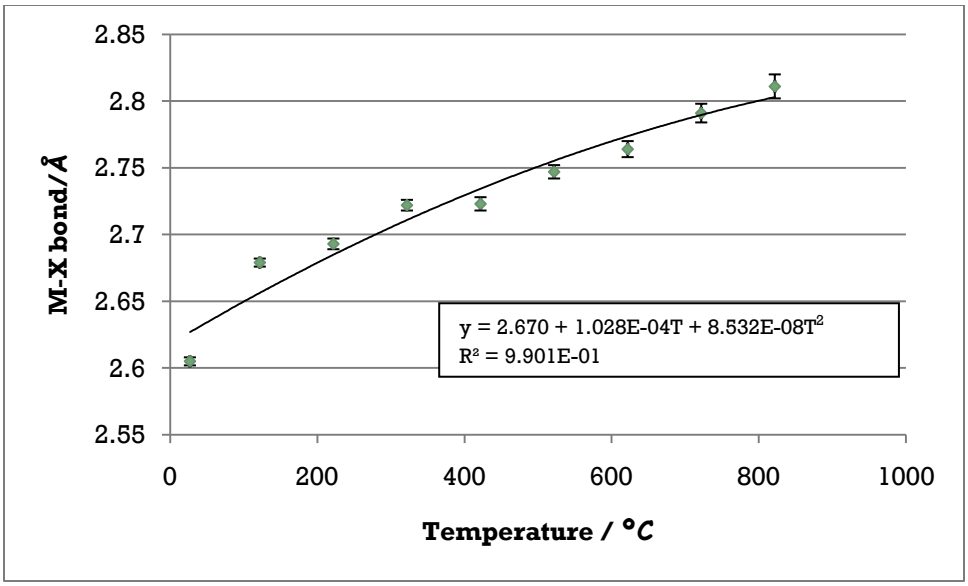

Fig 61: Graph showing change in M-X bond length as temperature increases. Error bars represent 1 esd.

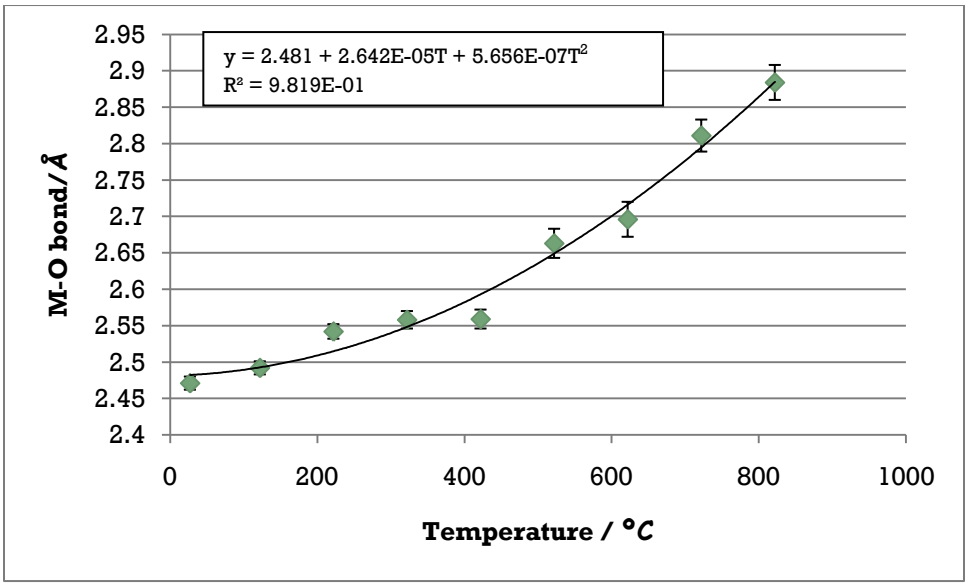

Fig 62: Graph showing change in M-O bond length as temperature increases. Error bars represent 1 esd.

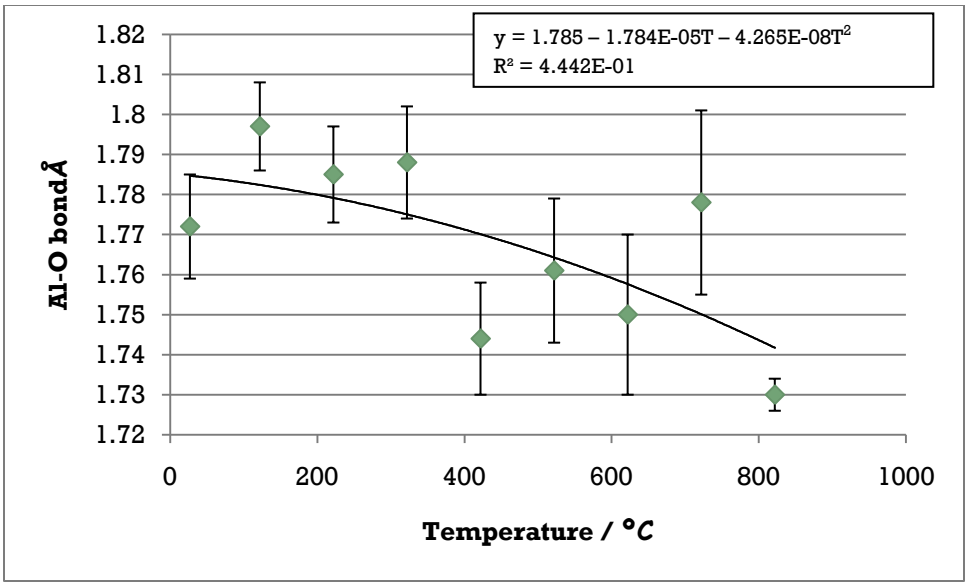

Fig 63: Graph showing change in Al-O bond length as temperature increases. Error bars represent 1 esd.

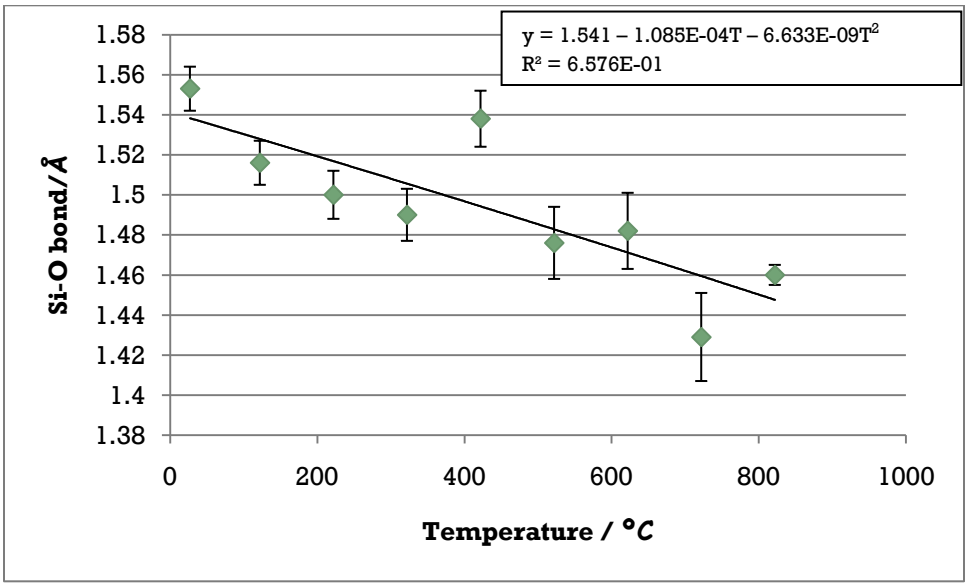

Fig 64: Graph showing change in Si-O bond length as temperature increases. Error bars represent 1 esd.

5.6b. High temperature study of silver exchanged chlorosodalites

- $Na_6Ag_2\,[SiAlO_4]_6.\,Cl_2$

High temperature study was carried out on the ion exchanged chlorosodalite and the atomic coordinate and thermal factor values are shown in Table 27.

Table 27: Atomic coordinate and thermal factor values for Na_6Ag_2 $[SiAlO_4]_6$. Cl_2 at various temperatures

Temp /°C	*a* / Å	M		O				Al	Si	X	CHI*2
		x	U_{iso} *x100*	*x*	*y*	*z*	U_{iso} *x100*	U_{iso} *x100*	U_{iso} *x100*	U_{iso} *x100*	
27	8.87409(4)	0.168649(1)	6.056(1)	0.142286(1)	0.444855(1)	0.147289(1)	3.805(1)	4.562(1)	3.639(2)	7.637(1)	1.197
122	8.88013(5)	0.169890(1)	7.049(2)	0.142476(1)	0.446011(2)	0.148245(1)	4.367(2)	5.062(2)	3.460(2)	8.491(2)	1.178
222	8.89207(5)	0.170026(2)	7.580(2)	0.141537(2)	0.442797(2)	0.147366(2)	4.589(1)	6.483(2)	3.846(1)	9.226(2)	1.149
322	8.91111(6)	0.173366(3)	8.777(2)	0.140715(2)	0.445288(1)	0.149385(2)	4.556(2)	5.984(1)	3.692(2)	10.939(2)	1.147
422	8.92644(7)	0.175554(2)	10.169(1)	0.139255(1)	0.449718(2)	0.150178(1)	4.759(2)	5.547(3)	4.292(1)	14.169(1)	1.15
522	8.94124(8)	0.177256(2)	10.178(2)	0.138060(1)	0.449812(2)	0.150967(2)	5.567(1)	4.034 (9)	5.275(9)	15.052(2)	1.187
622	8.95826(10)	0.178520(1)	11.354(1)	0.138838(1)	0.451164(2)	0.149312(2)	5.822(3)	4.935(4)	4.117(2)	17.274(2)	1.144
722	8.97523(11)	0.180677(2)	13.045(2)	0.139734(2)	0.449045(1)	0.149904(1)	5.367(2)	5.894(3)	3.727(3)	22.363(3)	1.119
822	8.99558(14)	0.184110(3)	12.688(2)	0.136874(2)	0.457949(1)	0.151450(2)	6.934(1)	3.456(3)	5.393(2)	24.872(2)	1.15

As can be seen from Table 28 and Figures 65-69 there is an increase in the size of the unit cell, M-X, and M-O bonds therefore suggesting that there is positive thermal expansion. Within a three esd error there are no consistent correlations in the Al-O and Si-O with composition and temperature

Table 28: High temperature studies of Na_6Ag_2 $[SiAlO_4]_6$. Cl_2

Temperature / °C	Unit cell /Å	Na-X bond/Å	Na-O bond/Å	Al-O bond/Å	Si-O bond/Å
27	8.87409(4)	2.592(4)	2.470(9)	1.692(20)	1.632(20)
122	8.88013(5)	2.613(4)	2.472(9)	1.695(20)	1.627(21)
222	8.89207(5)	2.619(5)	2.447(9)	1.705(16)	1.636(15)
322	8.91111(6)	2.676(6)	2.450(10)	1.720(21)	1.617(20)
422	8.92644(7)	2.714(7)	2.479(12)	1.725(18)	1.594(17)
522	8.94124(8)	2.745(7)	2.473(16)	1.739(18)	1.584(18)
622	8.95826(10)	2.77(7)	2.482(22)	1.724(19)	1.597(23)
722	8.97523(11)	2.809(7)	2.452(23)	1.732(23)	1.609(20)
822	8.99558(14)	2.869(9)	2.577(32)	1.742(23)	1.564(20)

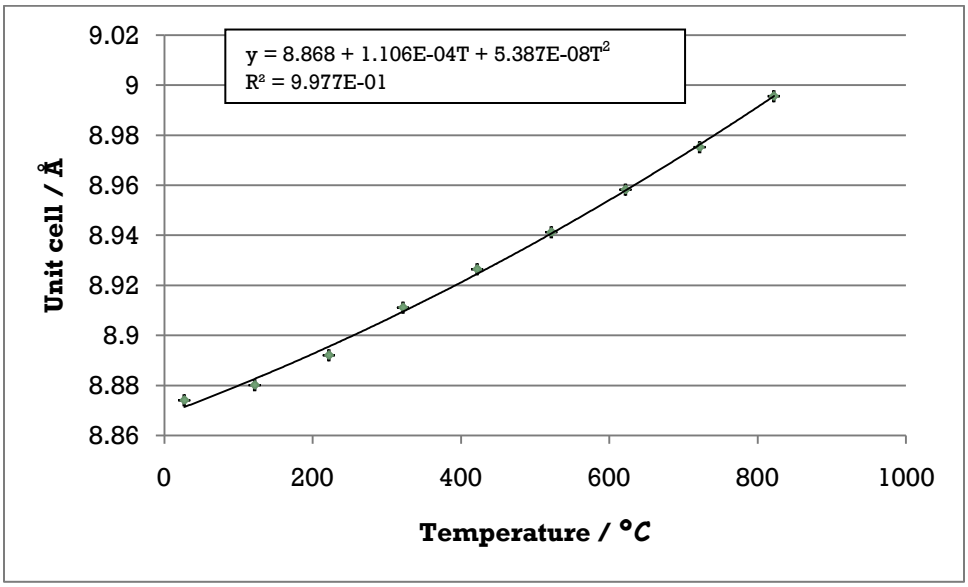

Fig 65: Graph showing change in unit cell size as temperature increases. Error bars represent 1 esd.

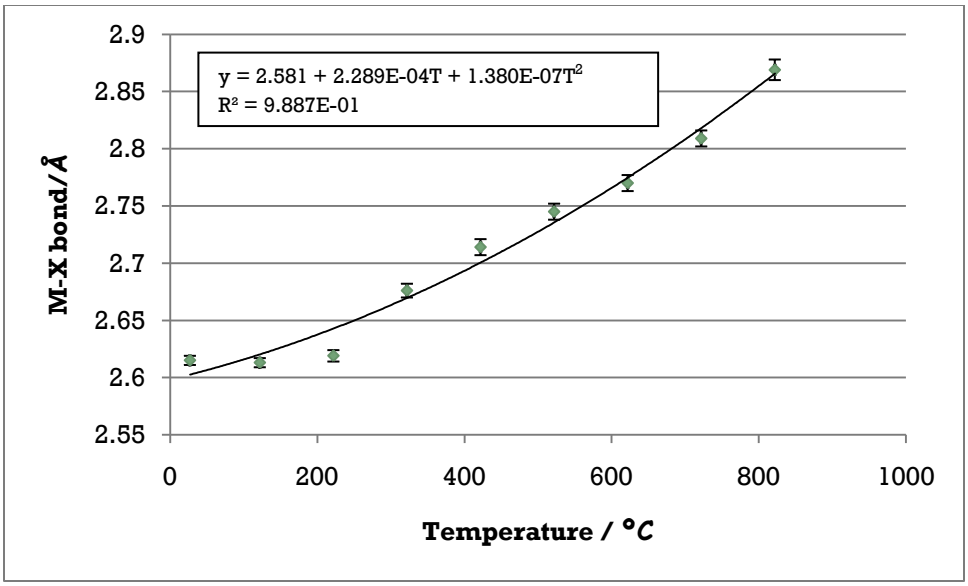

Fig 66: Graph showing change in M-X bond length as temperature increases. Error bars represent 1 esd.

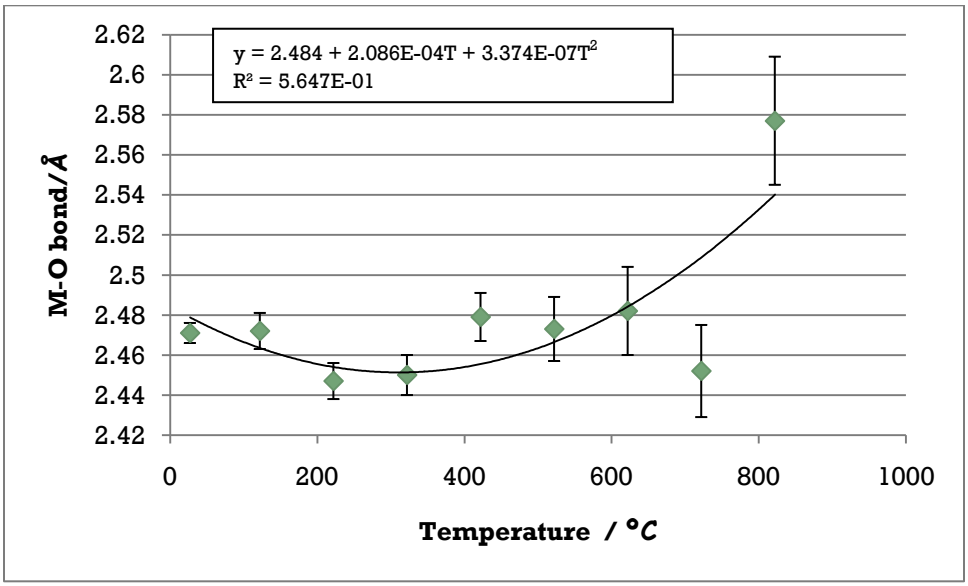

Fig 67: Graph showing change in M-O bond length as temperature increases. Error bars represent 1 esd.

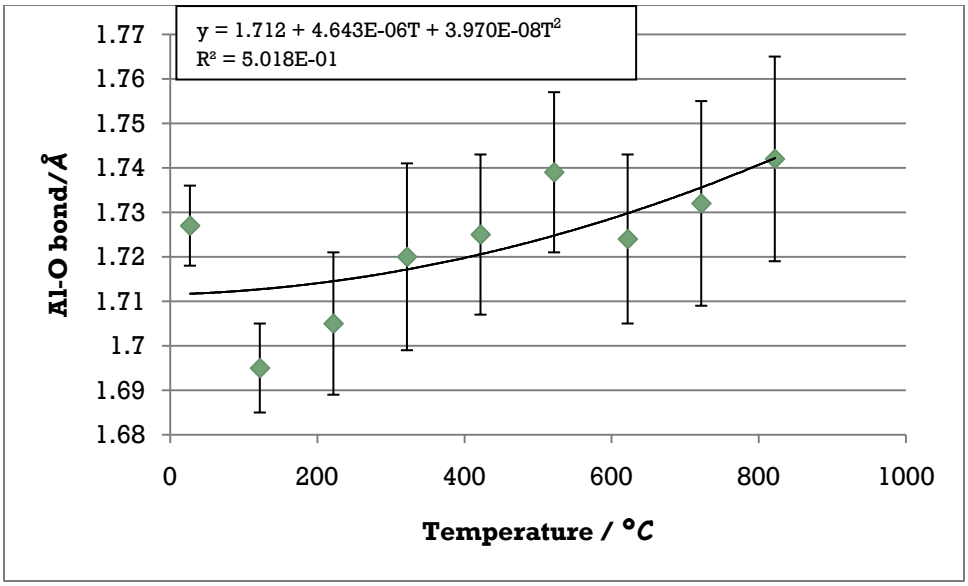

Fig 68: Graph showing change in Al-O bond length as temperature increases. Error bars represent 1 esd.

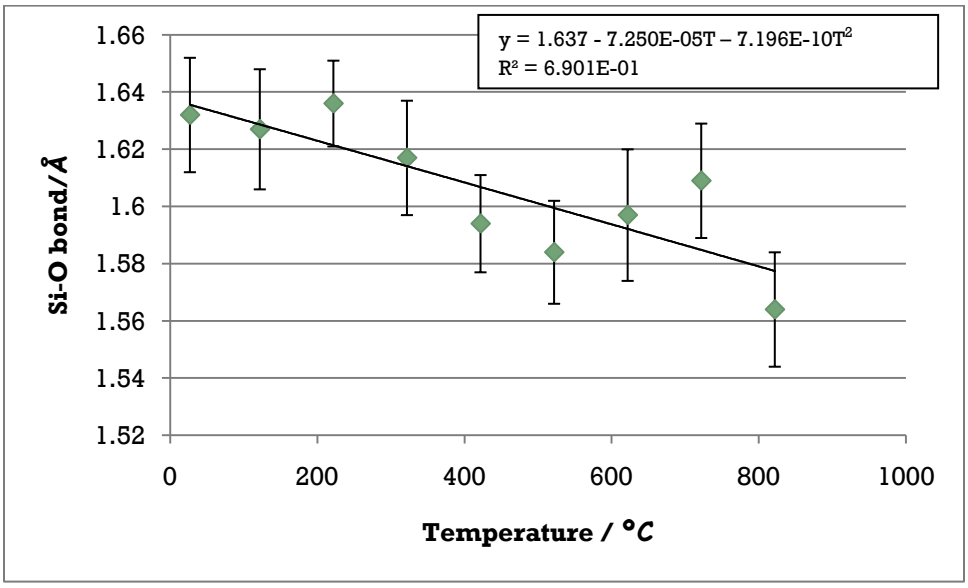

Fig 69: Graph showing change in Si-O bond length as temperature increases. Error bars represent 1 esd

- $Na_4\ Ag_4\ [SiAlO_4]_6.\ Cl_2$

High temperature study was carried out on the ion exchanged chlorosodalite and the atomic coordinate and thermal factor values are shown in Table 29.

Table 29: Atomic coordinate and thermal factor values for $Na_4Ag_4[SiAlO_4]_6Cl_2$ at various temperatures

Temp/ °C	*a* / Å	M		O				Al	Si	X	CHI*2
		x	U_{iso} *x100*	*x*	*y*	*z*	U_{iso} *x100*	U_{iso} *x100*	U_{iso} *x100*	U_{iso} *x100*	
27	8.87543(5)	0.170083(1)	6.905(1)	0.140009(1)	0.440072(2)	0.148847(2)	4.722(1)	6.337(1)	2.959(1)	12.645(2)	1.346
122	8.87764(5)	0.171182(2)	8.038(2)	0.137132(2)	0.441898(2)	0.149926(1)	4.299(2)	3.965(2)	3.622(3)	10.521(2)	1.26
222	8.89005(5)	0.169661(1)	8.567(2)	0.138919(2)	0.444672(1)	0.151060(2)	4.413(1)	3.588(1)	3.053(2)	10.191(1)	1.166
322	8.90863(7)	0.170973(2)	9.248(1)	0.135823(2)	0.445930(1)	0.150086(2)	4.369(2)	4.491(2)	2.977(1)	11.459(2)	1.118
422	8.92231(7)	0.173876(2)	10.263(2)	0.138166(2)	0.449135(2)	0.148336(1)	5.023(5)	4.574(2)	2.403(2)	15.551(2)	1.152
522	8.93673(8)	0.174749(1)	10.676(1)	0.138856(3)	0.450362(3)	0.146653(3)	5.533(3)	4.755(1)	2.017(2)	20.885(1)	1.104
622	8.95045(10)	0.175605(2)	11.686(2)	0.137966(1)	0.449141(2)	0.151293(2)	7.702(4)	3.956(2)	2.874(2)	26.909(2)	1.105
722	8.96386(11)	0.176875(1)	11.513(2)	0.131216(2)	0.454692(1)	0.153746(1)	6.174(2)	4.417(2)	2.147(3)	28.049(2)	1.121
822	8.98335(13)	0.179944 (1)	11.064(1)	0.135121 (11)	0.473005 (5)	0.149144 (12)	7.385 (4)	2.421 (41)	1.932 (38)	32.585 (2)	1.148

As can be seen from Table 30 and Figures 70-74 there is an increase in the size of the unit cell, M-X, and M-O bonds therefore suggesting that there is positive thermal expansion. Within a three esd error there are no consistent correlations in the Al-O and Si-O with composition and temperature.

Table 30: High temperature studies of $Na_4Ag_4[SiAlO_4]_6Cl_2$

Temperature / °C	Unit cell /Å	Na-X bond/Å	Na-O bond/Å	Al-O bond/Å	Si-O bond/Å
27	8.87543(5)	2.428(4)	2.418(9)	1.727(10)	1.623(10
122	8.87764(5)	2.430(4)	2.430(9)	1.744(11)	1.593(10)
222	8.89005(5)	2.466(5)	2.466(10)	1.738(13)	1.594(10)
322	8.90863(7)	2.476(6)	2.476(12)	1.748(15)	1.577(13)
422	8.92231(7)	2.487(6)	2.487(13)	1.719(13)	1.596(14)
522	8.93673(8)	2.497(6)	2.497(15)	1.703(14)	1.609(15)
622	8.95045(10)	2.722(7)	2.481(19)	1.745(23)	1.585(20)
722	8.96386(11)	2.746(8)	2.532(23)	1.788(24)	1.514(21)
822	8.98335(13)	2.801(9)	2.578(22)	1.788(22)	1.534(22)

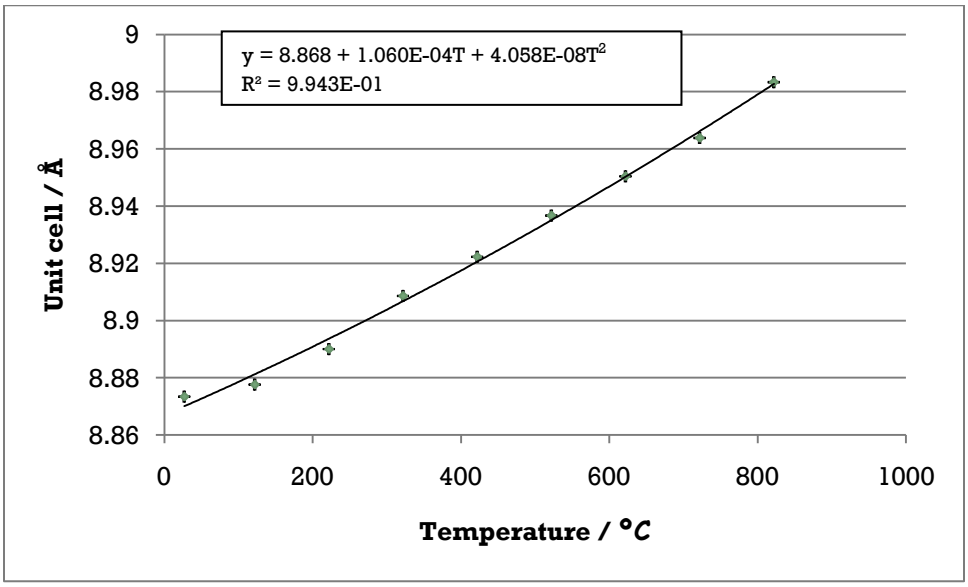

Fig 70: Graph showing change in unit cell size as temperature increases. Error bars represent 1 esd.

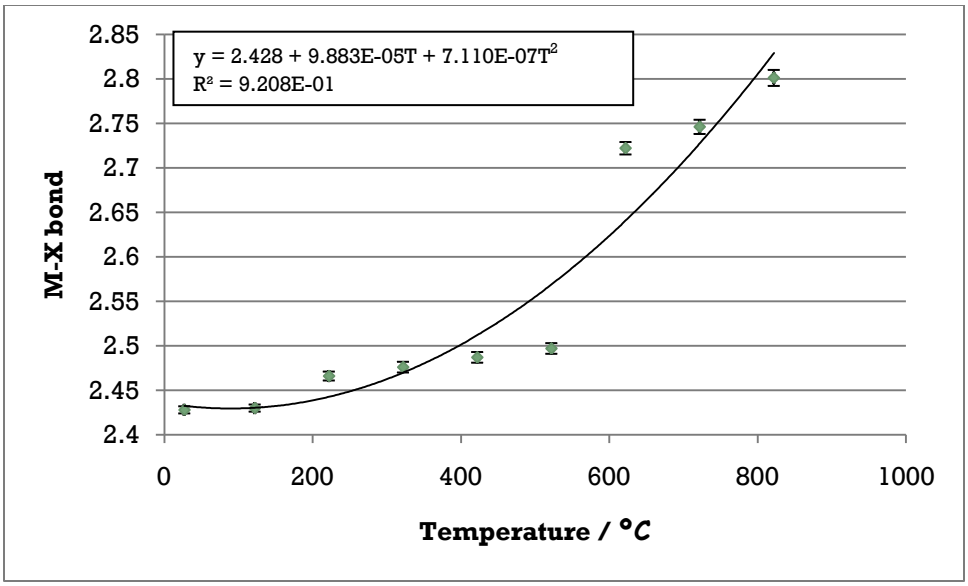

Fig 71: Graph showing change in M-X bond length as temperature increases. Error bars represent 1 esd.

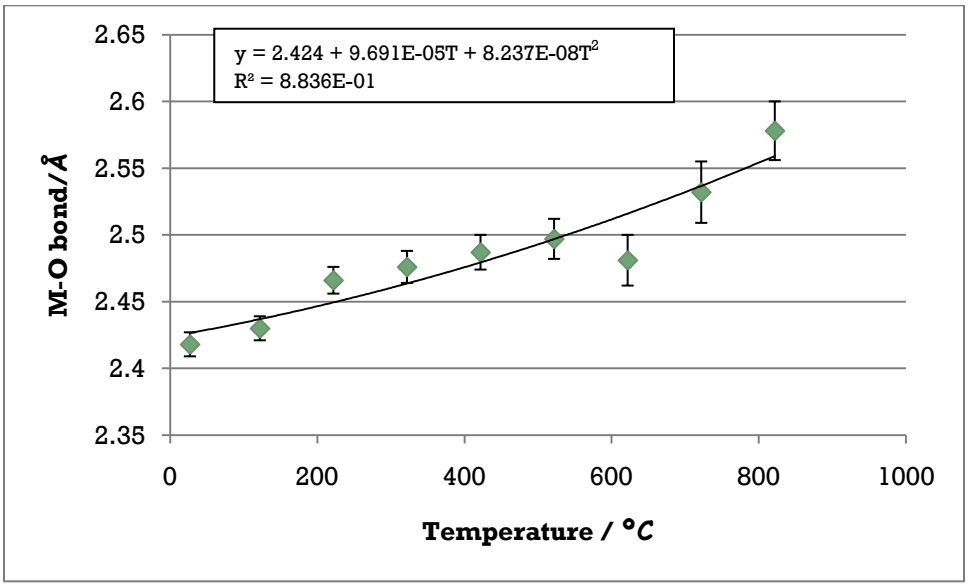

Fig 72: Graph showing change in M-O bond length as temperature increases. Error bars represent 1 esd.

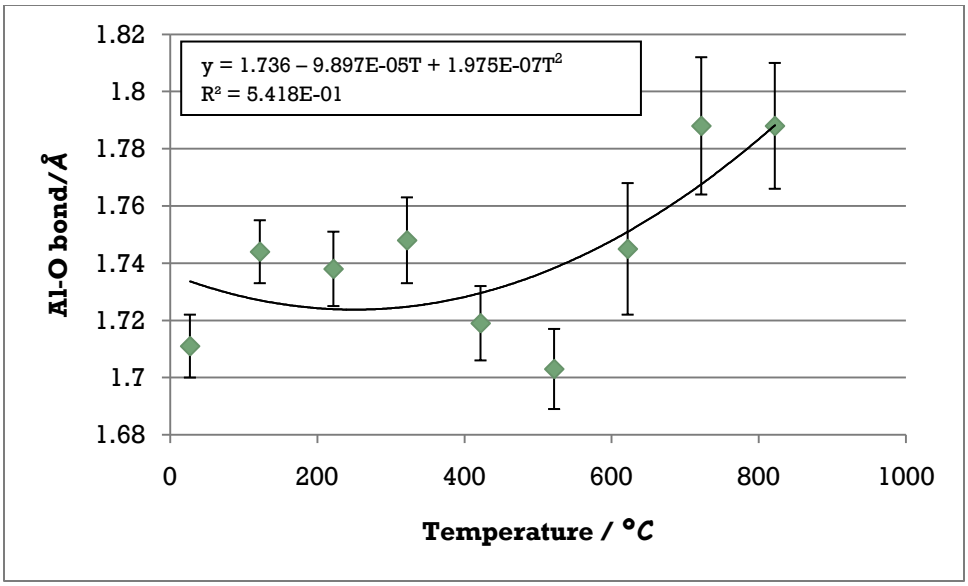

Fig 73: Graph showing change in Al-O bond length as temperature increases. Error bars represent 1 esd.

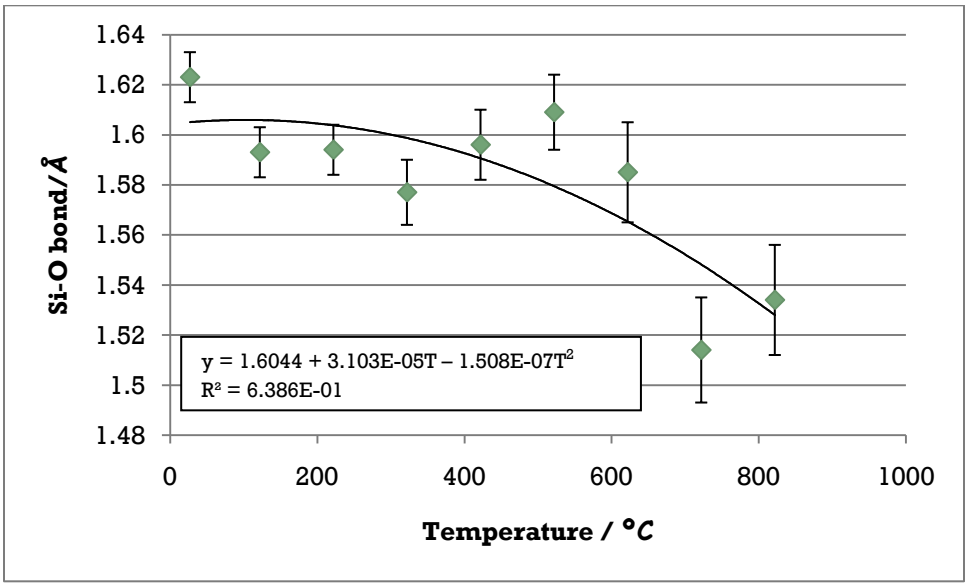

Fig 74: Graph showing change in Si-O bond length as temperature increases. Error bars represent 1 esd.

- $Na_2Ag_6[SiAlO_4]_6Cl_2$

High temperature study was carried out on the ion exchanged chlorosodalite and the atomic coordinate and thermal factor values are shown in Table 31.

Table 31: Atomic coordinate and thermal factor values for $Na_2Ag_6[SiAlO_4]_6Cl_2$ at various temperatures

Temp/ °C	*a* / Å	M		O				Al	Si	X	CHI*2
		X	U_{iso} *x100*	*x*	*y*	*z*	U_{iso} *x100*	U_{iso} *x100*	U_{iso} *x100*	U_{iso} *x100*	
27	8.8297(4)	0.165769 (10)	6.747 (2)	0.144661 (7)	0.438508(1)	0.149302(1)	4.356(1)	4.563(1)	2.683(2)	7.034 (2)	1.347
122	8.87701(4)	0.165259 (2)	7.499 (2)	0.140436 (2)	0.439443(2)	0.154109(2)	3.500(3)	2.070(2)	4.585(2)	6.375(2)	1.199
222	8.88854(5)	0.166069 (2)	9.412 (10)	0.136896(1)	0.443702(2)	0.149939(1)	2.457(2)	3.854(2)	2.582(2)	6.791(3)	1.199
322	8.90528(6)	0.168389 (2)	10.886 (2)	0.135944(2)	0.445938(1)	0.146381(2)	3.204(2)	3.259(3)	2.834(2)	7.487(2)	1.148
422	8.91901(8)	0.171118(2)	11.929(2)	0.134257(2)	0.451605(2)	0.149251(2)	3.354(2)	2.677(1)	1.666(1)	12.320(3)	1.137
522	8.9341(9)	0.174169(1)	13.153(!)	0.132620(3)	0.457669(3)	0.146955(3)	4.155(3)	2.603(1)	2.065(2)	14.239(4)	1.143
622	8.94899(11)	0.176004(2)	12.483(2)	0.127728(1)	0.464331(2)	0.148207(1)	5.378(3)	2.578(1)	1.413(3)	18.931(2)	1.115
722	8.96016(12)	0.179135(1)	12.967(1)	0.126577(2)	0.467713(2)	0.147606(2)	5.006(2)	2.641(2)	1.089(1)	30.318(5)	1.171
822	8.99152(13)	0.180196 (1)	12.913(2)	0.127403(2)	0.481446 (3)	0.145923(2)	7.579(2)	0.33(2)	3.971(2)	39.443 (1)	1.115

As can be seen from Table 32 and Figures 75-79 there is an increase in the size of the unit cell, M-X, and M-O bonds therefore suggesting that there is positive thermal expansion. Within a three esd error there are no consistent correlations in the Al-O and Si-O with composition and temperature.

Table 32: High temperature studies of $Na_2Ag_6[SiAlO_4]_6Cl_2$

Temperature / °C	Unit cell /Å	Na-X bond/Å	Na-O bond/Å	Al-O bond/Å	Si-O bond/Å
27	8.8297(4)	2.548(4)	2.432(9)	1.692(23)	1.656(23)
122	8.8770(4)	2.541(5)	2.446(9)	1.763(12)	1.602(16)
222	8.88854(5)	2.557(5)	2.485(11)	1.743(12)	1.588(9)
322	8.90528(6)	2.597(5)	2.496(10)	1.721(13)	1.597(10)
422	8.9190(8)	2.643(6)	2.531(12)	1.739(15)	1.558(11)
522	8.9341(9)	2.695(7)	2.571(11)	1.722(12)	1.547(20)
622	8.94899(11)	2.728(8)	2.628(15)	1.749(20)	1.496(15)
722	8.96016(12)	2.780(9)	2.643(23)	1.748(22)	1.487(16)
822	8.99152(13)	2.806(10)	2.770(24)	1.722(29)	1.489(15)

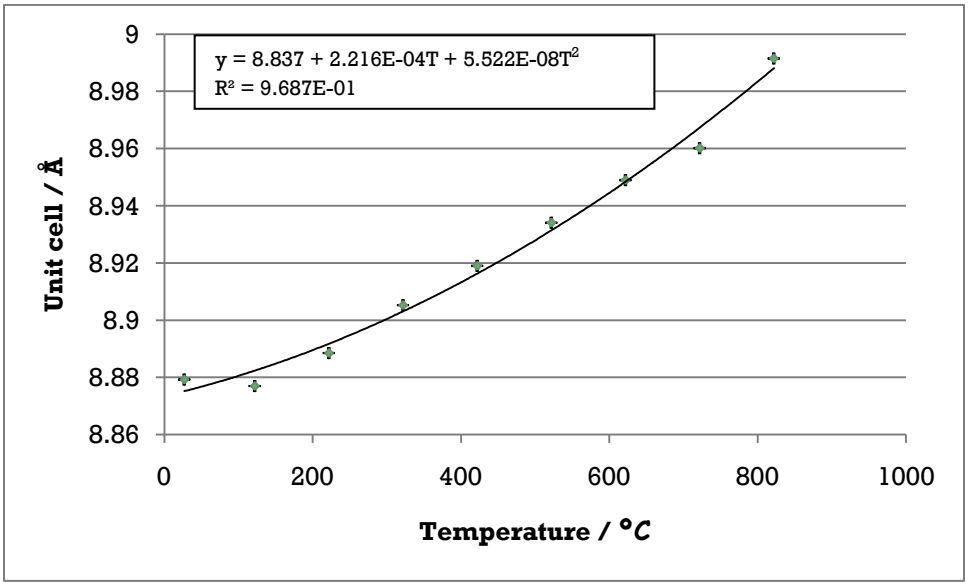

Fig 75: Graph showing change in unit cell size as temperature increases. Error bars represent 1 esd.

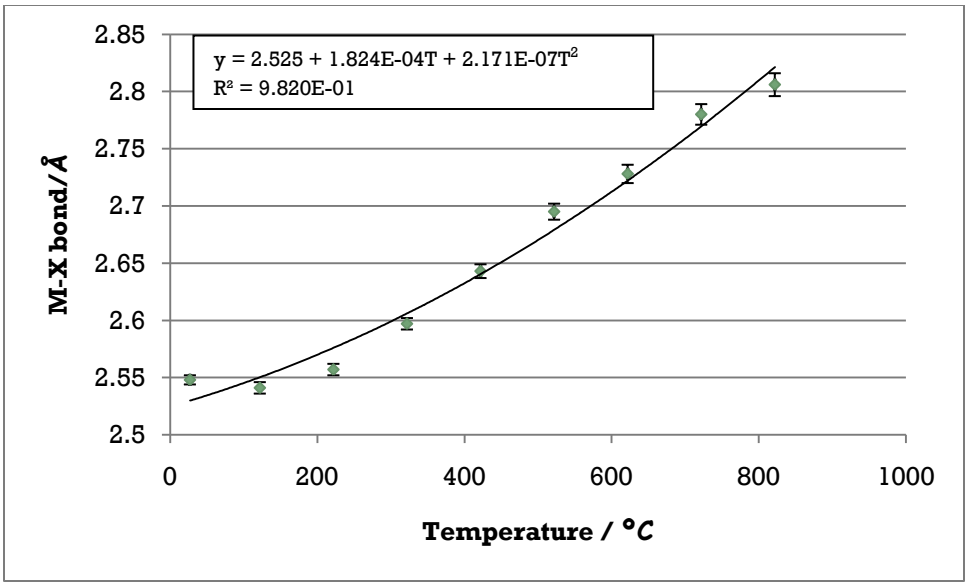

Fig 76: Graph showing change in M-X bond length as temperature increases. Error bars represent 1 esd.

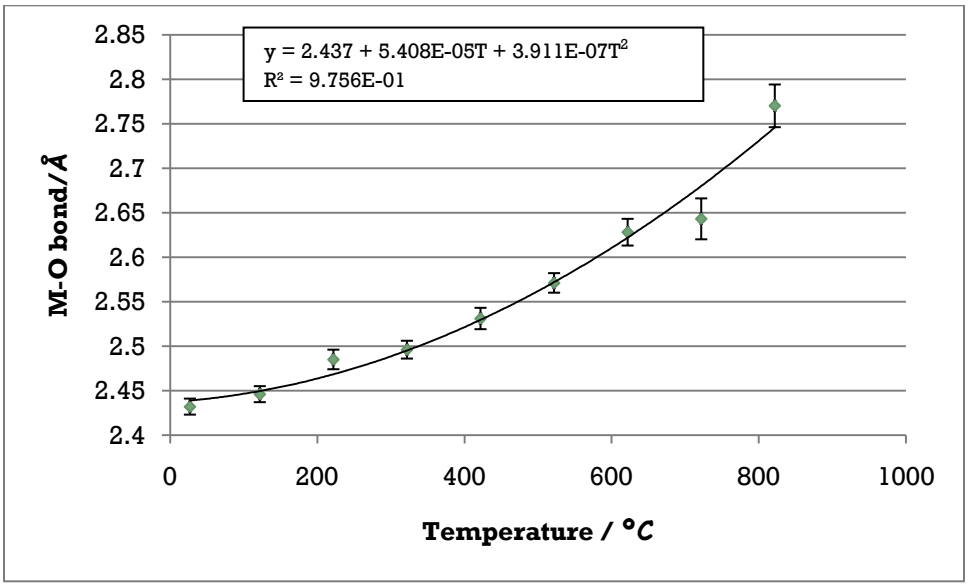

Fig 77: Graph showing change in M-O bond length as temperature increases. Error bars represent 1 esd.

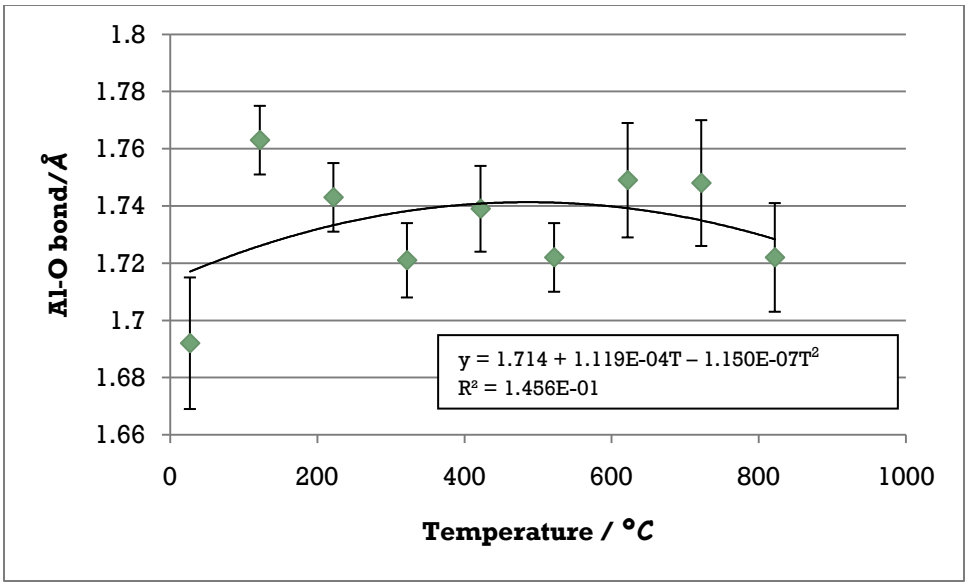

Fig 78: Graph showing change in Al-O bond length as temperature increases. Error bars represent 1 esd.

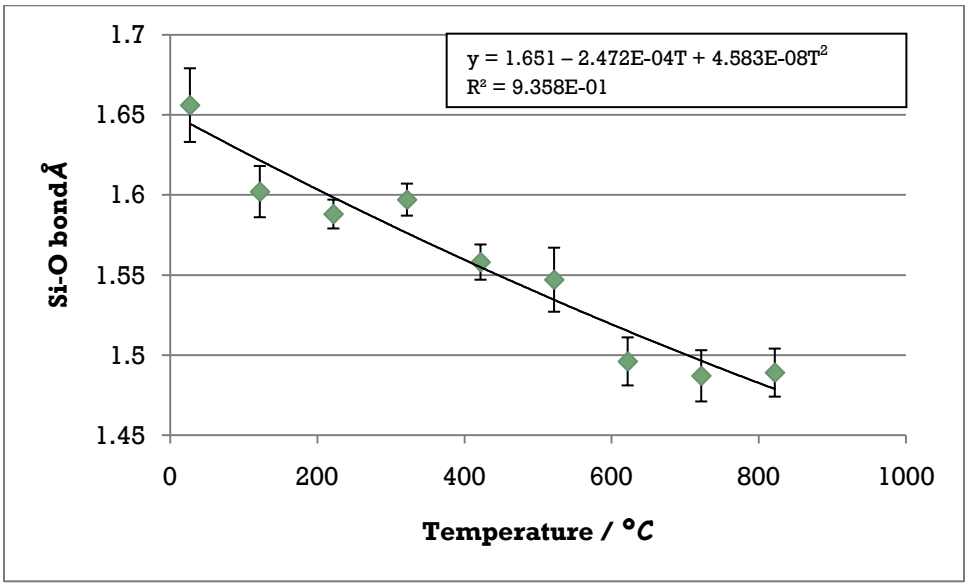

Fig 79: Graph showing change in Si-O bond length as temperature increases. Error bars represent 1 esd.

- $Na_0Ag_8[SiAlO_4]_6Cl_2$

High temperature study was carried out on the ion exchanged chlorosodalite and the atomic coordinate and thermal factor values are shown in Table 33.

Table 33: Atomic coordinate and thermal factor values for $Na_0Ag_8[SiAlO_4]_6Cl_2$ at various temperatures

Temp/ °C	*a* / Å	M		O				Al	Si	X	CHI* 2
		x	U_{iso} *x100*	*x*	*y*	*z*	U_{iso} *x100*	U_{iso} *x100*	U_{iso} *x100*	U_{iso} *x100*	
27	8.887969(5)	0.164247(36)	6.648 (22)	0.136913 (3)	0.439771 (16)	0.150429(3)	0.074(33)	0.956(5)	0.297 (5)	1.484 (19)	1.310
122	8.885130(5)	0.164828(28)	8.080 (23)	0.137216 (1)	0.442007 (13)	0.147987(1)	0.918(30)	0.551(4)	0.073(4)	3.548 (8)	1.233
222	8.865712(5)	0.164619(30)	9.791 (8)	0.133833 (4)	0.444913 (6)	0.150453(2)	0.258(30)	0.845(5)	0.609 (3)	2.701 (8)	1.235
322	8.914490(6)	0.164896(44)	10.497 (1)	0.132504 (20)	0.447228 (14)	0.148373(26)	0.411(38)	0.592(2)	0.156 (3)	2.566 (24)	1.249
422	8.912461(7)	0.164133 (1)	11.775 (1)	0.130159 (1)	0.451057 (3)	0.155277(1)	0.301(1)	1.094(1)	0.157 (1)	3.527 (1)	1.233
522	8.935641(8)	0.165643 (1)	12.762(11	0.128834 (23)	0.455205 (17)	0.149918(21)	0.375(36)	1.697(9)	0.215 (5)	7.454 (14)	1.314
622	8.9667(9)	0.165530 (3)	13.691 (1)	0.129035 (3)	0.454461 (2)	0.155410(2)	0.500(1)	1.243(1)	0.175 (1)	7.721 (1)	1.330
722	8.9789(10)	0.161039(45)	13.398 (4)	0.138223 (22)	0.457985 (6)	0.162969(19)	0.797(12)	0.511(4)	0.081 (4)	9.040 (2)	1.328
822	8.9947(11)	0.157044(22)	11.378 (3)	0.146453 (18)	0.459279 (5)	0.172337(8)	0.247 (9)	0.026(4)	0.189 (4)	16.631(13)	1.269

As can be seen from Table 34 and Figures 80-84 there is an increase in the size of the unit cell, M-X, and M-O bonds therefore suggesting that there is positive thermal expansion. Within a three esd error there are no consistent correlations in the Al-O and Si-O with composition and temperature.

Table 34: High temperature studies of $Na_0Ag_8[SiAlO_4]_6Cl_2$

Temperature / °C	Unit cell /Å	Na-X bond/Å	Na-O bond/Å	Al-O bond/Å	Si-O bond/Å
27	8.887969(5)	2.517(5)	2.431(10)	1.747(24)	1.613(24)
122	8.885130(5)	2.571(5)	2.446(11)	1.723(22)	1.625(20)
222	8.865712(5)	2.573(6)	2.475(12)	1.752(25)	1.585(9)
322	8.914490(6)	2.603(7)	2.495(13)	1.731(20)	1.591(12)
422	8.912461(7)	2.647(8)	2.517(15)	1.734(21)	1.592(11)
522	8.935641(8)	2.655(8)	2.612(20)	1.712(4)	1.593(10)
622	8.9667(9)	2.773(9)	2.634(22)	1.784(24)	1.437(15)
722	8.9789(10)	2.801(10)	2.764(24)	1.779(22)	1.439(12)
822	8.9947(11)	2.912(12)	2.880(26)	1.765(21)	1.432(13)

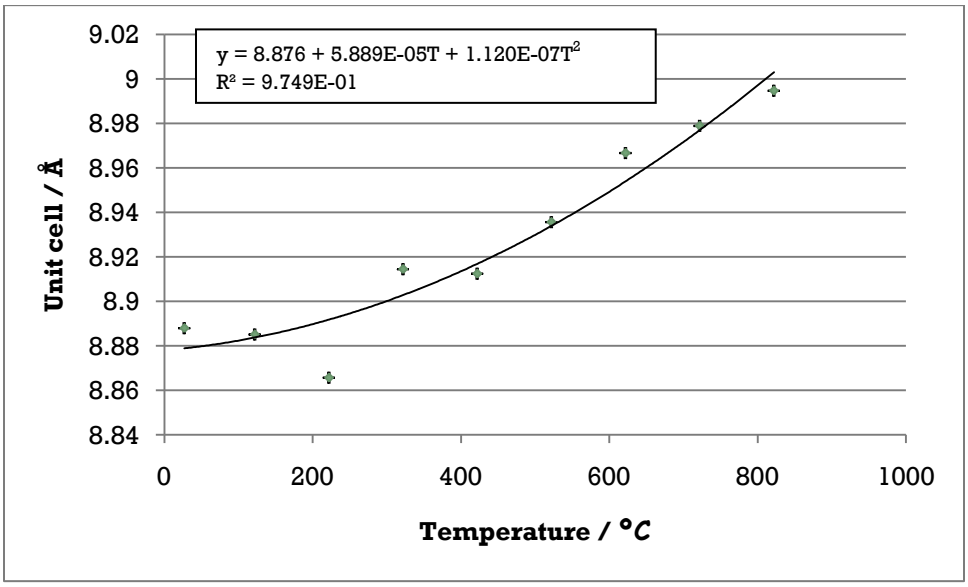

Fig 80: Graph showing change in unit cell size as temperature increases. Error bars represent 1 esd.

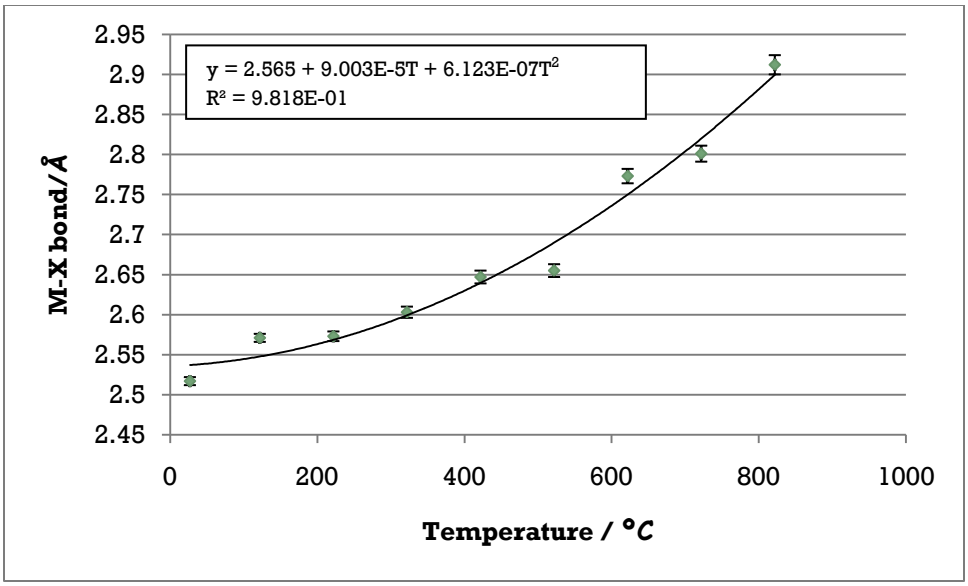

Fig 81: Graph showing change in M-X bond length as temperature increases. Error bars represent 1 esd.

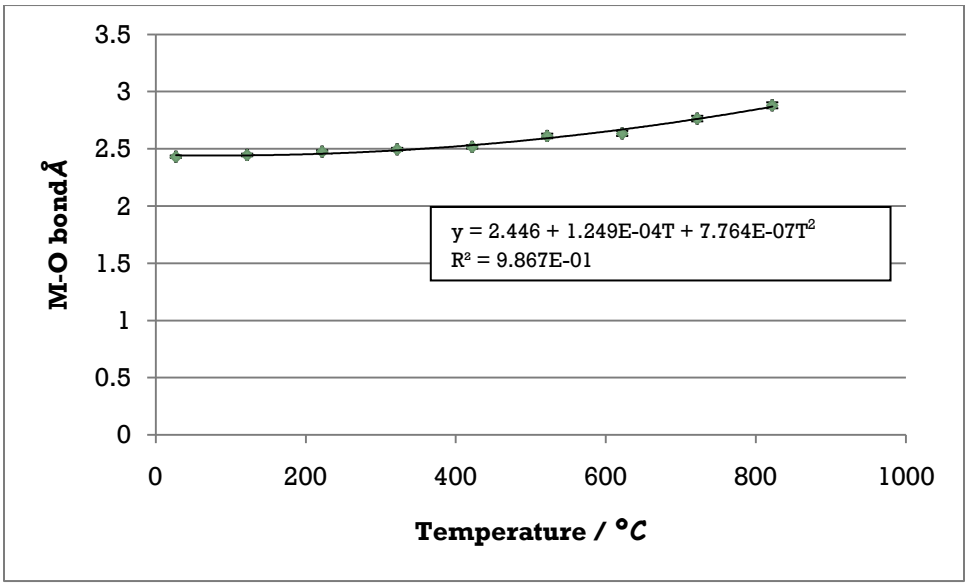

Fig 82: Graph showing change in M-O bond length as temperature increases. Error bars represent 1 esd.

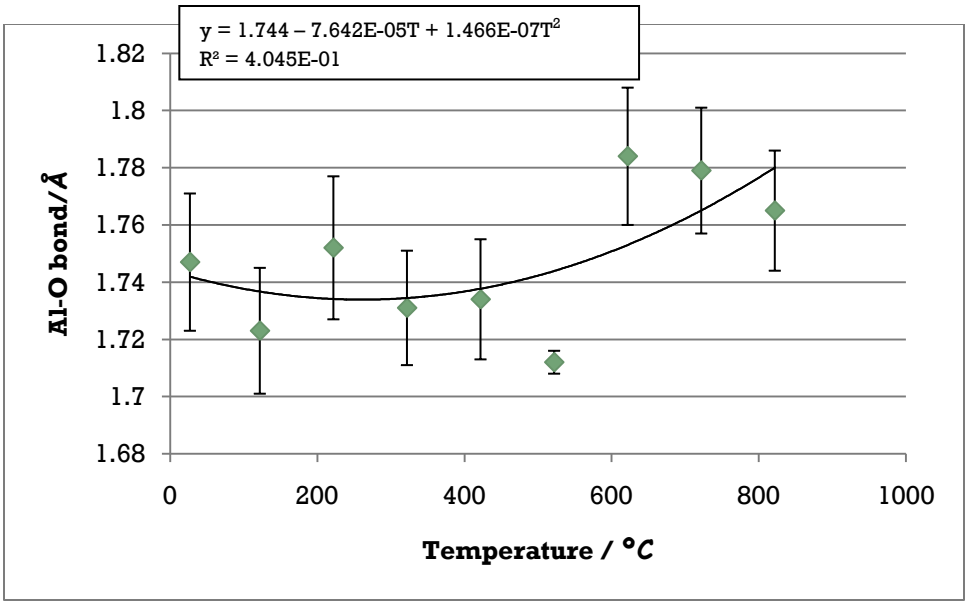

Fig 83: Graph showing change in Al-O bond length as temperature increases. Error bars represent 1 esd.

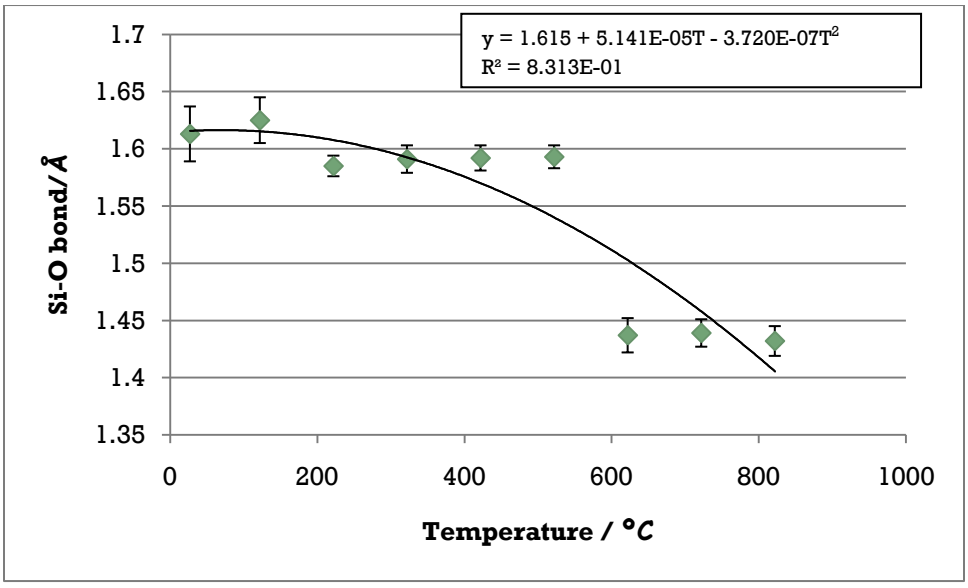

Fig 84: Graph showing change in Si-O bond length as temperature increases. Error bars represent 1 esd.

5.7. Discussion of Thermal expansion coefficients

The least squares fits of second order polynomials, $a = a_0 + bT + cT^2$ where T is in ºC, to the data are given as an insert on each graph in the sections above. Tables 35-37 show a summary of the regression data for all systems for unit cell, M-X bond and M-O bond lengths.

Table 35: Regression data of unit cell size for thermal expansion curves

Sodalite	**a_0 (Å)**	**10^6b**	**10^8c**	**R**
$Na_8Ag_0[SiAlO_4]_6Br_2$	8.922	122.7	7.553	0.9978
$Na_6Ag_2[SiAlO_4]_6Br_2$	8.918	111.1	7.617	0.9955
$Na_4Ag_4[SiAlO_4]_6Br_2$	8.911	94.60	7.675	0.9983
$Na_2Ag_6[SiAlO_4]_6Br_2$	8.909	94.67	6.703	0.9972
$Na_0Ag_8[SiAlO_4]_6Br_2$	8.913	71.23	9.123	0.9955
$Na_8Ag_0[SiAlO_4]_6Cl_2$	8.875	125.7	4.15	0.9996
$Na_6Ag_2[SiAlO_4]_6Cl_2$	8.868	110.6	5.387	0.9998
$Na_4Ag_4[SiAlO_4]_6Cl_2$	8.868	106.0	4.058	0.9971
$Na_2Ag_6[SiAlO_4]_6Cl_2$	8.837	221.6	5.522	0.9842
$Na_0Ag_8[SiAlO_4]_6Cl_2$	8.876	58.89	11.2	0.9749
$Na_8Ag_0[SiAlO_4]_6I_2$	8.991	162.5	5.059	0.9997

Table 36: Regression data of M-X bond for thermal expansion curves

Sodalite	**$a_{0\,(}$Å)**	**10^6b**	**10^8c**	**R**
$Na_8Ag_0[SiAlO_4]_6Br_2$	2.884	355.9	12.96	0.999
$Na_6Ag_2[SiAlO_4]_6Br_2$	2.729	176.4	22.22	0.9929
$Na_4Ag_4[SiAlO_4]_6Br_2$	2.621	203.6	21.21	0.9946
$Na_2Ag_6[SiAlO_4]_6Br_2$	2.633	170.9	16.73	0.9913
$Na_0Ag_8[SiAlO_4]_6Br_2$	2.670	102.8	8.532	0.9950
$Na_8Ag_0[SiAlO_4]_6Cl_2$	2.733	315.0	0.939	0.9887
$Na_6Ag_2[SiAlO_4]_6Cl_2$	2.581	228.9	13.80	0.9943
$Na_4Ag_4[SiAlO_4]_6Cl_2$	2.428	98.83	71.10	0.9595
$Na_2Ag_6[SiAlO_4]_6Cl_2$	2.525	182.4	21.71	0.9910
$Na_0Ag_8[SiAlO_4]_6Cl_2$	2.565	90.03	61.2	0.9818
$Na_8Ag_0[SiAlO_4]_6I_2$	3.088	344.1	17.2	0.9886

Table 37: Regression data of M-O bond for thermal expansion curves

Sodalite	**a_0 (Å)**	**10^6b**	**10^8c**	**R**
$Na_8Ag_0[SiAlO_4]_6Br_2$	2.342	131.1	5.568	0.997
$Na_6Ag_2[SiAlO_4]_6Br_2$	2.433	28.00	13.16	0.9747
$Na_4Ag_4[SiAlO_4]_6Br_2$	2.512	114.8	19.80	0.6071
$Na_2Ag_6[SiAlO_4]_6Br_2$	2.447	80.83	18.51	0.9246
$Na_0Ag_8[SiAlO_4]_6Br_2$	2.481	26.42	56.56	0.9909
$Na_8Ag_0[SiAlO_4]_6Cl_2$	2.352	20.7	10.79	0.9738
$Na_6Ag_2[SiAlO_4]_6Cl_2$	2.484	208.6	33.74	0.7511
$Na_4Ag_4[SiAlO_4]_6Cl_2$	2.424	96.91	8.237	0.940
$Na_2Ag_6[SiAlO_4]_6Cl_2$	2.437	54.08	39.11	0.9877
$Na_0Ag_8[SiAlO_4]_6Cl_2$	2.446	124.90	77.64	0.9867
$Na_8Ag_0[SiAlO_4]_6I_2$	2.344	73.5	32.9	0.9884

In a previous study by Hassan et al (2004) on sodium chlorosodalites, a least squares fit gave:

$a = 8.8837 + 9.8103E\text{-}05T + 4.8138E\text{-}08T^2$ and $R^2 = 0.9995$

My least squares fit for the same system was:

$a = 8.875 + 1.257E\text{-}4T + 4.15E\text{-}8T^2$ and $R^2 = 0.9996$

The derived values are similar, and probably within acceptable errors of each other.

Henderson and Taylor (1978) also studied this system and reported a least squares fit of:

$a = 8.879 + 9.18E\text{-}6T + 9.39E\text{-}9T^2$

Hassan et al (2004) did not discuss the discrepancy in their thermal expansion coefficients with that of Henderson and Taylor (1978), but they did note that the raw data matches reasonably closely. It is not possible to offer an explanation for this, even if Henderson and Taylor (1978) used temperature in Kelvin rather than Celsius it would not provide a good fit to the data.

Henderson and Taylor (1978) also fitted thermal expansion curves by for the sodium bromo and iodosodalites. The fit for the bromosodalite and iodosodalite respectively were:

$a = 8.9313 + 13.31E\text{-}6T + 9.81E\text{-}15T^4$

$a = 9.0066 + 7.98E\text{-}6T + 17.32E\text{-}9T^2$

My values for the bromosodalite and the iodosodalite respectively were:

$a = 8.992 + 12.27E\text{-}6T + 7.55E\text{-}8T^2$

$a = 8.991 + 162.5E\text{-}6T + 5.059E\text{-}8T^2$

There are again very large and unexplainable discrepancies.

The final point to discuss is how the thermal expansion coefficients change when the halide is fixed and silver is substituted by sodium. For the bromosodalite there seems to be a clear trend, with a steady decrease in the linear term. Unfortunately there is no clear trend for the chlorosodalite or when examining the M-X or M-O distance changes in either system. It is possible that these are due to insufficient data quality and better diffraction patterns, such as would be available from a synchrotron source, and are necessary.

Except for one outlier, Na_2Ag_6 chloride, you see a decrease in the unit cell coefficient of thermal expansion as you substitute Ag for Na (Table 35). In all cases this is due to the greater expansion of the M-X bond rather than M-O bond, but there is no clear trend in how the M-X or M-O values change as a function of the Na/Ag composition.

5.8. Discussion of tetrahedral tilt angles

Bromosodalites

As shown in Tables 38-43, there are changes in the AlO_4 and SiO_4 tilt angles for the bromosodalites as you change the Na/Ag ratio, but there is no apparent consistent trend except that, for all systems, the tilts decrease with increasing temperature .

Table 38: Calculated tilt angles and the percentage mean change for the Na/Ag bromosodalites

Sodalite	27°C			822°C			% change
	SiO4 tilt	AlO4 tilt	mean	SiO4 tilt	AlO4 tilt	mean	
$Na_{7.2}[SiAlO_4]_6Br_2$	21.9	20.3	21.1	13.5	12.2	12.8	39.1
$Na_{5.7}Ag_{2.3}[SiAlO_4]_6Br_2$	21.0	19.6	20.3	16.2	15.0	15.6	23.1
$Na_4Ag_4[SiAlO_4]_6Br_2$	20.1	18.5	19.3	19.4	16.6	18.0	6.8
$Na_{2.7}Ag_{5.3}[SiAlO_4]_6Br_2$	20.6	18.8	19.7	17.2	13.8	15.5	21.4
$Na_{0.3}Ag_{7.7}[SiAlO_4]_6Br_2$	21.6	19.2	20.4	-1.8	-1.5	-1.6	108.0

Table 39: Atomic coordinates for oxygen and calculated tilt angles for $Na_8[SiAlO_4]_6Br_2$ as the temperature is increased.

Temperature °C	x	y	z	SiO4 tilt	AlO4 tilt	mean
27	0.140608	0.44353	0.152567	21.9	20.3	21.1
122	0.140059	0.44559	0.153349	21.2	19.5	20.4
222	0.139596	0.448834	0.151994	20.1	18.6	19.4
322	0.136885	0.451066	0.152323	19.7	17.8	18.7
422	0.1388	0.454736	0.15399	18.1	16.4	17.2
522	0.134761	0.456109	0.153741	18.0	15.9	17.0
622	0.134586	0.459309	0.151922	16.8	15.0	15.9
722	0.13543	0.462693	0.152863	15.4	13.7	14.6
822	0.137266	0.46701	0.152892	13.5	12.2	12.8

Table 40: Atomic coordinates for oxygen and calculated tilt angles for $Na_6Ag_2[SiAlO_4]_6Br_2$ as the temperature is increased.

Temperature °C	x	y	z	SiO4 tilt	AlO4 tilt	mean
27	0.140672	0.445956	0.151873	21.0	19.6	20.3
122	0.139025	0.446467	0.151274	21.1	19.5	20.3
222	0.139743	0.446681	0.153267	20.9	19.2	20.0
322	0.138961	0.448638	0.153674	20.3	18.5	19.4
422	0.139813	0.44961	0.152601	19.8	18.3	19.0
522	0.140125	0.452245	0.152313	18.8	17.4	18.1
622	0.138829	0.454942	0.153224	18.0	16.4	17.2
722	0.140514	0.457448	0.153458	16.8	15.5	16.2
822	0.138726	0.459596	0.150877	16.2	15.0	15.6

Table 41: Atomic coordinates for oxygen and calculated tilt angles for $Na_4Ag_4[SiAlO_4]_6Br_2$ as the temperature is increased.

Temperature °C	x	y	z	SiO4 tilt	AlO4 tilt	mean
27	0.137652	0.44968	0.150665	20.1	18.5	19.3
122	0.136444	0.450546	0.147277	19.9	18.6	19.2
222	0.140112	0.446567	0.149742	20.9	19.6	20.3
322	0.135829	0.448397	0.151581	20.8	18.8	19.8
422	0.136307	0.450183	0.151776	20.1	18.2	19.1
522	0.135593	0.453095	0.145521	19.1	17.9	18.5
622	0.133084	0.457505	0.144925	17.7	16.3	17.0
722	0.129202	0.46011	0.146623	17.2	15.2	16.2
822	0.12484	0.456091	0.14766	19.4	16.6	18.0

Table 42: Atomic coordinates for oxygen and calculated tilt angles for $Na_2Ag_6[SiAlO_4]_6Br_2$ as the temperature is increased.

Temperature °C	x	y	z	SiO4 tilt	AlO4 tilt	mean
27	0.141994	0.446707	0.156683	20.6	18.8	19.7
122	0.138168	0.44423	0.157421	22.0	19.5	20.7
222	0.138004	0.449894	0.151534	20.0	18.3	19.1
322	0.133682	0.447229	0.150753	21.5	19.3	20.4
422	0.132665	0.451448	0.150514	20.1	17.9	19.0
522	0.13278	0.455079	0.150957	18.7	16.6	17.6
622	0.12938	0.458199	0.150889	17.9	15.5	16.7
722	0.130827	0.469932	0.147557	12.9	11.5	12.2
822	0.118134	0.463502	0.148938	17.2	13.8	15.5

Table 43: Atomic coordinates for oxygen and calculated tilt angles for $Ag_8[SiAlO_4]_6Br_2$ as the temperature is increased.

Temperature °C	x	y	z	SiO4 tilt	AlO4 tilt	mean
27	0.13436	0.446899	0.152689	21.6	19.2	20.4
122	0.13099	0.448996	0.154423	21.3	18.3	19.8
222	0.127361	0.453732	0.150776	20.0	17.1	18.5
322	0.124564	0.455521	0.148956	19.7	16.6	18.1
422	0.128967	0.455674	0.145764	19.0	16.9	17.9
522	0.125004	0.467565	0.1482	14.5	12.3	13.4
622	0.124608	0.470993	0.146088	13.1	11.2	12.2
722	0.120948	0.484213	0.148558	7.4	6.1	6.8
822	0.121466	0.503733	0.142762	-1.8	-1.5	-1.6

Chlorosodalites

As for the bromosodalites shown in Tables 44-49, there is again only one consistent trend in tilt angles for the chlorosodalites – for any system the tilts decrease with temperature.

Table 44: Calculated tilt angles and the percentage mean change for the Na/Ag chlorosodalites

Sodalite	27°C			822 C			% change
	SiO4 tilt	AlO4 tilt	mean	SiO4 tilt	AlO4 tilt	mean	
$Na_{7.2}[SiAlO_4]_6Cl_2$	23.0	21.7	22.4	17.9	16.1	17.0	24.2
$Na_{5.7}Ag_{2.3}[SiAlO_4]_6Cl_2$	21.2	20.5	20.9	17.1	15.5	16.3	21.9
$Na_{3.9}Ag_{4.1}[SiAlO_4]_6Cl_2$	23.2	21.9	22.6	11.3	10.3	10.8	52.2
$Na_{2.2}Ag_{5.8}[SiAlO_4]_6Cl_2$	23.0	22.4	22.7	8.3	7.2	7.8	65.8
$Na_{0.6}Ag_{7.4}[SiAlO_4]_6Cl_2$	23.7	21.8	22.8	15.5	13.3	14.4	36.7

Table 45: Atomic coordinates for oxygen and calculated tilt angles for $Na_8[SiAlO_4]_6Cl_2$ as the temperature is increased.

Temperature °C	x	y	z	SiO4 tilt	AlO4 tilt	mean
27	0.141439	0.439844	0.150827	23.0	21.7	22.4
122	0.138466	0.439672	0.151295	23.5	21.7	22.6
222	0.140288	0.441537	0.153043	22.6	20.9	21.8
322	0.140942	0.444006	0.151873	21.7	20.2	21.0
422	0.141096	0.444623	0.153072	21.4	19.9	20.7
522	0.138927	0.448856	0.152083	20.2	18.6	19.4
622	0.141275	0.451107	0.154302	19.1	17.6	18.3
722	0.139193	0.45224	0.15377	18.9	17.3	18.1
822	0.139365	0.455072	0.155685	17.9	16.1	17.0

Table 46: Atomic coordinates for oxygen and calculated tilt angles for $Na_6Ag_2[SiAlO_4]_6Cl_2$ as the temperature is increased.

Temperature °C	x	y	z	SiO4 tilt	AlO4 tilt	mean
27	0.142286	0.444855	0.147289	21.2	20.5	20.9
122	0.142476	0.446011	0.148245	20.8	20.0	20.4
222	0.141537	0.442797	0.147366	22.0	21.2	21.6
322	0.140715	0.445288	0.149385	21.2	20.1	20.7
422	0.139255	0.449718	0.150178	19.9	18.5	19.2
522	0.13806	0.449812	0.150967	20.0	18.4	19.2
622	0.138838	0.451164	0.149312	19.4	18.1	18.7
722	0.139734	0.449045	0.149904	20.0	18.8	19.4
822	0.136874	0.457949	0.15145	17.1	15.5	16.3

Table 47: Atomic coordinates for oxygen and calculated tilt angles for $Na_4Ag_4[SiAlO_4]_6Cl_2$ as the temperature is increased.

Temperature °C	x	y	z	SiO4 tilt	AlO4 tilt	mean
27	0.140009	0.440072	0.148847	23.2	21.9	22.6
122	0.137132	0.441898	0.149926	23.0	21.2	22.1
222	0.138919	0.444672	0.15106	21.7	20.1	20.9
322	0.135823	0.44593	0.150086	21.7	19.8	20.8
422	0.138166	0.449135	0.148336	20.2	18.9	19.6
522	0.138856	0.450362	0.146653	19.7	18.7	19.2
622	0.137966	0.449141	0.151293	20.2	18.6	19.4
722	0.131216	0.454692	0.153746	19.0	16.4	17.7
822	0.135121	0.473005	0.149144	11.3	10.3	10.8

Table 48: Atomic coordinates for oxygen and calculated tilt angles for $Na_2Ag_6[SiAlO_4]_6Cl_2$ as the temperature is increased.

Temperature °C	x	y	z	SiO4 tilt	AlO4 tilt	mean
27	0.144661	0.438508	0.149302	23.0	22.4	22.7
122	0.140436	0.439443	0.154109	23.3	21.5	22.4
222	0.136896	0.443702	0.149939	22.4	20.6	21.5
322	0.135944	0.445938	0.146381	21.7	20.3	21.0
422	0.134257	0.451605	0.149251	19.8	18.0	18.9
522	0.13262	0.457669	0.146955	17.7	16.1	16.9
622	0.127728	0.464331	0.148207	15.6	13.5	14.6
722	0.126577	0.467713	0.147606	14.3	12.3	13.3
822	0.127403	0.481446	0.145923	8.3	7.2	7.8

Table 49: Atomic coordinates for oxygen and calculated tilt angles for $Ag_8[SiAlO_4]_6Cl_2$ as the temperature is increased.

Temperature °C	x	y	z	SiO4 tilt	AlO4 tilt	mean
27	0.136913	0.439771	0.150429	23.7	21.8	22.8
122	0.137216	0.442007	0.147987	22.9	21.4	22.2
222	0.133833	0.444913	0.150453	22.4	20.1	21.2
322	0.132504	0.447228	0.148373	21.7	19.6	20.6
422	0.130159	0.451057	0.155277	20.6	17.5	19.1
522	0.128834	0.455205	0.149918	19.2	16.6	17.9
622	0.129035	0.454461	0.15541	19.4	16.3	17.9
722	0.138223	0.457985	0.162969	16.9	14.5	15.7
822	0.146453	0.459279	0.172337	15.5	13.3	14.4

Iodosodalite

As shown in Table 50, a decrease in the tilt angles is observed in the iodosodalites as the temperature is increased.

Table 50: Atomic coordinates for oxygen and calculated tilt angles for $Na_8[SiAlO_4]_6I_2$ as the temperature is increased.

Temperature °C	x	y	z	SiO4 tilt	AlO4 tilt	mean
27	0.141827	0.448432	0.158158	20.0	18.1	19.0
122	0.141001	0.450155	0.157477	19.5	17.6	18.5
222	0.144283	0.453482	0.158045	17.9	16.4	17.1
322	0.143235	0.453482	0.160572	18.0	16.2	17.1
422	0.14289	0.456286	0.158982	17.0	15.4	16.2
522	0.143742	0.459252	0.159458	15.8	14.3	15.1
622	0.145288	0.466366	0.161623	13.0	11.8	12.4
722	0.145876	0.469104	0.160167	12.0	10.9	11.4
822	0.145287	0.47732	0.160188	8.9	8.1	8.5

The changes in tilt angles suggest further investigation is warranted, but better quality data is necessary to draw meaningful conclusions. The best method to use would be to collect neutron diffraction data as this is much better at defining the oxygen atom positions.

6. Conclusions

Various methods were used to prepare the aluminosilicate sodalites $Na_8(Al_6Si_6O_{24})Br_2$, $Na_8(Al_6Si_6O_{24})Cl_2$, and $Na_8(Al_6Si_6O_{24})I_2$, the best samples were produced successfully with a high degree of crystallinity using the method of Stein. These sodalites were subsequently loaded with various amounts of silver by aqueous ion exchange to produce $Na_{8-x}Ag_x(Al_6Si_6O_{24})Br_2$ with x = 0, 2, 4, 6, 8, $Na_{8-x}Ag_x(Al_6Si_6O_{24})Cl_2$ with x = 0, 2, 4, 6 and 8, and $Na_8(Al_6Si_6O_{24})I_2$. Characterisation by X-ray powder diffraction and Rietveld refinements show that for the chloride and bromide systems the substitution of silver for sodium causes a contraction of the unit cell and M-X bonds in the MX4 tetrahedral units in the sodalite cages, with an expansion of the distance of the metal from the framework oxygen atoms. This can be attributed to the increased covalent bonding in an Ag-X bond vs. a Na-X bond.

High temperature X-ray powder diffraction studies on these systems show that all display positive thermal expansion from room temperature up to 822ºC. The coefficients of thermal expansion for the bromide system show a clear trend of decreasing with silver doping, but there were no clear trends for the chloride system or in the thermal expansion of the M-X or M-O distances in either system.

7. Further work

I did intend to carry out some high pressure work on the sodalites prepared but due to there not being enough time I did not manage to do this. Therefore future work could include high pressure studies on these ion exchanged sodalites to see how the nature of the halide and cation affect the bulk moduli.

During my work I also produced mixed halide sodalites:

$Na_8(AlSiO_4)BrCl$

$Na_8(AlSiO_4)BrI$

$Na_8(AlSiO_4)ClI$

Future work could include carrying out high temperature studies on these sodalites and the silver exchanged forms.